KINETICS OF THE FERRIC SULPHATE LEACHING OF SPHALERITE AND SPHALERITE/PYRITE MIXTURES

A STUDY OF THE CHEMICAL LEACHING OF BASE METAL MINERALS UNDER CONDITIONS SIMILAR TO THAT OF BIO-LEACHING BY THIOBACILLI

by

TERRY-ANN FOWLER

B.Sc. (Eng.) (Cape Town)

Dissertation Presented for Degree of

MASTER OF SCIENCE IN ENGINEERING

UNIVERSITY OF CAPE TOWN

DECEMBER 1995

SUMMARY

The work presented in this dissertation is an investigation of the ferric leaching of zinc from sphalerite. A further aspect of this study was an investigation of the influence of pyrite on the dissolution rate of sphalerite due to possible galvanic interactions. This study is one component of a larger study of the sub-processes involved in the bioleaching of sulphide minerals in which the ferric leaching of the sulphide mineral is assumed to be a chemical step with the bacteria oxidising ferrous iron to ferric iron and elemental sulphur, if formed, to sulphate.

The literature showed that two types of model have been used to describe the ferric leaching of the sphalerite. The first type was a shrinking-particle model in which the reaction was described by first order kinetics or an electrochemical mechanism. The second type included a mass transfer resistance in terms of a shrinking-core model described by half-order kinetics or a decaying diffusion coefficient.

All four of these models were tested for their ability to predict published data for the ferric leaching of sphalerite. It was found that the models fitted the data for the initial period of a leach up to conversions of about 50%. However, no one of the models was found to be successful in predicting the data for prolonged leaching to high conversions.

Because of this, a new model was developed based on the assumption of deactivation of the sphalerite surface due to precipitating products. This surface area deactivation model for the rate of conversion has the form:

$$\frac{dX}{dt} = k_{CR}(1-X)^{-2/3}\{\exp(k_I t)\}$$

where the $k_{CR}(1-X)^{-2/3}$ term is based on the shrinking-particle mechanism and the surface area deactivation term is exp ($k_I t$). When tested against ferric leach data from the literature it was found to be satisfactory for both the initial leach period and high conversion data at prolonged leach times.

In the experimental study the following factors were investigated: the effect of temperature between 30 °C and 55 °C; the size of the mineral particles in the range 106+90 μm to -45+38 μm; initial ferric iron concentration between 0.06 M to 0.5 M. Tests were run under conditions where the redox potential was controlled at fixed values ranging from 673 mV to 443 mV (vs Ag/AgCl) by the addition of 3% H_2O_2. In other tests the redox potential was not controlled but dropped during the course of the leach as the ferric iron was consumed. The Surface Area Deactivation Model was found to be a satisfactory fit for all of the leach data obtained in this study.

Using Arrhenius plots, the temperature dependence of the chemical reaction rate constant was calculated to be 47 $kJ.mol^{-1}$ and the activation energy calculated from the surface area deactivation rate constant was 43 $kJ.mol^{-1}$. In both cases, these values are in the range where the chemical reaction at the mineral surface is thought to control.

The surface area specific conversion rate decreased at the same rate for each particle size. This suggests a constant chemical rate per unit surface area and a constant specific rate of surface deactivation, in both cases independent of particle size. Examination of the leach residue by scanning electron micrography showed that at long leach times there was a layer of elemental sulphur attached to the surface of the sphalerite leading to its deactivation.

From the data obtained under controlled redox potential conditions, it was found that the reaction rate constants were a linear function of the redox potential. However, the gradient of the relationship changed at a redox potential of approximately 520 mV (vs Ag/AgCl). These results are consistent with the work of Crundwell (1988b) where the chemical reaction was shown to be dependent on the solution equilibrium of the iron species and the ionic species responsible for transfer of charge. From the data where the redox potential was not controlled, the reaction was limited by the amount of ferric iron available for the dissolution reaction.

The effect on the leach kinetics of possible galvanic interactions between pyrite and sphalerite were tested in two ways: the addition of pyrite concentrate to the sphalerite concentrate, and leaching of hand-picked samples of ore containing particles of combined unliberated pyrite and sphalerite in direct contact.

Where the pyrite concentrate was added to the sphalerite concentrate, no increase in the rate of zinc leaching was measured for pyrite/sphalerite mass ratios of 0.01, 0.1 and 1.0. On the other hand, in the ferric leaching of the particles of combined unliberated pyrite-sphalerite, the rate of zinc leaching was found to be greater than for sphalerite on its own under the same conditions. This suggests that for galvanic interactions to improve the rate leaching, the minerals have to be in intimate contact.

ACKNOWLEDGEMENTS

I would like to express my sincere thanks to the following organisations and people:

Gold Fields of South Africa for their financial support and Mr R. Beck, Mr R. Graham and Mr G. Martin for their interest in the project;

Professor G.S. Hansford for his advice and motivation during the course of this work and in particular, the preparation of this dissertation;

Dr. S.T.L. Harrison for her interest and advice during the initial stages of this project;

Mrs. R. Claassen for the electron-microscope work and Mrs. S. Vasic for all the chemical analyses;

The staff of the main workshop, the electronic workshop and the main laboratory for their help and assistance whenever required;

Dr. Frank Crundwell for his invaluable advice and criticism throughout the course of this work. In particular, I would like to thank him for his patience and understanding;

All those in the Chemical Engineering Department for their friendship and willingness to help;

My friends;
My parents, Peter and Audrey and family, Robyn, Roland, Justine and Nicole;
and Graeme.

TABLE OF CONTENTS

LIST OF FIGURES

LIST OF TABLES

LIST OF PHOTOMICROGRAPHS

NOMENCLATURE

$[Fe^{2+}]$	ferrous iron concentration	M
$[Fe^{3+}]$	ferric iron concentration	M
[MS]	metal sulphide concentration	$mol_{MS}.m^{-3}{}_{slurry}$
$[Zn^{2+}]$	zinc ion concentration	M
α	charge transfer coefficient ≈ 0.5	
A	diffusion area at time t	m^2
a	reaction order	
$a_{A/C}$	anodic/cathodic transfer coefficient	
A_o	total initial area available for reaction	m^2
A_s	specific particle area	$m^2{}_{solid}/m^3{}_{slurry}$
β	constant (rate-r_o relation) (Suni *et.al.*, 1989)	min^{-1}
b	stoichiometric coefficient	
d	particle diameter of unreacted core	m
D_e	effective diffusion coefficient in a porous structure	$m^2.hr^{-1}$
d_o	initial particle size	m
E	redox potential	mV
E_A	activation energy	$kJ.mol^{-1}$
E_h	redox potential for the Fe^{3+}/Fe^{2+} couple (Nernst equation)	mV
E^o	standard redox potential	mV
F	Faraday's constant	$kJ.mV^{-1}.mol^{-1}$
f	fraction of area blocked at time t	m^2
ϕ	overall constant (Rath *et.al.*, 1988)	
γ	= $(1-\alpha)F/RT$	
G_i	zinc grade of particle size fraction i	
η	overpotential	mV
j	experimental current density at redox potential E	$mA.m^{-2}$
j_o	exchange current density	$mA.m^{-2}$
K	Mass dimensionless "linear" rate constant (Palencia-Perez and Dutrizac, 1991)	
k	overall reaction rate constant	$hours^{-1}$

k'	rate constant not dependent on ferric or ferrous iron concentration	
k''	Rate constant dependent on iron concentration	$mol.m^{-2}.s^{-1}$
k_1	$= \left(\frac{3d_o \rho_B}{b k'}\right)$	
k_2	$= \left(\frac{k_s d_o}{4D_e}\right)$	
k_{22}	$= k_2 \exp(k_I t)$	
k_a	apparent rate constant for a surface reaction for an isometric particle excluding particle size	$\mu m.min^{-1}$
k_A	rate constant 1st order in surface reaction rate	$mol.m^{-2}.s^{-1}$
k_{CR}	chemical reaction rate constant	$hours^{-1}$
k_D	diffusion coefficient decay rate constant	$hours^{-1}$
k_I	surface area deactivation rate constant	$hours^{-1}$
k_o	overall constant determined from the product of the constants of the three relationships (T, d_o and $[Fe^{3+}]$).	
k_s	reaction rate constant dependent on unit surface	$m.hour^{-1}$
M	bivalent metal.	
M_{MS}	molar weight of MS	$kg.mol^{-1}$
M_o	initial value of leachable material	mol
MO	metal oxide	
MS	metal sulphide	
n	number of electrons involved in the reaction	
N	number of moles	mol
Q	flux of material	$mol.\ m^{-2}$
R	universal gas constant	$kJ.mol^{-1}.K^{-1}$
ρ_B	mass density of the reactant	$kg.m^{-3}$
ρ_{MS}	MS density	$kg.m^{-3}$
r_o	particle radius	m
SADM	surface area deactivation model	
SCE	standard calomel electrode	
τ	overall constant (Crundwell, 1988b)	
T	temperature	K

t	time	hours
w/v	solids weight per volume leach liquor	
ω_i	weight of any particular size fraction	
	(Suni *et.al.*, 1989)	g
X	is the fraction of zinc extracted from the sphalerite	

1. INTRODUCTION

The bioleaching of copper from low-grade ores is a well-established technology (Murr, 1980). Large dump and heap leaching operations, particularly in United States of America and Chile, are used in the extraction of copper from the ore. There is a growing interest in the bacterial leaching of other metals from low-grade sulphide ores as it is technically a viable process option (Marchant, 1986) especially for the oxidative pre-treatment of refractory gold-bearing sulphides (Bailey and Hansford, 1993).

Bioleaching of single mineral sulphides has been used commercially for the recovery of metals such as copper and uranium (Torma and Bosecker, 1982). In a ternary or multi-sulphide system, selective bioleaching of certain metals has been achieved (Torma and Subramanian, 1974). This phenomenon has been attributed to a galvanic interaction in which one mineral is passivated while the other undergoes oxidation. Selective leaching is being used for the pre-treatment of refractory gold ores where the main sulphides present are pyrite (FeS_2), pyrrhotite ($Fe_{1-x}S$) and arsenopyrite (FeAsS).

From the literature, it is evident that the following sub-processes might play important roles in the mechanisms and kinetics of leaching of metals from mixed mineral sulphides:

1. chemical oxidation by ferric iron
2. bacterial regeneration of ferric iron from ferrous iron
3. bacterial oxidation of sulphur
4. direct bacterial oxidation of particular sulphide minerals
5. galvanic interactions.

It is expected that bacterial oxidation of a mixed mineral sulphide can be described by a mathematical model built from those already developed for the sub-processes described above. It can then be assumed that it would be valuable to study these sub-processes separately.

The objective of this study is to be able to define a kinetic model for the chemical leaching of zinc from sphalerite. In particular, this project aims at investigating the sub-processes of chemical oxidation of sphalerite by ferric iron and galvanic interactions inherent in a multi-sulphide system. The hypothesis that has been set is

that the leaching of metals from a mixed mineral system (FeS_2/FeS/ZnS) can be described in terms of the kinetics of the sub-processes of chemical oxidation and galvanic interaction.

This hypothesis will be examined by developing a mathematical model for the kinetics of leaching of metals from a mixed sulphide mineral making use of the models developed for the sub-processes of chemical oxidation and galvanic interactions. In particular, the kinetics of the ferric sulphate leaching of sphalerite will be investigated.

The literature review (Chapter 2) highlights the need for this investigation on the following issues:

1. the chemical oxidation of sphalerite in a sulphate medium during prolonged leach periods;
2. the presence of other sulphide minerals in trace amounts and the effect they have in a chemical leaching system;
3. the nature of the products forming and their influence on the reaction kinetics.

A mixed sulphide, zinc ore from the Gamsberg deposit in the Namaqualand district of the Northern Cape Province provided a suitable material for the study of the relative roles of the different factors involved in the leaching of a mixed mineral ore. The Gamsberg ore body consists of a mixture of sulphide minerals formed by chemical precipitation of iron and manganese carbonates, silicates and sulphides (Rozendaal, 1982). The various metals, e.g. iron, zinc, lead, and manganese resulted from a metalliferous brine solution (Rozendaal, 1986). (See Appendix A for an overview of the geology and mineralogy of the Gamsberg ore deposit).

The ore body is divided into three zones:

1. the *Pyrite Ore Zone*, which is the stratigraphic base of the ore zone, primarily consists of pyrite (FeS_2) and sphalerite (ZnS) with minor amounts of other iron sulphides (these iron sulphides will be referred to as FeS_2 and include pyrite),
2. the *Pyrrhotite Ore Zone,* which contains larger amounts of pyrrhotite ($Fe_{1-x}S$ includes all crystal lattice forms found in the ore body), FeS_2 and other altered iron sulphides, ZnS and minor amounts of galena (PbS). The main difference between the *Pyrite Ore Zone* and the *Pyrrhotite Ore Zone* is the presence of minor amounts of graphite in the former that has influenced precipitation of FeS_2 instead of $Fe_{1-x}S$,

3. the *Magnetite Ore Zone*, which lies in the base of a Banded Iron Formation, has a higher grade of zinc than the other two zones but also a high content of manganese.

The mathematical model for the kinetics of leaching of zinc from a sphalerite concentrate has been developed from those models presented in the literature. This model has been verified by experimental data obtained as part of this study. The procedures for the experimental work were adapted from those described in the literature.

In the context of the broader objective of this study, further investigation will be able to test the following:

- during pure sphalerite leaching there is no direct bacterial attack and so oxidation of sphalerite in the presence of bacteria results from chemical oxidation of the mineral where the role of the bacteria is to regenerate ferrous iron to ferric iron, and to oxidise the elemental sulphur formed in the chemical leaching step;

- in a mixed mineral system, the above hypotheses apply but the chemical ferric leaching is enhanced by galvanic interactions.

2. LITERATURE REVIEW

The overall leaching reaction of sphalerite in a ferric solution is:

$$ZnS + Fe^{3+} \rightarrow Zn^{2+} + S^{o} + Fe^{2+} \qquad [2\text{-}1]$$

The important phenomena associated with this reaction are the reduction of ferric iron to ferrous iron and the kinetics related to the oxidation of the ferrous ion to the ferric ion state as well as the formation of elemental sulphur, S^{o}.

The chemical leaching of sulphide minerals is dependent on two aspects *viz.* the thermodynamics of leaching and the kinetics of leaching. The electrochemistry describes both the thermodynamics and the kinetics of the system.

Thermodynamic data are used to predict the general conditions that will enhance the dissolution of a mineral. This shows the tendency of a reaction to occur in a particular direction but provides no information on the rate of the reaction nor the mechanism.

In the case of chemical leaching, there are several steps in the overall conversion of reactants to products. Any one or more of these steps can be rate limiting (Levenspiel, 1972), i.e. the overall rate of reaction is dependent on this rate-limiting step. In sphalerite dissolution where ferric iron is necessary at the particle surface for reaction to occur, the following steps have been established as possible rate limiting factors:

1. diffusion of the ferric iron through the solid product (elemental sulphur or jarosite deposited on the surface of the particle) to the reacting surface;
2. chemical reaction of the ferric iron with the solid at the surface of the particle;
3. diffusion of the products away from the reacting surface through the product deposited on the particle surface.

This literature review shows that there are six aspects of the chemical leaching of zinc sulphide that are important. They are:

1. the mechanism and kinetic model describing the reaction,
2. the influence of impurities (Fe, Pb) within the leaching system or within the zinc sulphide lattice,
3. the formation of ferrous iron and its role in the dissolution process,

4. the formation of elemental sulphur and its role in the dissolution process,
5. the leach medium used - a ferric chloride medium or a ferric sulphate medium,
6. the influence of other mineral sulphides on the rate of sphalerite dissolution in a mixed mineral system.

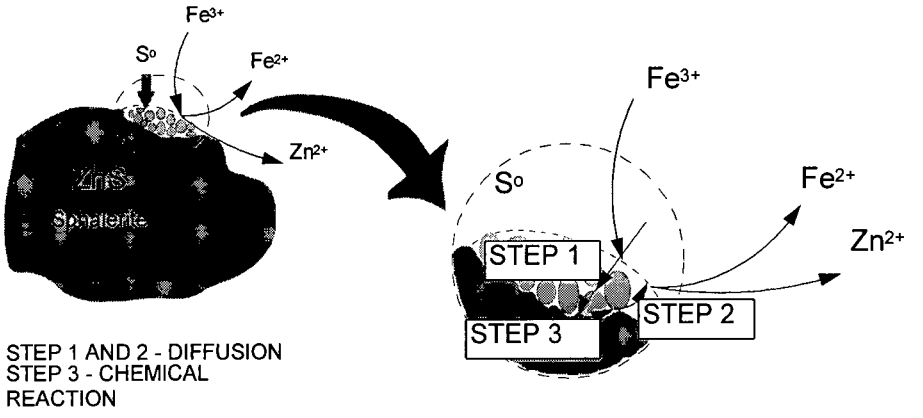

Figure 2-1 Stages in the leaching process.

In the presence of a mixed sulphide ore, galvanic interactions and the associated electrochemistry of the different minerals must also be considered.

2.1 The Kinetic Model Describing the Reaction

The dissolution processes of minerals have been described by different mathematical models. The shrinking-core model (discussed in Appendix A) is one such mathematical rate expression that has been used to describe the oxidation of sphalerite. In this model, it is assumed that the reaction rate is proportional to the mineral surface area. As the particle reacts, the surface area changes. The shrinking-core model accounts for the rate of change in the surface area as the reaction proceeds and the rate-determining step of either product-layer diffusion or chemical reaction at the unreacted core. This kinetic model has been used to describe the results of the sphalerite dissolution reaction where the rate of reaction at the surface of the particle was assumed to be rate limiting for this reaction (Jin *et al.*, 1984; Rath *et al.*, 1988). The rate equation takes the form:

$$1 - (1 - X)^{1/3} = k\,t \qquad [2\text{-}2]$$

where X is the fraction zinc extracted from the sphalerite

k is the overall reaction rate constant (hours^{-1}) and is dependent on the size, temperature and concentration of the reaction. Incidentally k^{-1} is the time taken for complete conversion (X = 1).

Table 2-1 shows the rate equations that have been used to describe the leaching of sphalerite.

REFERENCE	MODEL
Jin *et al.* (1984)	$1-(1-X)^{1/3} = \left[17.72 \times 10^3\ \rho_B^{-1}\ A_o\ [Fe^{3+}]^{0.5}\ \exp\left\{\frac{-E_A}{RT}\right\}\right] t$
Verbaan and Crundwell (1986)	$1-(1-X)^{1/3} = \left[\frac{6.605}{3\ M_o}\ A_o\ \exp\{17.3\ E_h\}\ \exp\left\{\frac{-E_A}{RT}\right\}\right] t$
Crundwell (1987)	$1-(1-X)^{1/3} = \left[\frac{\tau}{3M_o} A_o \exp\left\{\frac{-E_A}{RT}\right\}\ \left\{[Fe^{3+}_{AQ}] + [FeHSO_4^{2+}]\right\}^{1-\alpha}\right] t$
Rath *et al.* (1988)	$1-(1-X)^{1/3} = \left[\phi\ \rho_B^{-1}\ A_o [Fe^{3+}]^{0.62}\ \exp\left\{\frac{-E_A}{RT}\right\}\right] t$

Table 2-1 Summary of the kinetic models presented by other researchers.

2.1.1 The Development of the Kinetic Model Describing the Reaction

Two types of mechanism are presented in the literature to describe the kinetics of the dissolution of sphalerite. The first model describes the phenomena of the mechanism (this will be termed the phenomenological model) and the second model uses an electrochemical approach to describe the mechanism which is interpretative. In the first model, the overall reaction rate constant, k, is a function of particle size, temperature and ferric iron concentration (Jin *et al.*, 1984; Bobeck and Su, 1985; Rath *et al.*, 1988). The second model shows that the mechanism of the reaction is limited by charge transfer (Jin *et al.*, 1985; Verbaan and Crundwell, 1986; Rath *et al.*, 1988).

The overall reaction rate constant is a function of temperature, particle surface area and the ferric iron concentration. These parameters are incorporated into the

shrinking-core model by the product of their respective relationships to the overall reaction rate constant i.e.

$$k = k_o\, d_o^{-1}\, [Fe^{3+}]^a \exp\left\{\frac{-E_A}{RT}\right\} \qquad [2\text{-}3]$$

where $\exp\left\{\frac{-E_A}{RT}\right\}$ is the relationship between the temperature and the reaction rate constant which is determined from an Arrhenius plot with a calculated, inherent activation energy (E_A);

d_o^{-1} is the inverse relationship expected between initial particle size and the reaction rate constant because the larger the surface area per unit volume of solids (the smaller the particle size) the larger the rate of reaction;

and a is the reaction order.

The difference between the phenomenological model and the electrochemical model is the determination of the reaction order *a*.

NOTE: k_o is an overall constant determined from the product of the constants of the three above relationships (temperature, initial particle size and ferric iron concentration).

The variables, T, d_o and $[Fe^{3+}]$, have been investigated by several researchers (Jin *et al.*, 1984; Bobeck and Su, 1985; Rath *et al.*, 1988). The dissolution rate, when the chemical reaction at the mineral surface is rate limiting, is strongly dependent on the temperature of the reaction. Dissolution data obtained for different leaching temperatures are used to calculate the activation energy of the reaction from an Arrhenius plot.

All workers show that the smaller the particle size, d_o, the higher the rate of dissolution. The literature on the bioleaching of metal sulphide ores shows that particle size is an important factor in modelling the rate of dissolution. Early studies showed that decreasing the particle size increased the rate of leaching significantly (Bryner and Anderson, 1957; Malouf and Prater, 1961).

The particle size and surface area concentration are associated in that as the particle size reduces, the surface area concentration increases. One of the earliest recognitions of the importance of surface area on leach rate was made by Malouf and Prater (1961) (Hansford and Chapman, 1992). Torma *et al.* (1970, 1972) observed a linear relationship between zinc bioleach rate and surface area concentration in a batch reactor. A similar relationship was found by Gormely *et al.* (1975) for a continuous bioreactor. Mathematical models developed have shown a dependence on the surface area of the ore.

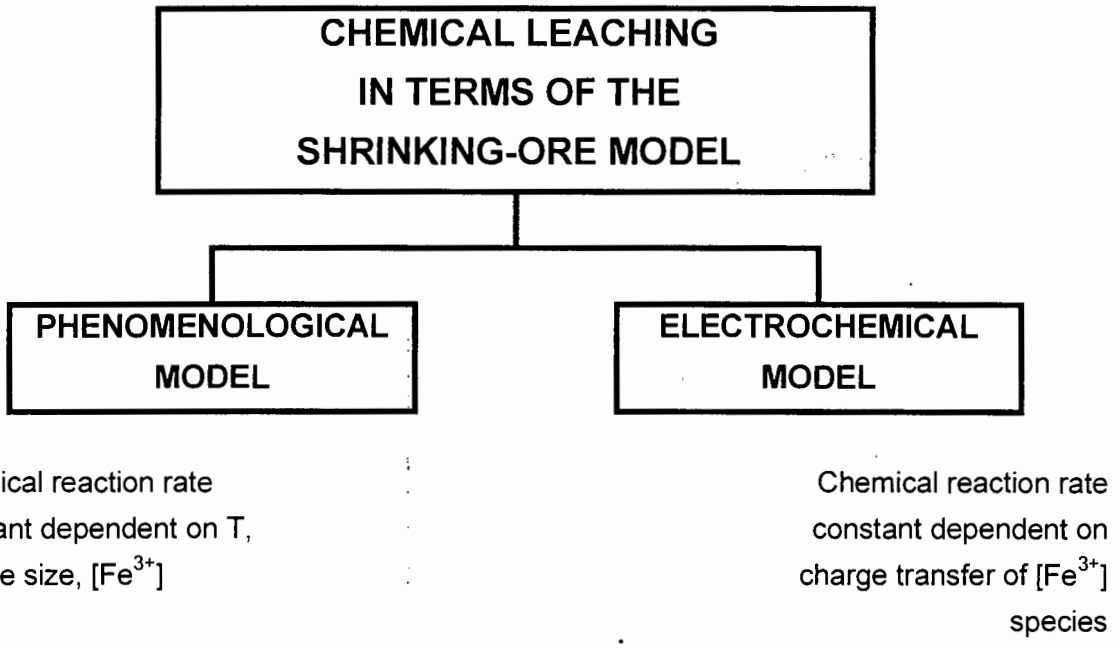

Figure 2-2 Diagram showing the different models used to describe the chemical leaching of sphalerite.

Different methods were presented to determine the particle surface area. The most simple method of determining the surface area was used by Hansford and Chapman (1992) who assumed that each particle was a sphere and calculated it as such. The disadvantage of this method is that the calculated surface area underestimates the surface area of irregular particles. Other methods used for surface area calculation were the BET method (Verbaan and Crundwell, 1986; Crundwell, 1988b) and the air permeability method (Bailey, 1993). These methods may overestimate the surface area available to the bacteria for attachment.

The literature showed that at some ferric iron concentration, the order of the reaction changed from approximately one half to zero (Jin *et al.*, 1984; Bobeck and Su, 1985; Crundwell, 1988a; Rath *et al.*, 1988). However, the ferric iron concentration at which this change was shown to occur was not consistent for these researchers. Data obtained by Jin *et al.* (1984) showed an increase in the reaction rate for increasing amounts of ferric iron until a maximum concentration of 0.8 M. After this, there was no dependence of the reaction rate on the ferric iron concentration. This was also observed by Bobeck and Su (1985) but the concentration of ferric iron at which the change in the reaction order was observed was 0.1 M.

A similar trend was calculated from the work of Rath *et al.* (1988) and gave a maximum concentration of ferric iron comparable with that of Jin *et al.* (1984).

REFERENCE	$[Fe^{3+}]$ (M)	REACTION ORDER *a*	E_A ($kJ.mol^{-1}$)
Jin *et al.* (1984)	0.8	0.5	58
Bobeck and Su (1985)	0.1	0.5	50
Crundwell (1988a)	0.3	0.5	79
Rath *et al.* (1988)	1.0	0.62	58

Table 2-2 Comparison of reaction orders and activation energies as used in kinetic models derived by various researchers.

The order of the reaction has been shown to be 0.5 by many researchers (Su, 1976; Bobeck and Su, 1985; Jin *et al.*, 1984; Crundwell, 1988a). Su (1976) and Bobeck and Su (1985) showed the dependence of the order of the reaction on the ferric iron for concentrations of less than 0.1 M. At ferric iron concentrations higher than this, the order of the reaction changed to zero. This observation was validated by research work by Jin *et al.* (1984) who also measured a reaction rate of 0.5 with respect to the ferric iron concentration. The difference that they found was that the order of reaction changed at a concentration of ferric iron of 0.8 M which was higher than the ferric iron concentration observed by Bobeck and Su (1985). At ferric iron concentrations higher

than 0.8 M, Jin *et al.* (1984) showed no rate dependence on the [Fe^{3+}] and proposed that an adsorption mechanism dominated at this stage of the leaching reaction.

The second type of model suggested that the mechanism of the leaching of sphalerite was an electrochemical dissolution reaction with the rate controlling step dependent on the composition of the sphalerite and solution conditions (Jin *et al.*, 1985; Verbaan and Crundwell, 1986; Rath *et al.*, 1988).

Assuming that the leaching occurred through a corrosion couple on the ZnS surface and that the electrochemical charge transfer reaction was the rate-determining step, Jin *et al.* (1985) derived an electrochemical model incorporating the ferric iron effect and the chloride ion effect when leaching sphalerite in a ferric chloride solution. The ferric and chloride ions first adsorbed on to the surface of the sulphide mineral and then charge transfer occurred between these adsorbed ions and the ZnS lattice.

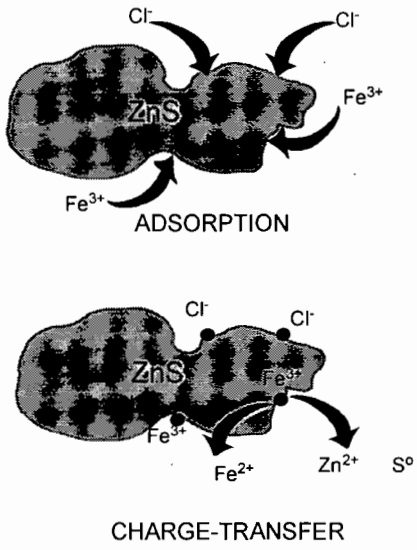

Figure 2-3 The mechanism of the electrochemical dissolution of sphalerite leaching proposed by Jin *et al.* (1985).

The model described the change in order observed at high ferric iron concentrations from one-half to zero which had not been accounted for in the generalised model described by Jin *et al.* (1984) and Rath *et al.* (1988).

For the oxidative leaching of sphalerite, Verbaan and Crundwell (1986) proposed an electrochemical charge-transfer mechanism in which the mineral surface potential was

approximated by the Nernst[1] equation for the Fe^{3+}/Fe^{2+} redox couple. The electrochemical model kinetics, analogous to the corrosion mechanism, could be described by the Butler-Volmer[2] equation (Verbaan and Crundwell, 1986; Rath *et al.*, 1988) for the two half-cell reactions at the mineral surface:

$$\begin{aligned} ZnS &\rightarrow Zn^{2+} + S^{\circ} + 2e^{-} \quad \text{(anodic)} \\ 2Fe^{3+} + 2e^{-} &\rightarrow 2Fe^{2+} \quad \text{(cathodic)} \end{aligned} \qquad [2\text{-}4]$$

Verbaan and Crundwell (1986) formulated the overall leaching rate in terms of Faraday's law and the shrinking-core model.

$$1-(1-X)^{1/3} = \left[\frac{6.605}{3\,M_o} A_o \exp\{\gamma E_h\} \exp\left\{\frac{-E_A}{RT}\right\}\right] t \qquad [2\text{-}5]$$

where $\gamma = (1-\alpha)F/RT$

α is the charge transfer coefficient ≈ 0.5

A_o is the total initial area available for reaction

M_o is the initial value of leachable material

E_h is the redox potential for the Fe^{3+}/Fe^{2+} couple described by the Nernst equation.

Crundwell (1987) found that when the ferrous iron concentration was constant and the ferric iron concentration varied, the model showed a "Nernstian" response, i.e. a plot of *log (Initial Rate)* versus *Redox Potential* gave a straight line with slope of 0.5F/RT. This "Nernstian" response was not observed when the ferric iron concentration was kept constant and the ferrous iron concentration was varied. The "non-Nernstian" response was the motivation for further study of the role of the Fe^{3+}/Fe^{2+} couple during ZnS leaching (Crundwell, 1988b).

This detailed study by Crundwell (1988b) established that the rate-determining step was the rate of charge transfer across the Helmholtz layer and the space-charge region. The redox potential is a measure of the activity ratio of $[Fe^{3+}]_{TOTAL}$ and

[1] See Appendix C (Equation C-1) for the Nernst equation

[2] See Appendix C (Equation C-2) for the Butler-Volmer Equation

$[Fe^{2+}]_{TOTAL}$ ions for the electrolyte system consisting of ferric and ferrous sulphate complexes. The distribution of the iron species in solution was calculated. The dominant species was $FeSO_4^+$ (85 %) followed by $FeHSO_4^{2+}$ (10 - 15 %). Crundwell (1987) argued that $FeHSO_4^{2+}/FeHSO_4^+$ and $[Fe^{3+}{}_{AQ}]/[Fe^{2+}{}_{AQ}]$ were the electro-active species. He proposed that the $FeSO_4^+$ species was less electro-active because it is an inner-sphere complex, while the $FeHSO_4^{2+}$ and $[Fe^{3+}{}_{AQ}]$ were more electro-active because they are outer-sphere complexes. The model presented is:

$$1-(1-X)^{1/3} = \left[\frac{\tau}{3M_o} A_o \exp\left\{\frac{-E_A}{RT}\right\} \left\{[Fe^{3+}_{AQ}] + [FeHSO_4^{2+}]\right\}^{1-\alpha}\right] t \qquad [2\text{-}6]$$

where the effect of only the electro-active outer-sphere couples was incorporated, and the reaction order, *a*, was approximately 0.5.

2.1.2 A Comparison of the Kinetic Models

A comparison was drawn between the models developed by the different researchers to determine which model fitted the leaching data obtained from Crundwell (1988b) for a sphalerite concentrate. Basic conditions were set for the comparison and are:

Activation Energy	46	$kJ.mol^{-1}$
$[Fe^{3+}]$	0.274	M
Temperature	78	°C
Initial Particle Size (average)	54	μm

Table 2-3 Basic conditions used for the comparison of the kinetic models.

The phenomenological models presented by Jin *et al.* (1984) and Rath *et al.* (1988) were very similar in that the basic form of the equation was the same due to their assumption that sphalerite dissolution was governed by the chemical reaction at the mineral surface.

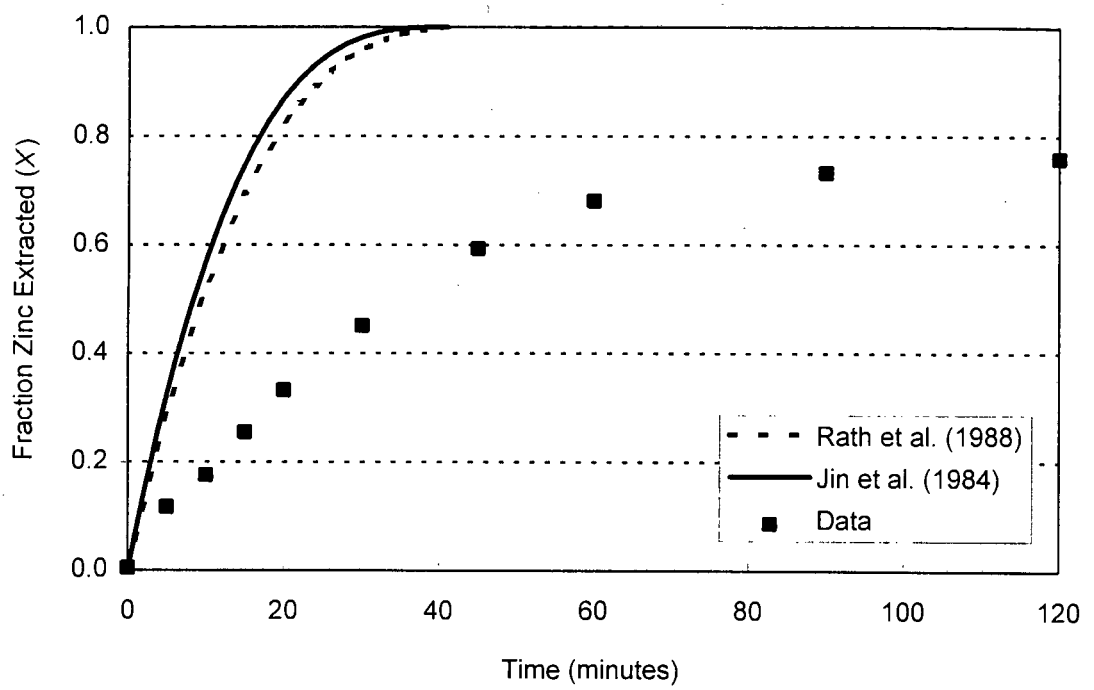

Figure 2-4 Comparison of the models presented by Jin *et al.* (1984) and Rath *et al.* (1988) with data obtained from Crundwell (1988b) for the leaching of a sphalerite concentrate (ex-Gamsberg) under the same leaching conditions.

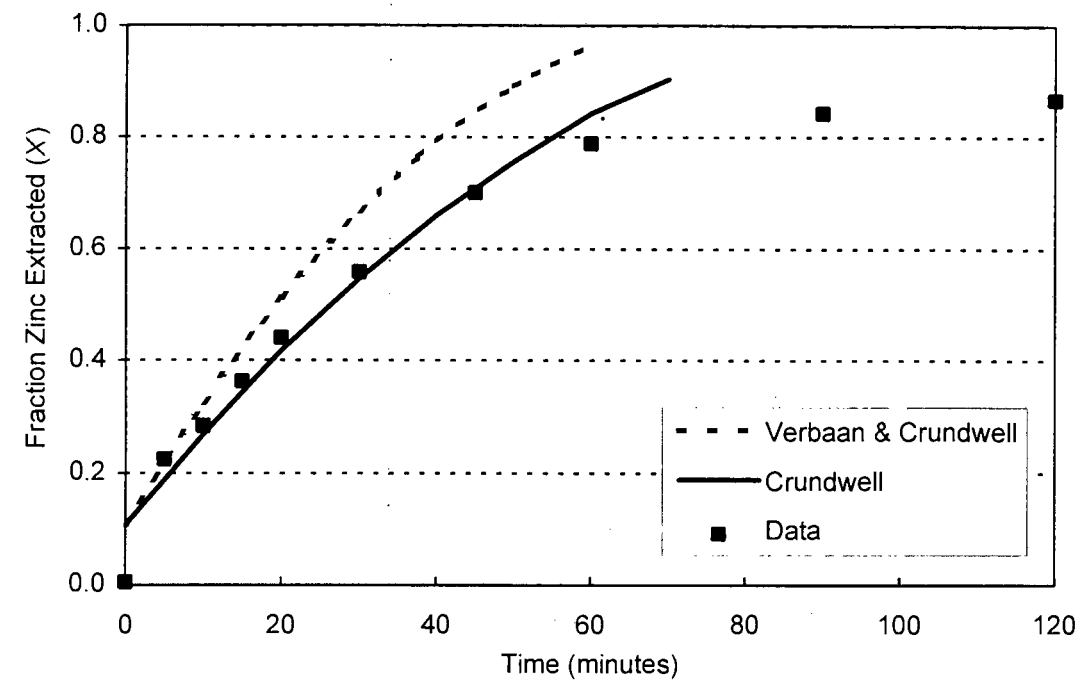

Figure 2-5 Comparison of the models presented by Verbaan and Crundwell (1986) and Crundwell (1987) with leaching data of the Gamsberg ore.

These researchers investigated the reaction during the initial stages of occurrence and modelled it as such. For prolonged leaching periods, these models predicted that the sphalerite ore was completely leached. Bobeck and Su (1985) claimed that this did not happen if the reaction was to continue for an extended period. Leaching data obtained for the Gamsberg ore from Crundwell (1988b) suggested that complete conversion of ZnS to Zn^{2+} may not occur because of coating of the particle caused by the products of reaction.

This is shown in Figure 2-4 and Figure 2-5, where the models are presented under similar conditions to those used in obtaining the data.

The electrochemical model developed by Crundwell (1987) allowed for the fractured material that was found to surround the Gamsberg ore. This material dissolved rapidly which resulted in the initial conversion shown in Figure 2-5.

2.2 The Influence of Impurities (Fe, Pb) in the Zinc Sulphide Crystal Lattice

The presence of impurities within the sphalerite crystal lattice also increased the dissolution rate of zinc. Studies by Romankiw and DeBryn (1965) showed that the presence of iron, the most common impurity present in the sphalerite (Crundwell, 1988b), increased the ionic character of the Zn–S bond and thus the mineral exhibited increased dissolution rates.

Su (1976), Bobeck and Su (1985), Crundwell (1988a) and Palencia-Perez and Dutrizac (1991) showed that the leaching rate increased in a linear manner with increasing iron content within the lattice. Associated with the increase in iron content within the sphalerite lattice was a decrease in the activation energy.

Lead, either as part of the crystal lattice or present as galena (PbS), was shown experimentally to inhibit dissolution of ZnS (Crundwell, 1988b). The results obtained were explained by assuming that a lead sulphate precipitate had formed on the surface of the particles; this caused the rate limiting step to change from the chemical reaction at the mineral surface to the diffusion through the product. The experimental work of Lochmann and Pedlik (1995) showed that passivation did occur but the degree of this passivation caused by anglesite ($PbSO_4$) could not be determined as other product layers formed and all contributed to diffusion limitations.

ORIGIN OF SPHALERITE	IRON CONTENT	E_A (kJ.mol^{-1})	REFERENCE
Pure Sphalerite Crystal	0.0 %	64.5	Bobeck and Su (1985)
Wards (natural pure sphalerite)	0.55 %	59.5	Crundwell (1988a)
Rosh Pinah (impure flotation concentrate)	1.79 %	44.1	Crundwell (1988a)
Zincor (impure flotation concentrate)	2.56 %	51.6	Crundwell (1988a)
St. Joe (impure flotation concentrate)	5.2 %	46.9	Bobeck and Su (1985)
Black Mountain (impure flotation concentrate)	8.02 %	31.7	Crundwell (1988a)
Gamsberg (impure flotation concentrate)	8.62 %	43.3	Crundwell (1988a)

Table 2-4 Activation energies reported for the leaching of sphalerite in ferric chloride media (Palencia-Perez and Dutrizac; 1991).

2.3 The Formation of Ferrous Iron and its Role in the Dissolution Process

Ferrous iron, Fe^{2+}, present in the solution was shown to reduce the rate of dissolution of sphalerite (Crundwell, 1988b). Crundwell (1988b) attributed this effect to the ferrous iron decreasing the concentration of the electro-active ions present that were required for dissolution.

The solution redox potential is dependent on the ratio of $[Fe^{3+}]$ to $[Fe^{2+}]$. At high concentrations of ferric iron, the redox potential is high. The presence of ferrous iron at high concentrations in a leaching system causes a decrease in the redox potential.

The redox potential has been shown to be influenced by the concentration of solids in a bioleaching system (Komnitsas and Pooley, 1990). Their observations which sustained the work by Sakaguchi *et al.* (1976) showed that as the concentration of solids increased, the redox potential decreased. The explanation for this was that the

bacteria-to-solids ratio was low at high solids concentration. As the redox potential is a measure of the relative amounts of ferric iron to ferrous iron, the observations of Komnitsas and Pooley (1990) and Sakaguchi *et al.* (1976), can be interpreted as follows. At a high solids concentration, the ferric iron was consumed by the chemical reaction. The abundance of the ferrous iron in solution caused the lowered measured redox potentials.

In a review paper, Bailey and Hansford (1993) reported this to have important implications during the oxidation of a mixed sulphide mineral ore. From an analysis of the results of Komnitsas and Pooley (1990) on an arsenopyrite/pyrite system, Hansford and Bailey (1992) showed that the period before significant oxidation of the pyrite phase occurred, increased with increasing concentration of solids. This was attributed to a lower redox potential increasing the preference for arsenopyrite oxidation. From the application of the logistic equation to this data, Hansford and Bailey (1992) showed that the rate constants of the bio-oxidation of both the arsenopyrite and pyrite decreased with decreasing redox potential.

2.4 The Formation of Elemental Sulphur and its Role in the Dissolution Process

From their experimental data, Su (1976) and Bobeck and Su (1985) concluded that the decrease in the reaction rate in the later stages of sphalerite oxidation was caused by formation of a protective sulphur layer. However, Boon and Heijnen (1993), in an extensive evaluation and review of data on zinc leaching reported in the literature, concluded that the diffusion rate limitation due to the formation of S^{o} does not occur. This conclusion was drawn in their review of the literature on the chemical leaching of sphalerite from the fact that the rate of dissolution decreased when ferric sulphate was used as the leach medium during batch experiments.

This was considered to be due to the fact that formation of jarosite did not occur when a ferric chloride leach medium was used. A further contributing factor was that if diffusion through the sulphur layer were rate limiting then the activation energy of the reaction would be lower (about 20 $kJ.mol^{-1}$). Boon and Heijnen (1993) attributed the decrease in the reaction rate, observed by Bobeck and Su (1985), to the detrimental effect caused by the increase in ferrous iron concentration rather than diffusion through the sulphur layer.

This conclusion by Boon and Heijnen (1993) was sustained by observations of Jin *et al.*(1984). This work examined reaction residues at various levels of zinc extraction by SEM and identified the products of reaction by energy dispersive X-ray analyses and X-ray diffraction. These analyses showed the formation of a layer of sulphur at the surface of the particles and that this sulphur product layer was very porous. These phenomena were supported by scanning electron micrographs reported by Rath *et al.* (1988).

2.5 Leaching in Either a Ferric Chloride Solution or a Ferric Sulphate Solution

Using the results of Dutrizac and MacDonald (1978) and Jin *et al.* (1985) for ferric chloride batch leaching, Crundwell (1988b) confirmed that the electrochemical model he had developed for the leaching of sphalerite in ferric sulphate could describe the leaching mechanism in ferric chloride solutions. It successfully gave the order of dependence of the rate on the concentrations of Fe^{3+}, Fe^{2+} and Cl^-. The difference, as noted by Crundwell (1988b), for leaching in either a sulphate medium or a chloride medium was that inactive ionic species are formed in sulphate leaching while in chloride leaching, no complexes that formed were inactive. The relevance of this is that the charge transfer in chloride solutions is not dominated by a particular ionic species as it is in sulphate solutions.

Palencia-Perez and Dutrizac (1991) established similar kinetics in both ferric sulphate and ferric chloride systems. They showed a linear correlation between the leaching rate and the solid-solution iron content for both sulphate and chloride systems with corresponding activation energies that were similar. They concluded from these findings that the mechanism of the sphalerite leaching reaction was controlled by the charge-transfer on the sphalerite surface.

2.6 The Influence of Other Mineral Sulphides in a Mixed Mineral System

Sulphide minerals assume electrode potentials in aqueous solutions. A direct consequence of this is that when two sulphide minerals are in contact in a leaching system, they form a galvanic cell where the minerals act as electrodes. Oxidation-reduction processes or reactions occur at each electrode and influence the chemical and bioleaching of the sulphides, in particular, that of mixed sulphides systems (Mehta

and Murr, 1983; Natarajan and Iwasaki, 1983). The more noble mineral acts as the cathode and is galvanically protected by the cathodic reaction (Mehta and Murr, 1983):

$$\tfrac{1}{2}O_2 + 2H^+ + 2e^- = H_2O \qquad [2\text{-}7]$$

This means that the mineral with the lower rest potential acts as the anode according to the anodic reaction

$$MS = M^{2+} + S^o + 2e^- \qquad [2\text{-}8]$$

where MS is the metal sulphide
M is the bivalent metal.

The overall reaction of the system is as follows:

$$MS + \tfrac{1}{2}O_2 + 2H^+ = M^{2+} + S^o + H_2O \qquad [2\text{-}9]$$

The magnitude of the galvanic current, which was reported by Natarajan (1988), was dependent on a number of factors which influence the rate of metal dissolution; they were:

- the rest potential difference between sulphide minerals in contact
- the anode to cathode area ratio
- the electrolytic properties such as pH, conductivity, availability of oxygen, and the presence of other redox couples
- the presence or absence of bacteria.

Table 2-5 indicates that the measured rest potential of sulphide minerals varied according to the type of solution and its pH (Mehta and Murr, 1983). It has been shown that the rest potential of sphalerite is influenced by its iron content (Peters and Majima, 1968; Majima, 1969).

SULPHIDE	SOLUTION	TEMPERATURE °C	REST POTENTIAL mV	REFERENCE
Pyrite (FeS_2)	1M H_2SO_4	25	630	Attia and El-Zeky (1990)
	1M $HClO_4$	25	620	Attia and El-Zeky (1990)
	-	-	450	Graham (1993)
Chalcopyrite ($CuFeS_2$)	1M H_2SO_4	20	520	Attia and El-Zeky (1990)
Galena (PbS)	1M H_2SO_4	20	280	Attia and El-Zeky (1990)
	1M HCl	25	290	Attia and El-Zeky (1990)
Pyrrhotite ($Fe_{1-x}S$)	9K Medium pH = 2.5	25	120 - 110	Natarajan and Iwasaki (1983)
	-	-	120	Graham (1993)
Sphalerite (ZnS)	1M H_2SO_4	20	-240	Attia and El-Zeky (1990)
	-	-	-180	Graham (1993)

Table 2-5 Rest potentials for some sulphide minerals in strong acidic solution.

From Table 2-5, the order of the galvanic series is as follows:

$$ZnS < FeS < PbS < Cu_2 \approx CuS < CuFeS_2 < FeS_2$$

where ZnS is the least *noble* and FeS_2 is the most *noble*.

Prediction of selective oxidation in binary systems follows the rest potential or galvanic series where the more active mineral is leached and the more noble mineral is cathodically protected. In a multi-sulphide combination, similarly the least noble mineral will undergo anodic oxidation and the most noble of the combination will act as the cathode. The sulphides, whose rest potentials assume intermediate values, undergo anodic oxidation in the presence of the more noble mineral but are galvanically passivated in comparison with the less noble mineral. Various types of possible combinations of galvanic currents come into existence in such systems and

thus it becomes difficult to predict the exact manner in which the anodic dissolution proceeds (Natarajan, 1988).

2.6.1 Galvanic Interactions

Work on the investigation of the galvanic effects in the bioleaching of sulphide minerals was reviewed by Mehta and Murr (1983). Early workers (Buehler and Gottschalk, 1910) showed that the rate of oxidation of certain natural sulphides was greatly increased by the presence of either marcasite or pyrite. The reason given for this enhanced oxidation rate was that the iron salts and sulphuric acid formed in the oxidation of the iron sulphide acted as oxygen carriers. Further investigation by these researchers (Gottschalk and Buehler, 1912) showed that in the oxidation of pyrite and marcasite with the supply of iron as the oxidant, the one sulphide showed significant oxidation and the other was galvanically protected. This was attributed to the difference in the rest potentials of the two sulphide minerals.

This phenomenon was shown for a different system by Dutrizac and MacDonald (1973) who found that the rate of dissolution of chalcopyrite was accelerated in the presence of pyrite, molybdenite (MoS_2) and stibnite (Sb_2S_3), but was retarded in the presence of galena. Scanning electron micrographs of leached samples of low-grade copper-bearing ore (Berry *et al.*, 1978) showed that where the chalcopyrite and pyrite were in direct contact with each other, the chalcopyrite was corroded whereas the pyrite surface was found to be almost unaffected. This observed corrosion rate was accelerated in the presence of micro-organisms.

From their literature review, Mehta and Murr (1982) concluded that these observations were purely qualitative and no investigation was undertaken to understand quantitatively the kinetics of the phenomenon of the galvanic interactions present. In their study, they investigated the galvanic interaction between chalcopyrite and pyrite by varying the quantity of each mineral and then measuring the amount of metal dissolution under sterile conditions and in inoculated systems.

Results showed that the rest potential of a mixture of chalcopyrite and pyrite assumed a value between that of the pure chalcopyrite and the pure pyrite. Highest dissolution rates of copper were observed in a system where there was an equal ratio of chalcopyrite to pyrite (by mass). This was further enhanced by bacteria, which

increased the corrosion current of the system from five $\mu A.cm^{-2}$ under abiotic conditions to ten times that in inoculated systems. From these results, the authors concluded that due to the different rest potentials present in a mixture of sulphides, galvanic interactions did occur and contributed to the leaching process. This phenomenon for the use of selective leaching in a mixed sulphide ore was verified by other investigators (Jyothi, Sudha and Natarajan, 1989).

As part of their experimental procedure, many researchers (Mehta and Murr, 1983; Natarajan and Iwasaki, 1983; Natarajan, 1988; Jyothi *et al.*, 1989) used scanning electron micrographs to examine the leaching surface of the mineral sulphides. These showed preferential attack of the less noble sulphide in contact with the more noble sulphide. In all micrographs where pyrite was the most noble sulphide, there was very little oxidation of the pyrite present, while the less noble mineral in close contact with the pyrite showed marked oxidation. Scanning electron microscopy was used to support the phenomenon of selective leaching by being a visual verification of this occurrence.

Attia and El-Zeky (1990) investigated selective bioleaching for the recovery of precious metals from complex sulphide ores and tailings. Their data for lead dissolution did not follow the galvanic series trend. Instead it showed retardation of the dissolution of the galena. This was attributed to the formation of lead sulphate ($PbSO_4$) that controlled the level of soluble lead in the liquor. It was observed that pyrite dissolution gradually increased until, after twenty-four days of the experimental test period, pyrite oxidation became significant. This was explained by the fact that the pyrite acted as the cathode in the system while the less noble minerals were being oxidised.

Simultaneously, refractory gold and silver became exposed to the solution and began to take part in the galvanic interactions. It was postulated that as gold and silver have rest potentials of 1498 mV and 799 mV respectively, they, in conjunction with the pyrite, acted as the cathodes in the system until such time as the minerals less noble than pyrite were almost completely oxidised. From this stage onwards, they acted as the cathode and the pyrite was then subjected to anodic dissolution.

2.6.2 The Role of Bacteria in an Electrochemically Leaching System

In a system where thiobacilli and associated species were present, Mehta and Murr (1983) observed a difference in the corrosion current i.e. the equilibrium rest potential, under abiotic conditions in comparison with that of an inoculated system. They attributed the increase in the current to the bacterial activity in the inoculated system. This was in accordance with the work of Jyothi *et al.* (1989) who also observed that the mineral electrode potentials in the inoculated sulphide solution were higher than those under abiotic conditions. However, they suggested that this increase could have been due to the higher ferric ion (Fe^{3+}) concentration (redox potential) at the electrode surface resulting from bacterial activity.

Although galvanic contact in a system was a factor contributing to the selective leaching of multi-sulphide minerals, the presence of thiobacilli was shown to accelerate the galvanic dissolution. (Mehta and Murr, 1982; Mehta and Murr, 1983; Natarajan and Iwasaki, 1983; Natarajan, 1988; Natarajan, 1992b).

Two roles have been suggested for the bacteria in a mixed sulphide bioleaching system:

- due to bacterial activity, current density in the system is increased and this, in turn, increases the dissolution of the specific metal ion (Mehta and Murr, 1983);
- the presence of the bacteria helps to remove the accumulated layers on the leaching surface (Natarajan, 1988; Mehta and Murr, 1982) thus reducing the layer of sulphur reaction product. This is important if the principal rate-limiting step is the transport process of electrons through the layer of sulphur. (Mehta and Murr, 1982; Graham, 1993).

Conclusive evidence on the role of the bacteria in a system where the galvanic interactions are significant, is still to be established (Nicol, 1993). However, the presence of bacteria in a galvanic system did enhance the rate of dissolution of zinc from a mixed sulphide system (Natarajan, 1988). Possible reaction mechanisms for the galvanic dissolution of the active material have been presented by Jyothi *et al.*, 1989:

Mehta and Murr (1983) reported that in a chalcopyrite/pyrite system, the presence of *Thiobacillus ferrooxidans* increased the dissolution rate of copper by 2.1 times that of

the abiotic leach. Further experimentation showed that the zinc dissolution rate from a zinc sulphide/pyrite system was increased by a factor of 1.3 in the presence of thiobacilli and associated species.

2.6.3 Anode to Cathode Area

Natarajan (1988) leached sphalerite by adding different mass ratios of pyrite, chalcopyrite and galena in the presence of *Thiobacillus ferrooxidans*. The results of these shake flask experiments showed that as the mass ratio of sphalerite to chalcopyrite increased, i.e., more sphalerite was added to the chalcopyrite, the dissolution of zinc from the sphalerite decreased. This was explained by the fact that as more sphalerite than chalcopyrite was added to the system, the surface area of sphalerite particles increased. As the sphalerite underwent anodic dissolution in the system, it showed that the smaller anodic surface in contact with a larger cathode favoured higher anodic dissolution.

Interpretation of the results obtained by Mehta and Murr (1983) on the effect of galvanic interaction generated by the addition of different amounts of pyrite to constant amounts of chalcopyrite, supported this finding by Natarajan (1988) that the smaller the anode to cathode ratio, the higher the oxidation of the anode. Their results showed that as the amount of pyrite (cathode) added to the leaching system increased with respect to a fixed amount of chalcopyrite (anode), the rate of copper dissolution increased.

2.6.4 Applied Potentials in a System

Natarajan (1992b) studied the effect of applied potentials on zinc dissolution from a sphalerite concentrate mixed with other sulphide minerals. Electro-bioleaching tests at applied potentials in the range -600 mV to +600 mV (SCE) were conducted. A plot of *Dissolved Zinc* (mg.ℓ^{-1}) versus *Applied Potential* (mV, vs SCE), peaked at two characteristic points (approximately -450 mV to -500 mV and +400 mV) corresponding to current and to zinc dissolution maximum.

This, according to Natarajan (1992b) implied higher leaching rates for sphalerite at two specific applied potentials. These peaks corresponded to the cathodic and anodic sides of the polarisation diagram. In the presence of bacteria, an expected increase in

the dissolution of zinc was measured. In a binary mixture of pyrite and sphalerite, zinc dissolution was found to be at a maximum at -500 mV.

In the presence of chalcopyrite, zinc dissolution was decreased in comparison with leaching in the presence of pyrite. However, this was expected from the galvanic interaction influence of the minerals in contact. At -500 mV, the dissolution of pyrite and chalcopyrite was minimised while at positive potentials (+400 mV to +600 mV), there was random bulk dissolution of all three sulphides with no selectivity.

Probable mechanisms for the dissolution of a mixed sulphide mineral containing sphalerite, pyrite and chalcopyrite have been discussed under different conditions: (Natarajan, 1992c)

- a negative applied potential of -500 mV where dissolution of sphalerite was favoured

$$ZnS + 2H^{+} = Zn^{2+} + H_2S \qquad \text{at } -500 \text{ mV} \qquad [2\text{-}10]$$

- positive potentials

$$\begin{aligned} ZnS &= Zn^{2+} + S^{\circ} + 2e^{-} \\ FeS_2 &= Fe^{2+} + 2S^{\circ} + 2e^{-} \qquad \text{at 400 mV} \\ CuFeS_2 &= Cu^{2+} + Fe^{2+} + S^{\circ} + 4e^{-} \qquad \text{at 600 mV} \end{aligned} \qquad [2\text{-}11]$$

At an applied potential of -500 mV (SCE), the production of elemental sulphur would be eliminated (Equation 2-10). Any detrimental effect on the dissolution rate that may be caused by a sulphur layer forming would thus be removed.

2.7 Summary

The literature review showed that the kinetics of the dissolution of sphalerite has been studied extensively. The mechanism of the dissolution process has been found to vary yet the oxidation rate is dependent on the particle size (or surface area), temperature and ferric iron concentration. The kinetic models developed from these studies adequately describe the initial stages of leaching. However, for prolonged

leach periods, the models developed do not predict the data presented in the literature for the ferric sulphate leaching of a sphalerite concentrate. This highlights the need for this study to investigate the leaching reaction for prolonged leach periods.

Diffusion limitation due to the porous sulphur layer was a controversial opinion as no qualitative work has been done on this particular issue. The leaching kinetics were shown to be similar in ferric sulphate solutions and ferric chloride solutions but in a ferric sulphate medium, jarosite may form; however, this may not result in diffusion limitation. Diffusion limitations caused by these products jarosite and elemental sulphur) may develop if leaching was to be prolonged. The need to investigate the nature of the products formed and their influence on reaction kinetics arises from these sections of the literature review.

The literature showed that in a mixed mineral system, certain phenomena were observed. These were: selective dissolution of the least noble mineral in a mixed sulphate ore; a smaller anodic surface area in contact with a larger cathode surface area favours higher anodic dissolution; applied potentials increase selective dissolution of a mineral from a mixed sulphide system. This implies that when considering a mixed mineral system, the role of the other sulphide minerals and the effect that these may have on the dissolution process must be investigated.

3. MODEL DEVELOPMENT and comparison with published data on the ferric leaching of sphalerite.

The literature showed that the rate expressions already developed vary (athough these are all based on the basic shrinking-core model) and are specific to a certain sphalerite ore type. (See Appendix D for a summary of other researchers' work). The models presented in the literature were derived to describe the initial rate of the reaction where the chemical reaction at the mineral surface was limiting.

This chapter begins by examining with the use of the shrinking-particle model where the chemical reaction is first order with respect to ferric iron. This is then compared to the data presented in the literature. This model will be referred to as the FIRST-ORDER MODEL.

More recent research shows that the chemical reaction can be described as an electrochemical reaction dependent on the ferric iron and ferrous iron in solution. The next model, the ELECTROCHEMICAL MODEL, is a shrinking-particle model where the electrochemical reaction is dependent on the ferric/ferrous ratio instead of the ferric iron concentration (First-Order Model).

The previous two models, the First-Order Model and the Electrochemical Model, do not predict the data adequately. Some researchers show the kinetics of the electrochemical reaction to be half-order in ferric iron concentration. The following model accounts for diffusion limitations (shrinking-core model) and includes in the derivation the electrochemical reaction that is half-order with respect to ferric iron. It is referred to as the HALF-ORDER KINETICS MODEL.

The Half-Order Kinetics Model did not predict the data presented from the literature for the leaching of the Gamsberg sphalerite concentrate. The next step in the model development was to manipulate the diffusion coefficient, D_e, of the Half-Order Kinetics Model to decrease with time. This model was termed the D_e DECAY MODEL.

The model derived for the purpose of this study reverts to the assumption that the electrochemical reaction at the mineral surface is the rate limiting step. The difference between the ELECTROCHEMICAL MODEL and this model is that the mineral surface is assumed to be deactivated as a product layer forms. This deactivation process is assumed independent of the leaching reaction. This model is termed the SURFACE AREA DEACTIVATION MODEL and was derived for the purpose of this study to predict the leaching of sphalerite for prolonged leach periods. The data presented by Crundwell (1988b) on the ferric sulphate leaching of the Gamsberg sphalerite concentrate, is used as an initial examination of the Surface Area Deactivation Model. The results obtained are compared to the results presented in his work. These results are also compared to the data obtained from this experimental study.

Figure 3-1 shows the progression of the development of these models as Step A, Step B, Step C and Step D.

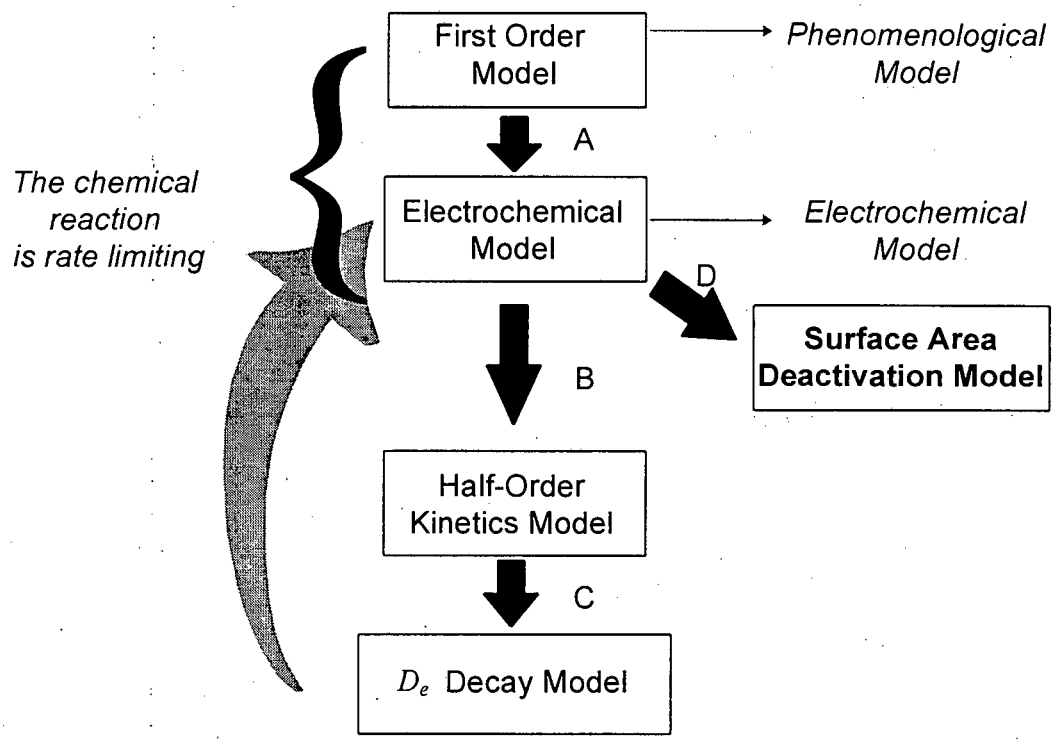

Figure 3-1 Schematic representation on the development of the mathematical expression used to describe the dissolution of sphalerite.

3.1 The First Order Model

This model assumes that the reaction at the mineral surface is first order with respect to ferric iron. It is this reaction that is the rate limiting step. The equation is the standard model presented in Levenspiel (1972). The progress of the reaction is unaffected by the presence of any product layer and the quantity of material reacting is proportional to the available surface of the unreacted core.

$$-\rho_B \frac{d\,d}{d\,t} = bk'\left[Fe^{3+}\right] \qquad [3\text{-}1]$$

This can be written in terms of fractional conversion noting that:

$$1-X = \left(\frac{d}{d_o}\right)^3 \qquad [3\text{-}2]$$

The final form of the equation written in terms of fractional conversion is:

$$\frac{d\,X}{d\,t} = k_1 (1-X)^{2/3}\left[Fe^{3+}\right] \qquad [3\text{-}3]$$

This model was fitted to the data of Jin *et al.* (1984) and Rath *et al.* (1988) to test its applicability for this study. Figure 3-2 shows that the First Order Model describes the initial reaction curve for the ferric chloride leach of the sphalerite.

The data presented in the literature for the dependence of the reaction on temperature, particle size and ferric iron concentration was modelled according to the First-Order Model. The kinetic constants that have been calculated are used to determine the activation energy for the reaction, the inverse relationship between the particle size and the reaction order, *a*. Table 3-1 gives the values obtained in the literature by the original authors and the values from the rate constant calculated by the First Order Model.

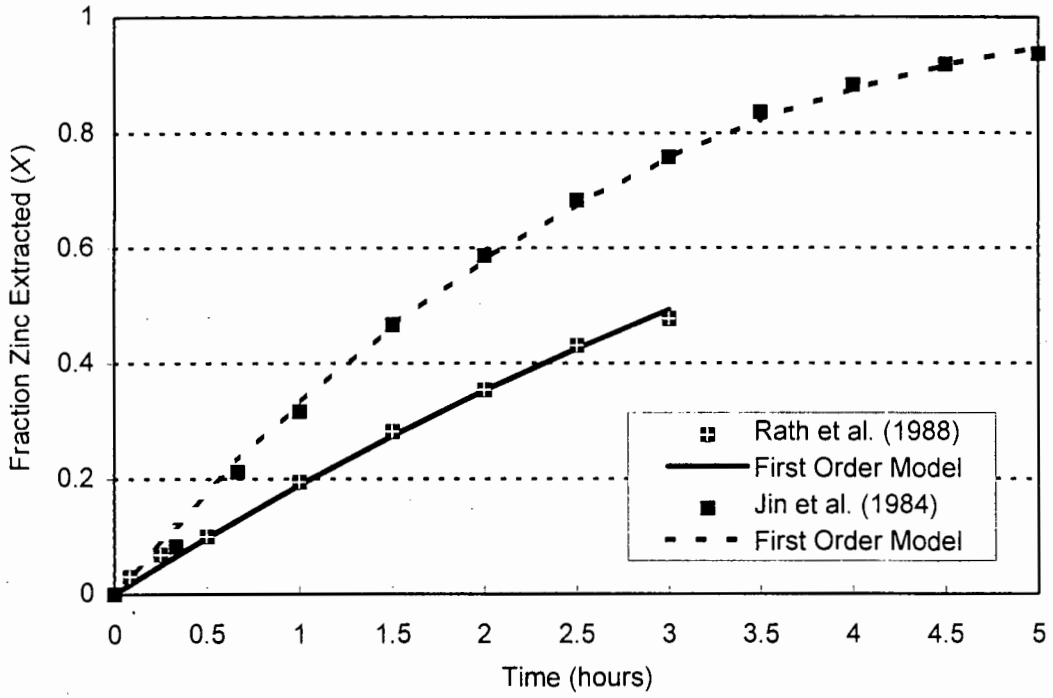

Figure 3-2 A plot of the data of Rath *et al.* (1988) and Jin *et al.* (1984) for the fraction of zinc extracted versus time. The conditions of these experiments are particle size = -105+53 μm, temperature = 50°C and $[FeCl_3]$ = 0.6 M and particle size = -63+53 μm, temperature = 65°C and $[Fe^{3+}]$ = 0.6 M respectively. The First-Order Model was fitted to the data.

AUTHOR	ACTIVATION ENERGY ($kJ.mol^{-1}$)		PARTICLE SIZE CONSTANT (μm^{-1})		REACTION ORDER		OVERALL REACTION RATE CONSTANT	
	Original	This Study	Original	This Study	Original	This Study	Original	This Study
Jin *et al.* (1984)	58.4	60.5	0.019	0.113	0.5	1	8.86×10^{3}	2.51×10^{5}
Rath *et al.* (1988)	58	58.3	0.037	0.003	0.62	1	72.64	369.08

Table 3-1 Comparison of the variables of the models derived by the original authors and those calculated from the First Order Model.

The value for the activation energy calculated by the First Order Model compared with that calculated by Jin *et al.* (1984) and Rath *et al.* (1988). However, the dependence of the reaction rate constant on the initial particle size differed significantly. The change in the dependence of the ferric iron concentration resulted from the forced change in the reaction order from either 0.62 or 0.50 to 1.00. The First-Order Model has been used to predict the leaching of sphalerite from a concentrate of the Gamsberg ore. Figure 3-3 shows the data presented by Crundwell (1988b) and the models derived from the kinetic rate constants determined from the First Order Model. The models are a better representation of the Gamsberg sphalerite concentrate. In particular, the model prediction based on the data of Jin *et al.* (1984) is an adequate representation of the initial stages of the reaction curve where the chemical reaction at the mineral surface is rate limiting.

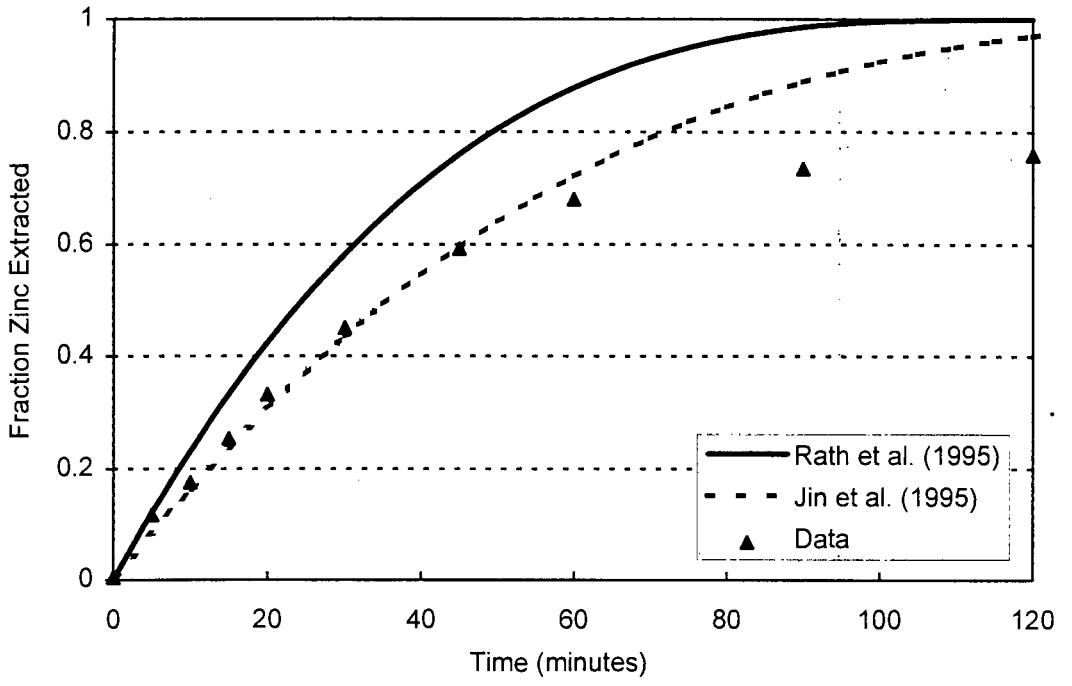

Figure 3-3 The First Order Model prediction derived from the data of Jin *et al.* (1984) and Rath *et al.* (1988). This has been compared with the data presented by Crundwell (1988b) under similar conditions.

For prolonged leach periods, both models predict complete dissolution of the sphalerite, whereas the data shows a lesser extent of sphalerite dissolution. It was assumed that this difference was because Jin *et al.* (1984) and Rath *et al.* (1988) used ferric chloride as a leach medium and Crundwell (1988b) used ferric sulphate. The implication of this is that jarosite or any other sulphate precipitates that may form in a ferric sulphate leach can not form in other media and thus cause the reaction to become diffusion limiting.

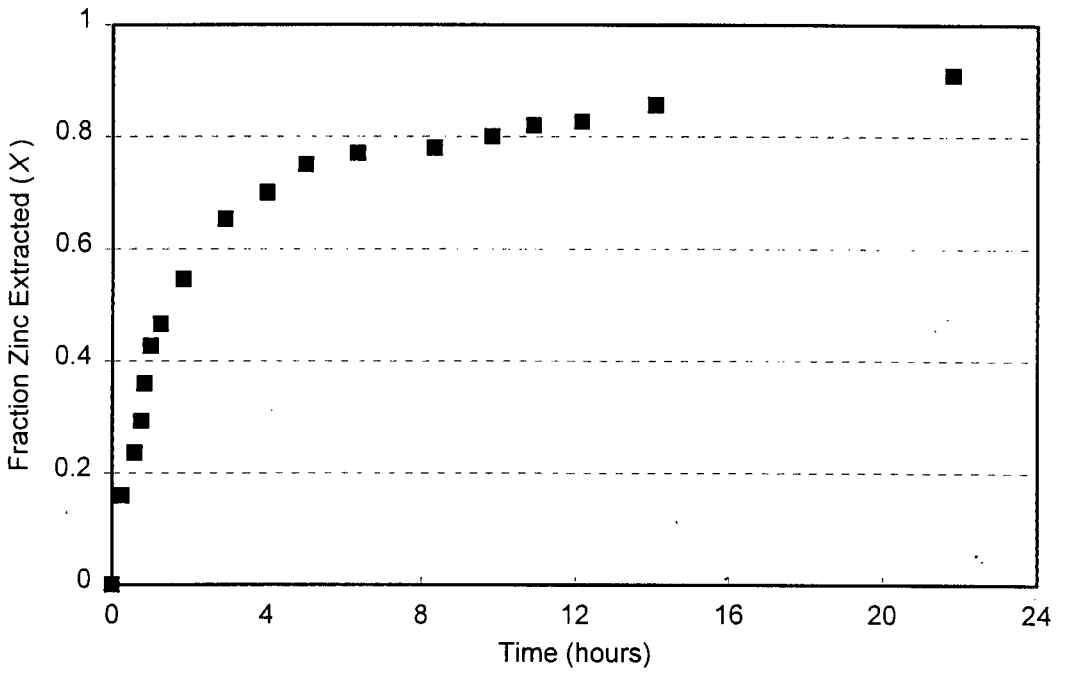

Figure 3-4 The dissolution data of Bobeck and Su (1985) showing that during prolonged leaching periods the reaction is possibly inhibited by the formation of sulphur.

However, Bobeck and Su (1985) leached sphalerite under similar conditions in a ferric chloride medium, but extended the leach period to twenty-four hours. From their data, they concluded that the dissolution process was controlled initially by the chemical reaction at the mineral surface but that this changed to become diffusion limiting as a sulphur layer formed on the mineral surface.

The data of Crundwell (1988b) for the leaching of the Gamsberg concentrate under the same conditions has been modelled according to the First-Order Model. The model shows an adequate fit of the data for the initial stages of leaching. As expected, during extended periods of leaching the model deviated from the data as it did not account for the possible inhibitory effect caused by the formation of sulphur and iron sulphate precipitates. It was on this basis that the First-Order Model was rejected for the purpose of this study.

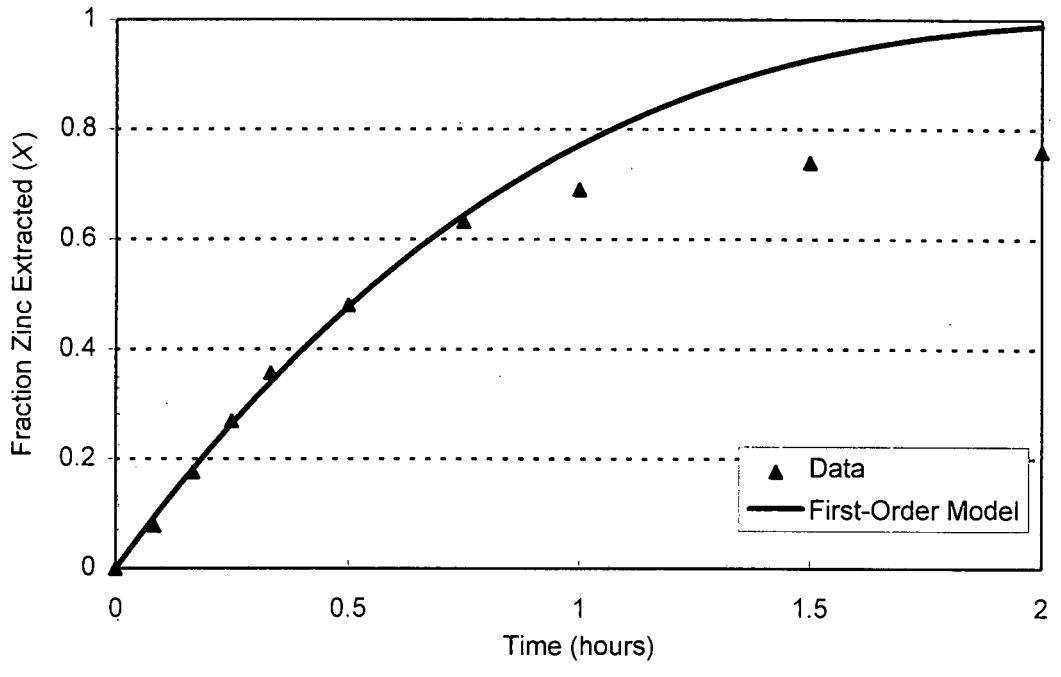

Figure 3-5 The data presented by Crundwell (1988b) with a First Order Model fit.

3.2 The Electrochemical Model

Verbaan and Crundwell (1986) showed that the reaction was dependent on the solution redox potential or the ratio of ferric iron to ferrous iron. The Electrochemical Model assumes that the chemical reaction mechanism at the mineral surface is described by an electrochemical mechanism dependent on the square root of the ferric iron to ferrous iron ratio.

The derivation of this model is presented in Appendix E. The final form of the equation is:

$$\frac{dX}{dt} = k_1 (1-X)^{2/3} \left(\frac{[Fe^{3+}]}{[Fe^{2+}]} \right)^{1/2} \qquad [3\text{-}4]$$

Figure 3-6 shows the comparison of the Electrochemical Model and the data (Crundwell, 1988b). The initial stages of leaching are well described, but the model predicts that the sphalerite reaches complete dissolution.

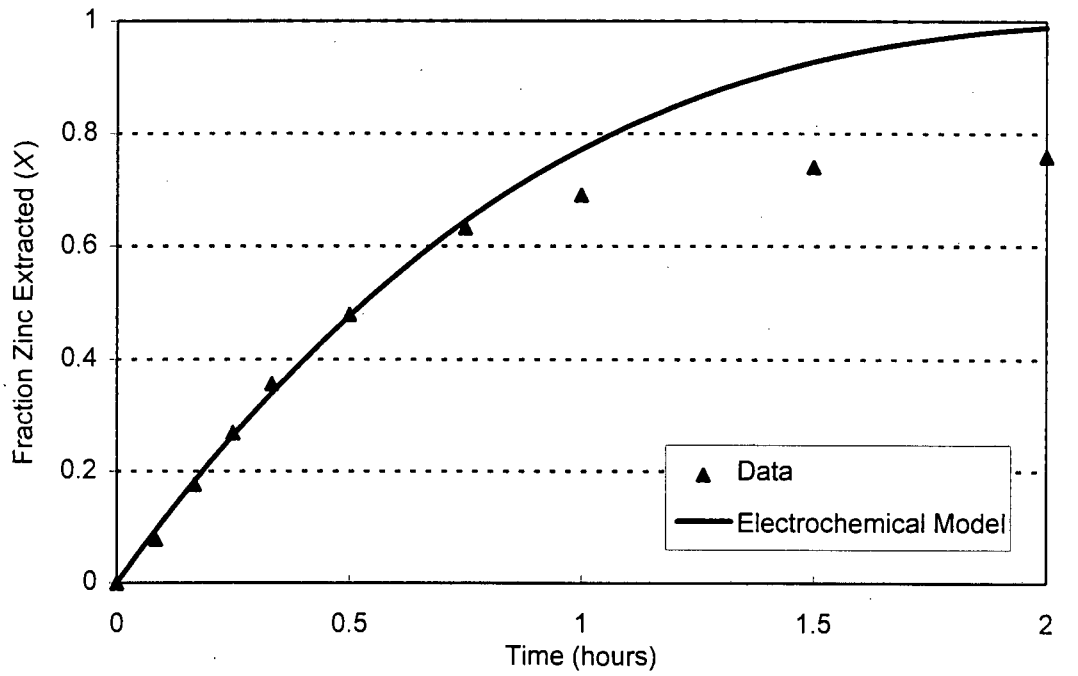

Figure 3-6 The data presented by Crundwell (1988b) with the Electrochemical Model prediction.

The Electrochemical Model predicts that the chemical reaction will be rate limiting during the initial stages of dissolution. This model does not account for any product layer forming or any precipitate that may inhibit the chemical reaction. For prolonged leach periods, this model is not an adequate prediction of the data (Crundwell; 1988b). For this reason, this model has been disregarded for the purpose of this study.

The failure of the First-Order Model and the Electrochemical Model to fit the data for the ferric sulphate leaching of the Gamsberg sphalerite concentrate was, due to the fact that both models predict complete dissolution of the mineral over prolonged leach periods. The data showed that the rate of dissolution of the sphalerite does change.

3.3 The Half-Order Kinetics Model

The Half-Order Kinetics Model is an attempt to model all the data for prolonged leach periods by assuming that the reaction is controlled by the chemical reaction at the mineral surface and by the product layer diffusion. The Half-Order Kinetics Model also assumes that the reaction kinetics are half-order in ferric iron and ferrous iron concentrations. Appendix E shows the full derivation of this model.

$$\frac{dX}{dt} = \frac{k_1}{[Fe^{2+}]^{1/2}} (1-X)^{2/3} [Fe^{3+}]_c^{1/2} \qquad [3\text{-}5]$$

where

$$[Fe^{3+}]_c^{1/2} = -k_2(1-X)^{1/3}\left[1-(1-X)^{1/3}\right] + \sqrt{\left\{k_2(1-X)^{1/3}\left[1-(1-X)^{1/3}\right]\right\}^2 + [Fe^{3+}]} \qquad [3\text{-}6]$$

Figure 3-7 shows the Half-Order Kinetics Model prediction with the data presented by Crundwell (1988b). This model does not describe the initial stages of the reaction curve as accurately as the previous two models. The model does predict that the overall conversion of the sphalerite to be less than previously shown by the First-Order Model and the Electrochemical Model. However, the overall model prediction is not an adequate description of the data and on this basis it was not used for the purpose of this study.

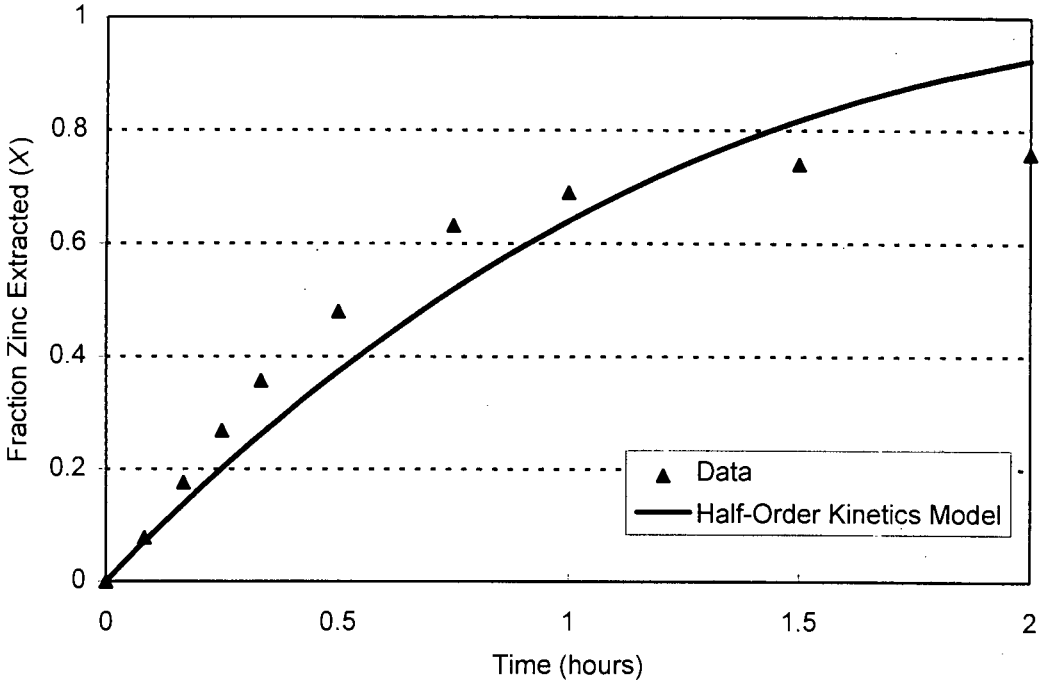

Figure 3-7 The Half-Order Kinetics Model fitted to the data presented by Crundwell (1988b).

3.4 The Diffusion Coefficient (D_e) Decay Model

During leaching, it was observed that a sulphur layer does form (Jin *et al.*, 1984; Bobeck and Su, 1985; Rath *et al.*, 1988; Lochmann and Pedlik, 1995). It was assumed that diffusion limitations of the reactants to the mineral surface caused by this layer are negligible (Jin *et al.*, 1984; Rath *et al.*, 1988). However, Morin *et al.* (1985) proposed that the kinetics of the leaching of galena (PbS) were controlled by the aqueous diffusion of ferric iron in the pores of the sulphur layer and the chemical reaction at the surface. It was shown that if this diffusion limitation was accounted for in the kinetic model, an improved representation of the end of reaction curve is obtained.

The Diffusion Coefficient (D_e) Decay Model is based on that presented by Morin *et al.* (1985) where the chemical reaction and product layer are assumed to be the rate controlling steps with the diffusion coefficient decreasing with time. The difference between the work presented by Morin *et al.* (1985) and this model is that it is assumed

that in this model, the reaction is dependent on the half-order reaction of ferric iron in solution. (The term "decay" has been used in naming this model as the theory in manipulating this model originates from that of catalyst "decay").

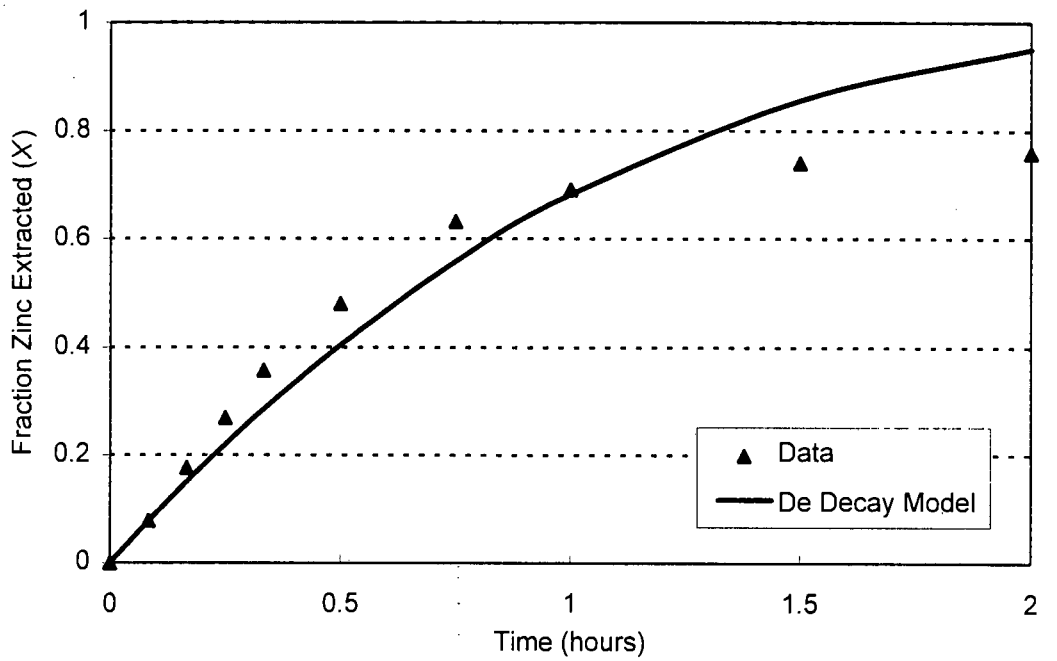

Figure 3-8 The Diffusion Coefficient Decay Model fitted to the data presented by Crundwell (1988b).

The final equation is similar to the Half-Order Kinetics Model. Appendix E shows the full derivation of this model.

$$\frac{dX}{dt} = \frac{k_1}{[Fe^{2+}]^{1/2}} (1-X)^{2/3} [Fe^{3+}]_c^{1/2} \qquad [3\text{-}7]$$

but now

$$[Fe^{3+}]_c^{1/2} = -k_{22}(1-X)^{1/3}\left[1-(1-X)^{1/3}\right] + \sqrt{\left\{k_{22}(1-X)^{1/3}\left[1-(1-X)^{1/3}\right]\right\}^2 + [Fe^{3+}]} \qquad [3\text{-}8]$$

where

$$k_{22} = k_2 \exp(k_D t) \qquad [3\text{-}9]$$

Figure 3-8 shows the Diffusion Coefficient Decay Model prediction and the data presented by Crundwell (1988b). The overall model prediction is similar to the model prediction of the Half-Order Kinetics Model. As the model does not predict the data, it is considered an inadequate description of the reaction curve for the data presented by Crundwell (1988b).

3.5 Summary

The four models examined do not adequately describe the data presented. The first two models, the First-Order Model and the Electrochemical Model, are shrinking-particle models where diffusion limitations through a product layer are not accounted for. The difference between these two models is the dependence of the ferric iron concentration. The First-Order Model assumed that the reaction is first order dependent on the ferric iron. The Electrochemical Model is half-order dependent on the ratio of ferric iron and ferrous iron.

The following two models, the Half-Order Kinetics Model and the Diffusion Coefficient Decay Model, are shrinking-core models. This means that any diffusion limitations caused by a product layer forming are accounted for. The difference between the Diffusion Coefficient Decay Model and the Half-Order Kinetics Model is that the diffusion coefficient is manipulated to decrease with time.

Figure 3-9 shows the difference between the four models under the same conditions. The First-Order Model and the Electrochemical Model predict complete conversion of the zinc from the sphalerite. The Half-Order Kinetics Model does not predict complete conversion but does not account for the passivation that does occur according to the data. Even though the Diffusion Coefficient Decay Model shows a more accurate fit

to the data because the diffusion coefficient is manipulated to decrease with time, the prediction is not a suitable fit.

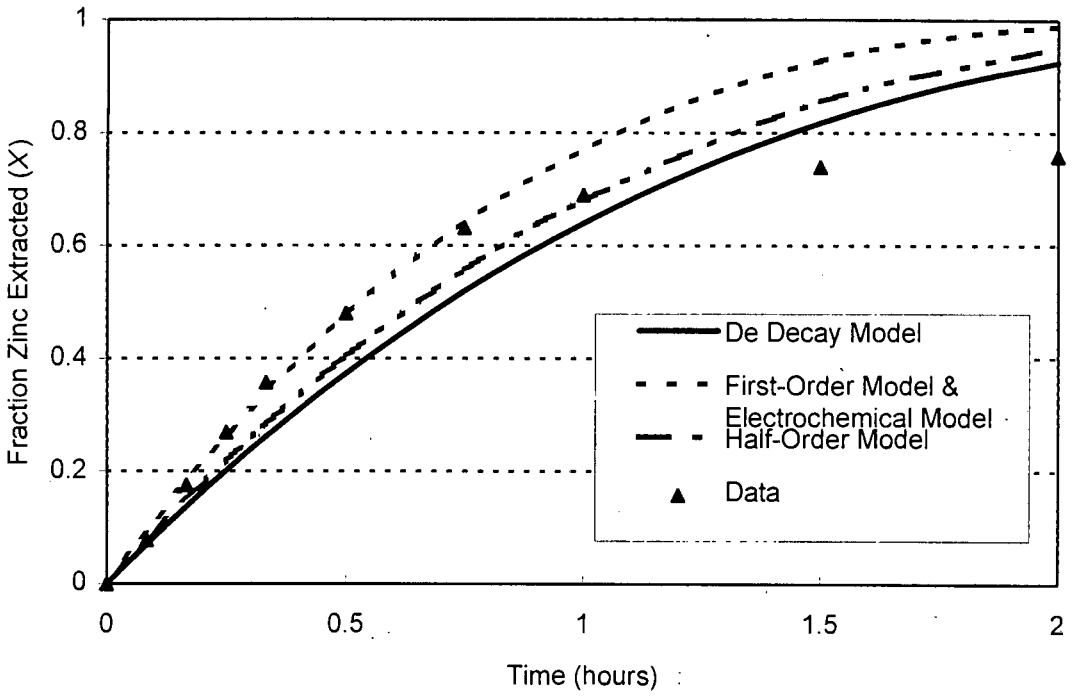

Figure 3-9 A plot of the data presented (Crundwell, 1988b) and the model prediction of the first four models presented.

The First-Order Model and the Electrochemical Model adequately describe the data during the initial stages of leaching. The Half-Order Kinetics Model and the Diffusion Coefficient Decay Model do not describe the data during the initial stages of the reaction but do appear to be a better fit of the data during prolonged leach periods.

3.6 The Surface Area Deactivation Model

The Surface Area Deactivation Model assumes the following:

- the surface of the mineral is deactivated with time during the leaching process
- this deactivation process is independent of the leaching reaction
- the dependence of the reaction on the ferric iron concentration and the ferrous iron concentration is to be determined and is not included in the derivation

- the available area is shrinking and is diminished by (1 - f) (where f is the fraction of diffusion area that is blocked)
- the rate of change of diameter is small compared to the rate of change of fraction of diffusion area that is blocked, f.

$$-\rho_B \frac{d\,d}{d\,t} = bk'' \qquad [3\text{-}10]$$

To account for diffusion limitations let

A = diffusion area at time t
f = fraction of area blocked at time t

The particle surface area increases due to dissolution (Growth in Area term). Simultaneously, the particle surface area is deactivated because of product formation (Shrinkage in Area term). The net area available for leaching is thus the difference of these two terms:

Accumulated Area = Growth in Area - Shrinkage in Area

where
Accumulated Area = $f A /_{t+\Delta t} - f A /_t$
Growth in Area = $k_l (1\text{-}f) A \Delta t$
Shrinkage in Area = $k_{-l} (1\text{-}f) A \Delta t$
= 0 as the reaction of dissolution is irreversible

Thus

$$\frac{d\,f\,A}{d\,t} = k_l (1 - f) A \qquad [3\text{-}11]$$

The available area is shrinking and is diminished by (1 - f) so Equation 3-10 becomes:

$$-\rho_B \frac{d\,d}{d\,t} = bk''(1 - f) \qquad [3\text{-}12]$$

Expressing particle diameter in terms of fraction conversion

$$1-X = \left(\frac{d}{d_o}\right)^3 \qquad [3\text{-}13]$$

Using the Product Rule, Equation 3-11 becomes

$$A\frac{df}{dt} + f\frac{dA}{dt} = k_1(1-f)A \qquad [3\text{-}14]$$

It was assumed that the rate of change of diameter is small compared to the rate of change of f (fraction of diffusion area that is blocked) therefore

$$f\frac{dA}{dt} = 0 \qquad [3\text{-}15]$$

and Equation 3-14 becomes

$$\frac{df}{dt} = k_1(1-f) \qquad [3\text{-}16]$$

Integrating Equation 3-16 gives

$$f = 1 - \exp\{-k_1\} \qquad [3\text{-}17]$$

Substituting this into Equation 3-12 gives

$$-\rho_B\frac{dd}{dt} = bk''\left(\exp\{-k_1 t\}\right) \qquad [3\text{-}18]$$

In terms of fractional conversion, combining Equation 3-13 and Equation 3-18 gives:

$$-\rho_B\left(\frac{d\, d_o\,(1-X)^{1/3}}{dt}\right) = bk''\left(\exp\{-k_1 t\}\right)$$

$$(1-X)^{-2/3}\frac{d_o\,\rho_B}{3bk''}\frac{dX}{dt} = \left(\exp\{-k_1 t\}\right) \qquad [3\text{-}19]$$

$$\frac{dX}{dt} = (1-X)^{2/3}\frac{3\,b\,k''}{d_o\,\rho_B}\left(\exp\{-k_1 t\}\right)$$

The final form of the equation is

$$\frac{dX}{dt} = k_{CR}\,(1-X)^{2/3}\exp\{-k_1 t\} \qquad [3\text{-}20]$$

The model has been used to fit the data by Bobeck and Su (1985) presented in Figure 3-3. The Surface Area Deactivation Model describes the data for a ferric chloride leach where the reaction becomes inhibited and the rate of conversion of sphalerite decreases (Figure 3-9). This model describes the initial stages of the reaction curve as well as the curve observed during prolonged leach periods.

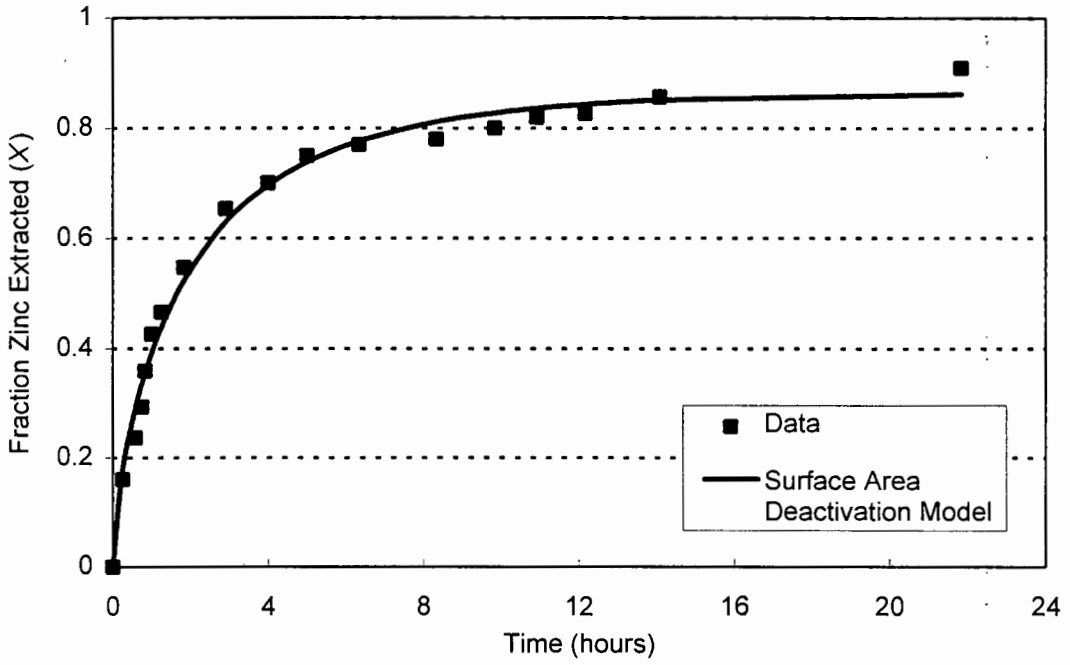

Figure 3-10 The Surface Area Deactivation Model fitted to the data presented by Bobeck and Su (1985).

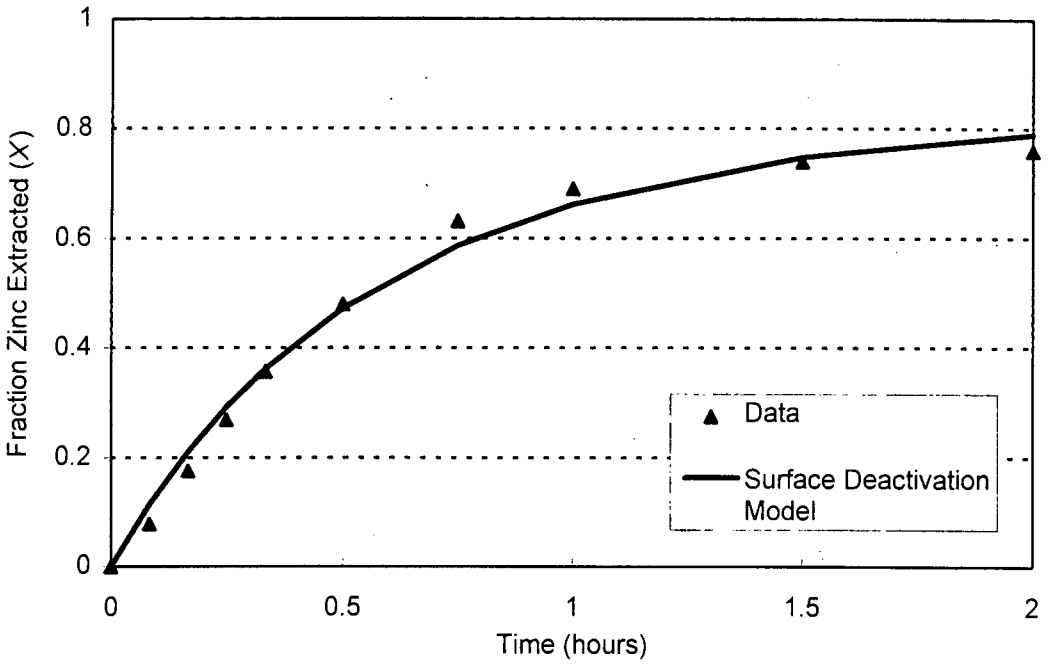

Figure 3-11 A plot of the data presented by Crundwell (1988b) with the Surface Area Deactivation Model.

The Surface Area Deactivation Model was also applied to the data presented by Crundwell (1988b) on the leaching of the Gamsberg sphalerite concentrate using a ferric sulphate medium. Figure 3-10 shows the leaching data presented in the literature and the Surface Area Deactivation Model fit for a chemical leach in a ferric sulphate medium.

Figure 3-11 shows that the initial stages of the leaching data are well described by the Surface Area Deactivation Model. This was expected as the chemical reaction rate constant, k_{CR}, was a generalised rate constant still to be evaluated in terms of temperature, initial particle size and ferric iron or ferrous iron concentration. By including the surface area deactivation term, the later stages of the leaching data were well defined by the Surface Area Deactivation Model.

This model is an adequate description of the data for a ferric sulphate leach of the Gamsberg ore. This model was further investigated in this study by reformulating

the data presented by Crundwell (1988b). These reformulated data will be compared with the experimental results of this study.

3.6.1 Investigation of the Surface Area Deactivation Model using the Data presented by Crundwell (1988b)

The activation energy of the reaction has been calculated as 37.7 $kJ.mol^{-1}$, from an Arrhenius plot of the chemical reaction rate constant, k_{CR}. This is lower than that calculated by Crundwell (1988b) who calculated an activation energy of 46 $kJ.mol^{-1}$.

The difference between the two values calculated for the activation energy of the same ore is due to the difference in the calculation of the reaction rate constant from which the activation energy was calculated. The chemical reaction rate constant for the Surface Area Deactivation Model differs from the chemical reaction rate constant for the shrinking-particle model presented by Crundwell (1988b) as a result of the assumptions made in the derivation of the Surface Area Deactivation Model.

The dependence of the reaction on the ferric iron concentration and the ferrous iron concentration is included in the reaction rate constant k_{CR} for the Surface Area Deactivation Model. The chemical reaction rate constant must be investigated in terms of the relationship of the ferric iron and ferrous iron present. The First-Order Model and the Electrochemical Model accurately described the initial stages of the leach data. Because of this, the validity of the dependence of the chemical reaction on the ferric iron concentration and ferrous iron concentration according to the First-Order Model and the Electrochemical Model are investigated.

The chemical reaction rate constant, k_{CR}, was investigated by plotting k_{CR} versus the iron species in solution. Figure 3-11 is a plot of the chemical reaction rate constant versus the ferric iron concentration i.e. first-order dependence. This plot shows no linear dependence of the chemical reaction rate constant on the ferric iron concentration. This shows that the First-Order Model is an inaccurate description of the kinetics of the reaction and justifies its exclusion from this study.

Figure 3-12 is a logarithmic plot of the chemical reaction rate constant versus the square root of the ratio of the ferric iron concentration and the ferrous iron concentration. This plot shows that a linear regression of the data yields a slope of 0.206 instead of the expected 0.5. This inconsistency demonstrates that the Electrochemical Model in terms of the dependence of the chemical reaction on the ferric iron and ferrous iron is inadequate. This is supported by the findings of Crundwell (1988b) who showed that this type of model is an inadequate description of the kinetics of the chemical reaction.

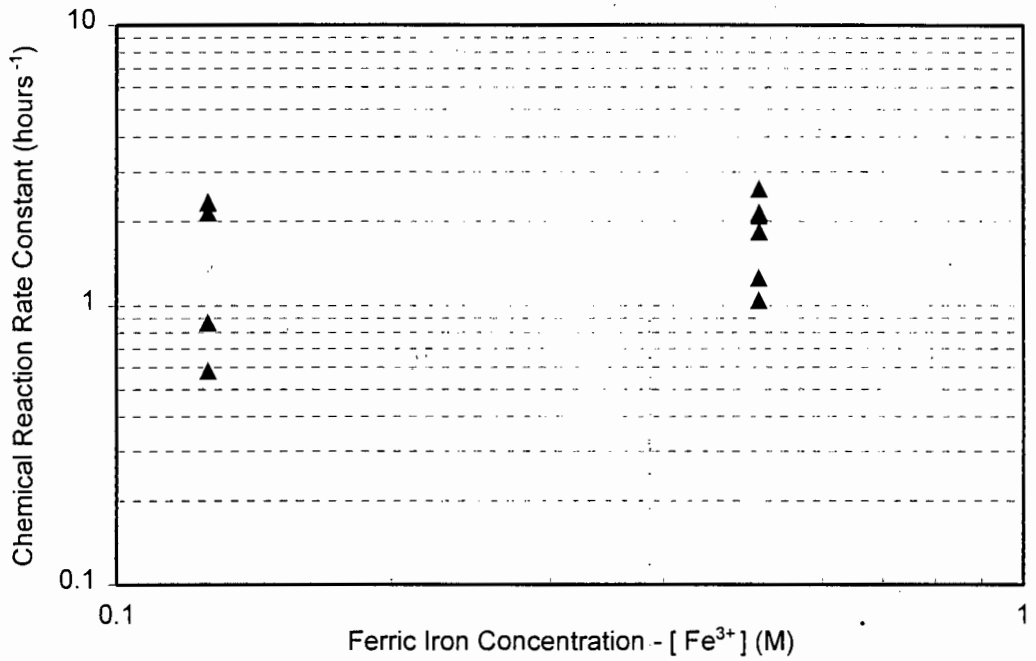

Figure 3-12 A plot of the chemical reaction rate constant versus the ferric iron concentration.

Crundwell (1988b) proposed that the chemical reaction was dependent on the charge transfer of electro-active ions across the Helmholtz layer. Figure 3-13 shows the relationship between the reaction rate constant, k_{CR}, and the sum of the electro-active, outer-sphere equilibrium species (Fe^{3+}_{AQ} and $FeHSO_4^{2+}$). The slope of the best fit of this plot is 0.547. This result is comparable with the value of 0.545 calculated by Crundwell (1988b) for the same data but using the reaction rate constant as defined by the model he presented. The significance of the slope being

equal to one-half is that if the Fe^{3+}/Fe^{2+} couple is not reversible at the mineral surface, then the reaction order with respect to the electro-active species should be approximately equal to 0.5 Crundwell (1988b). This implies that the chemical reaction is dependent on the equilibrium species as the reaction order is one-half with respect to the electro-active species corresponding to irreversible Fe^{3+}/Fe^{2+} couple at the mineral surface

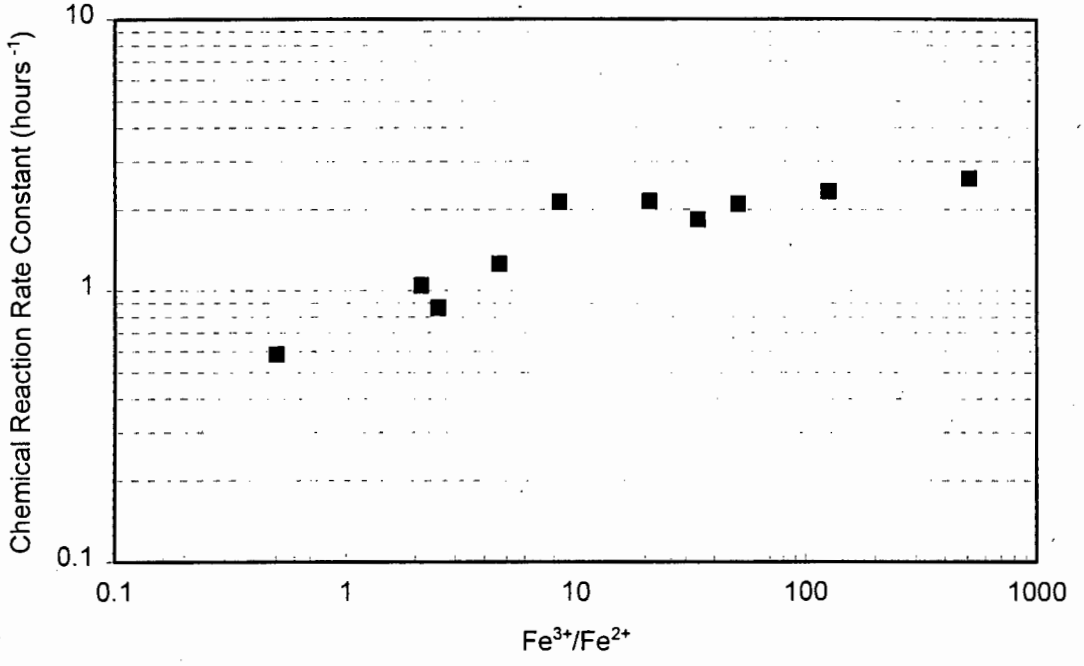

Figure 3-13 The relationship between the reaction rate constant and the ferric/ferrous iron ratio.

The Surface Area Deactivation Model is an adequate fit of the data presented by Crundwell (1988b) for the ferric sulphate leaching of the Gamsberg sphalerite concentrate. The reaction kinetics are shown to be independent of the ferric iron concentration and justifies the exclusion of the First-Order Model. The chemical reaction rate constant is shown to be linearly dependent on the ferric/ferrous iron ratio. However, the expected dependence on the slope of the linear regression is not one-half. Because of this, the reaction is not dependent on the ferric/ferrous couple. This shows that the assumption, that the reaction kinetics being dependent on the ferric/ferrous couple, of the Electrochemical Model is incorrect and justifies the exclusion of this model from the study.

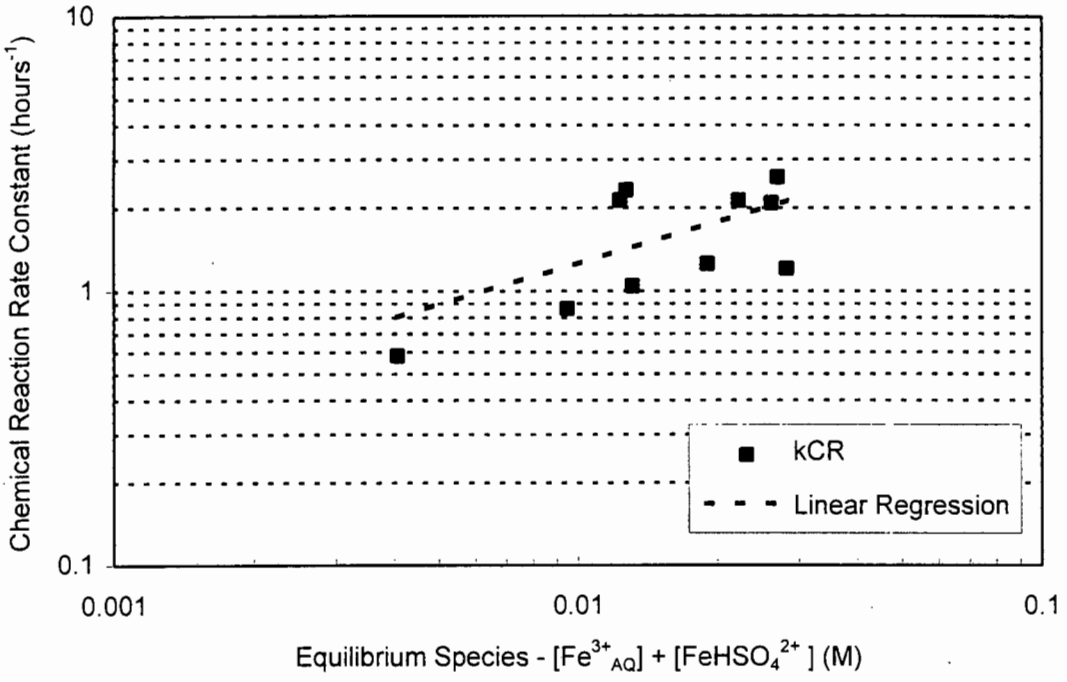

Figure 3-14 The relationship between the reaction rate constant and the electro-active species.

The results obtained in this section for the data presented by Crundwell (1988b) support the assumptions he made in the development of his model to describe the kinetics of the chemical reaction at the mineral surface. These results will be used as a comparison for the experimental work of this data to confirm the validity of these assumptions

4. MATERIALS AND METHODS

4.1 Introduction

This chapter describes the experimental materials used and procedures followed in performing the experimental work of this study. Many of the procedures were adopted from the literature. Such instances have, where necessary, been noted and included in this section.

The material used is described and the procedure for the preparation of the ore is detailed. The characterisation of the different types of materials used is shown. The details of the chemical analysis of the ore types are given.

The batch reactors and other experimental apparatus are described. This is followed by the experimental procedure and the standard conditions for experimentation. The methods of mineralogical investigation are given.

4.2 Preparation and Characterisation of the Ore

The ore samples were obtained from the Gamsberg ore deposit (Aggenuys, North Cape Province, South Africa) which is a mixed sulphide primarily made of sphalerite, pyrite and pyrrhotite.

- Sphalerite, pyrite and pyrrhotite concentrates, were supplied by Gold Fields Research Laboratories, Southdale, Johannesburg. These samples were milled and wet-screened to a size fraction of -75+53 μm. Samples of the sphalerite concentrate, of size fractions -106+90 μm, -53+45 μm and -45+38 μm, were also supplied.
- A number of samples, in which the sphalerite was finely disseminated throughout the rock, were hand-picked from the deposit. These samples were crushed, milled and screened to a size fraction of -75+53 μm.
- Bore core samples taken during preliminary geological exploration work, were crushed, milled and screened to the appropriate size fractions and included in this study. These bore core samples were from the *Pyrrhotite Ore Zone.*

A proportion of the sphalerite concentrate supplied by Gold Fields Research Laboratories, Southdale, Johannesburg, was further separated by means of magnetic separation into samples of varying iron and manganese concentrations (concentration of these elements was determined by separation current).

All of the ore samples were washed with sodium sulphide (Na_2S) to clean and sulphidise the mineral surface according to the reaction: (Somasundaran and Moudgil, 1988).

$$MO + NaS^- \rightarrow MS + NaO^- \qquad [4\text{-}1]$$

This method was shown to enhance the initial leaching rate by converting all metal oxides to sulphides (Equation 4-1). (Jin *et al.*, 1984; Crundwell, 1987; Suni *et al.*, 1989).

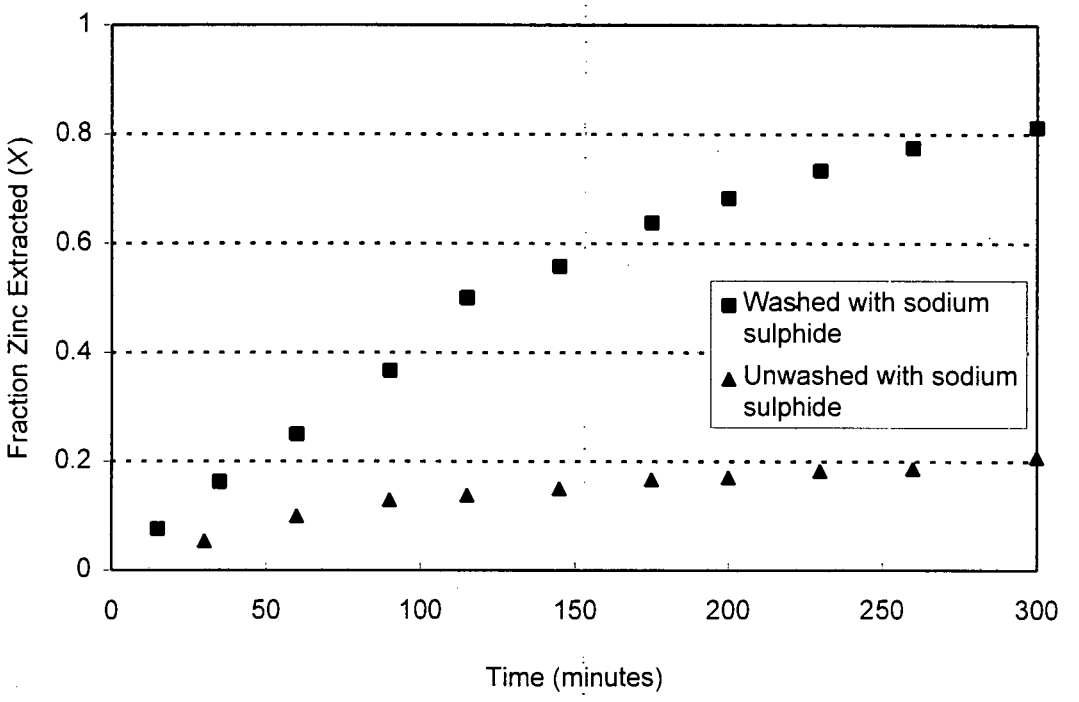

Figure 4-1 Leaching results of Jin *et al.* (1984) showing the effect of washing the concentrate with Na_2S solution.

The ore sample for each experiment was added to a 0.5 M solution of Na_2S and agitated on a magnetic stirrer (Gallenkamp). This was allowed to settle for one minute and then decanted. The washed ore was rinsed with excess de-ionised

water while being filtered. The ore was then allowed to dry before being used for experimentation. A Malvern Particle Size Analyser (Malvern Instruments, Malvern, England) was used to determine the distribution of particle size within a size fraction of each sample.

Each of the ore samples was assayed for Zn, Fe_{TOTAL}, S_{TOTAL} and Mn. Table 4-1 shows the chemical assay for the different ore types used in the experimental work.

ORE SAMPLE	CONCENTRATION (%)				
	ZINC	IRON	SULPHUR	MANGANESE	LEAD
A	52.75	8.09	33.80	1.40	0.16
B	52.22	7.93	32.47	1.27	0.22
C	53.26	7.84	32.50	1.19	0.24
D	51.92	7.27	33.75	1.10	0.26
E	27.98	8.21	23.55	0.93	1.20
F	11.75	12.59	31.95	0.52	0.18
G	9.06	15.69	29.40	0.33	1.48
H	7.13	22.65	43.90	0.27	0.18

A ZnS Concentrate: -106+90 μm
B ZnS Concentrate: -75+53 μm
C ZnS Concentrate: -53+45 μm
D ZnS Concentrate: -45+38 μm
E ZnS from Pyrrhotite Zone (Zn finely disseminated): -75+53 μm
F Bore Core Sample from Pyrrhotite Zone: -75+53 μm
G Gamsberg Concentrate (Ore Zone unknown): -75+53 μm
H FeS_2 Concentrate: -53+45 μm

Table 4-1 Chemical compositions of the sphalerite ore samples.

The metallic elements, Zn, Fe_{TOTAL}, Pb and Mn, were determined by digesting the ore in acid (see Appendix C) and then using atomic adsorption spectrophotometery on the resulting solution (Varian Spectra AA30 Spectrophotometer). The sulphur content of the sulphide materials used in this study was determined in a LECO Sulphur Determinator, SC32 DB64. The furnace temperature was 1350 °C.

The relative amounts of the different sulphide minerals, ZnS, $Fe_{1-x}S$ and FeS_2, were determined by X-ray diffraction at a scan speed of 1 s/0.05° (Siemens Cristalloflex D500 X-ray Diffractometer). Specific surface area of the different size fractions was measured using the N_2 BET method.

4.3 Experimental Apparatus

Batch reactors were used in this research. The reactors used were two litre culture glass vessels (Quickfit FV2ℓ) fitted with four stainless steel baffles (Figure 4-2). A variable speed overhead motor (Heidolph RZR 50) fitted with an impeller having a pitched-blade turbine was used (Figure 4-3). The reactor baffling and impeller were designed to optimise suspension of solid particles in a flat-bottomed reactor and conform to typical turbine agitation proportions (Nagata; 1975).

The stirred batch reactors were placed in a waterbath in order to maintain the temperature at the required level. Temperature of the waterbath was maintained by a Labotec (South Africa) heater stirrer. To eliminate any evaporation of the leach liquor, the system was fitted with a condenser (Liebig Condenser C1/13).

The redox potential and pH were measured using a combined pH/redox probe (ASI pH/ORP (3-in-1) Model No. RH101431) and controlled for the duration of the experiment. The reference electrode was a silver/silver chloride electrode. Redox potential and pH meters and controllers were designed by the Chemical Engineering Department (UCT) and supplied by Hitech Micro Systems (Cape Town, South Africa). Redox potential was controlled by the addition of 30 $g.\ell^{-1}$ hydrogen peroxide (H_2O_2) to the system. Where necessary, the pH was controlled by addition of a 500 $g.\ell^{-1}$ solution of sulphuric acid (H_2SO_4).

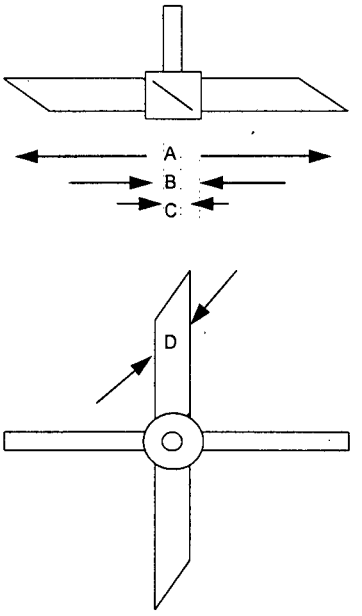

DIMENSIONS: A: 70 mm; B: 13 mm; C: 6 mm; D: 27 mm; Pitch Angle = 45°

Figure 4-2 Pitched-blade turbine.

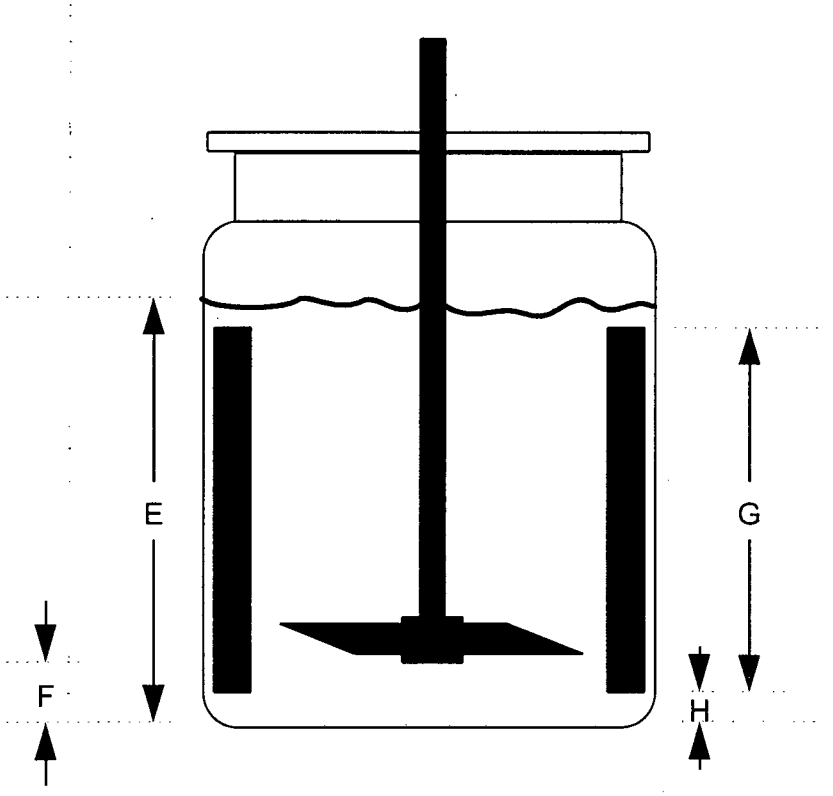

DIMENSIONS: E: 150 mm; F: 25 mm; G: 140 mm; H: 5 mm

Figure 4-3 Schematic diagram of the batch reactor.

4.4 Experimental Procedure

Table 4-2 shows the standard conditions of each experiment:

$[Fe^{3+}]$	0.5 M
pH	< 1.6
Solids density	20 $g.\ell^{-1}$
Temperature	40 °C
Size fraction	-75+53 μm
Redox Potential	585 mV (vs Ag/AgCl)
Impeller speed	800 rpm

Table 0-1 Standard conditions of each experiment.

The ferric iron concentration was set at 0.5 M in order to ensure that the amount of ferric iron for the dissolution reaction would not be limiting. (Crundwell; 1988b). The pH was set at a value less than 1.6 so as to eliminate the possibility of jarosite formation (Bailey; 1993). The temperature was 40°C as this is the optimal temperature at which thiobacilli exist (Brierley, 1978). The redox potential was maintained at a value of 585 mV (vs Ag/AgCl) to ensure that there is no change in the specific rate of reaction due to a change in solution redox potential. This value was chosen as the work of Natarajan (1992b) showed that there was no selective leaching in a mixed sulphide ore in the range 400 mV (vs SCE) to 600 mV (vs SCE). The impeller speed was set at 800 rpm to minimise mass transfer limitations.

The leaching solution consisted of an aqueous solution of 0.1 M solution of sulphuric acid (9.8 $g.\ell^{-1}$ H_2SO_4) and 0.25 M ferric sulphate ($Fe_2(SO_4)_3.xH_2O$) or (27.924 $g.\ell^{-1}$ Fe^{3+}). Analytical grade reagents and de-ionised water were used for these leaching solutions.

Once initial conditions of the leach solution were stabilised, 30 g of prepared concentrate was added to 1.5 litres of the solution to give a solid-to-liquid ratio of two percent. Samples were drawn at 30 minutes and after the first hour of the batch test, and then every hour thereafter until three hours had passed since the start of the experiment. Samples were drawn at three to four hourly intervals until a total leach period of thirty-two hours had passed. During experiments where the temperature of the leach liquor was maintained at a higher level than the 40 °C

maintained under standard conditions, samples were drawn more frequently and the total leach period was reduced.

The redox potential and pH were recorded at the time each sample was taken. The amount of hydrogen peroxide added by the controlling apparatus was also determined at this point. The volume of hydrogen peroxide added to the system was determined as follows: the initial mass of the hydrogen peroxide to be added by the controlling apparatus was recorded prior to the start of the experiment using a *laboratory* balance (Denver Instruments Model No. XL- 3100); thereafter the mass of the hydrogen peroxide remaining was recorded at each sample. From these mass measurements it was possible to determine the volume of hydrogen peroxide added.

Each sample volume was measured and filtered using a *Millipore*® filter (Sterifil Aseptic System with sterile, individually sealed, 0.45 μm filter paper). This was then analysed for Zn, Fe_{TOTAL}, and Mn using atomic adsorption spectrophotometery. Solid residues were investigated under a scanning electron microscope.

4.5 Mineralogical Investigation of the Sphalerite Samples

Fresh samples of the concentrate were cleaned and examined using an ISI ABT 130DS scanning electron microscope (SEM). The SEM uses energy dispersive X-ray (EDX) and back-scatter electron detectors. The samples were prepared by mounting them on a microscope stub, and carbon coating them to a thickness of approximately 25 nm. In addition to this, photographs were taken of samples of the ore during leaching. All images are back-scattered electron images.

5. RESULTS AND DISCUSSION

The factors influencing the kinetics of the reaction were investigated using the Gamsberg ore, in particular, a sphalerite concentrate. The Surface Area De-activation Model that was developed for the purpose of this study (Chapter 3) was fitted to the data obtained. The kinetic rate constant was evaluated in terms of the activation energy of the reaction, the influence of the size of the leaching particle and the dependence of the reaction on the Fe^{3+}/Fe^{2+} iron ratio and the ferric iron concentration in the solution. The role of the solids concentration was determined under conditions where the redox potential was not controlled.

The Gamsberg ore body contains several sulphide minerals of which sphalerite is the most prevalent. Pyrite and pyrrhotite occur in minor amounts in the ore body. The effect of the addition of a pyrite concentrate in trace amounts to the sphalerite concentrate was investigated at controlled redox potentials to determine whether it had any effect on the leaching rate of the sphalerite. Samples, hand-picked from the ore body for their mineralogical characteristics, were investigated to determine whether or not the galvanic interactions between pyrite and sphalerite increased the rate of dissolution of zinc if the minerals were in direct contact with each other.

Scanning electron micrographs and XRD techniques were used to examine the nature of the products formed.

5.1 Determination of the Chemical Oxidation Rate Equation of the Sphalerite Concentrate in a Sulphate Medium for Prolonged Leach Periods

This section determines the kinetics of the chemical reaction of sphalerite in a sulphate medium. The sphalerite concentrate was used for this part of the experimental work The standard conditions presented in Table 4-1, were changed accordingly to investigate the variable under consideration.

5.1.1 Temperature Dependence of the Reaction

In order to determine the effect of temperature on the rate of reaction, the sphalerite concentrate, of size fraction -75+53 μm, was leached at different temperatures in the

range of 30°C to 55°C. The ferric sulphate leach medium had a ferric iron concentration of 0.5 M. The redox potential was controlled at 585 mV (vs Ag/AgCl) by the addition of 3 % H_2O_2.

Figure 5-1 shows the dependence of the chemical reaction versus time as temperature increases. The Surface Area Deactivation Model was used to predict the data.

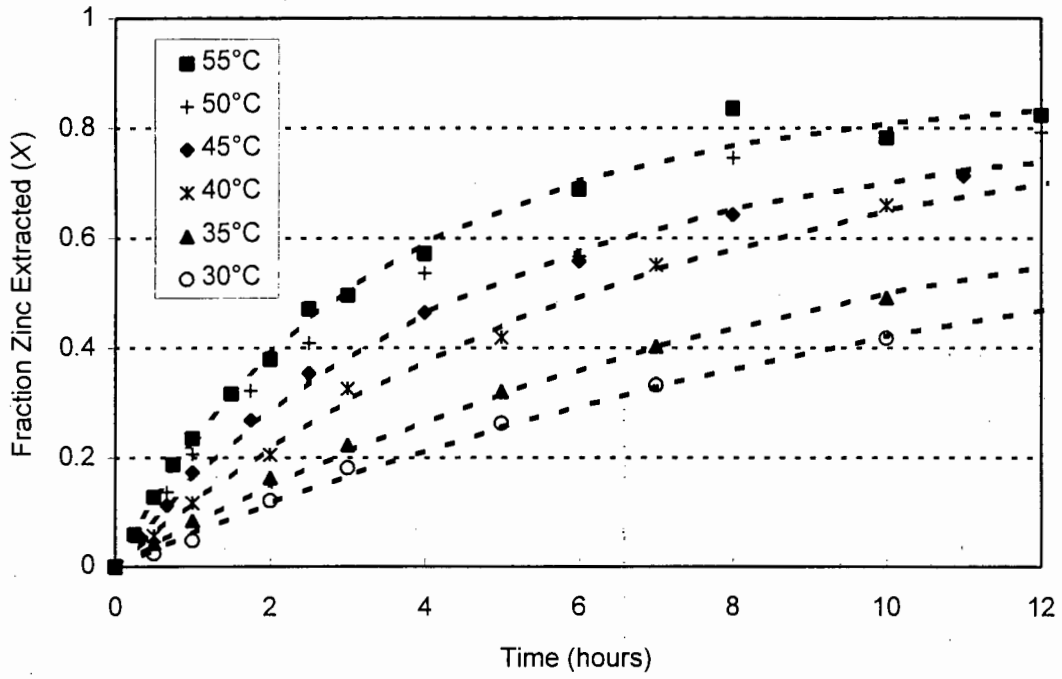

Figure 5-1 The temperature dependence of the dissolution reaction.

Figure 5-1 shows that as the temperature increases from 30 °C to 55 °C, the rate of dissolution, or the fraction of zinc extracted versus the time, increases as expected. At a temperature of 55 °C, the rate of dissolution of the sphalerite is almost zero after twelve hours of leaching and it is expected that the dissolution reaction is almost complete. At a temperature of 30 °C, the fraction of zinc extracted from the sphalerite is approximately 0.45 after twelve hours of leaching. Even though the fraction of zinc extracted at lower temperatures was less than the fraction zinc extracted for the higher temperatures, in particular at a temperature of 55 °C, the dissolution process had not stopped for these experiments and the fraction of zinc extracted did increase for prolonged leach periods as predicted by the Surface Area

Deactivation Model. This means that at lower temperatures, the reaction proceeds at a slower rate.

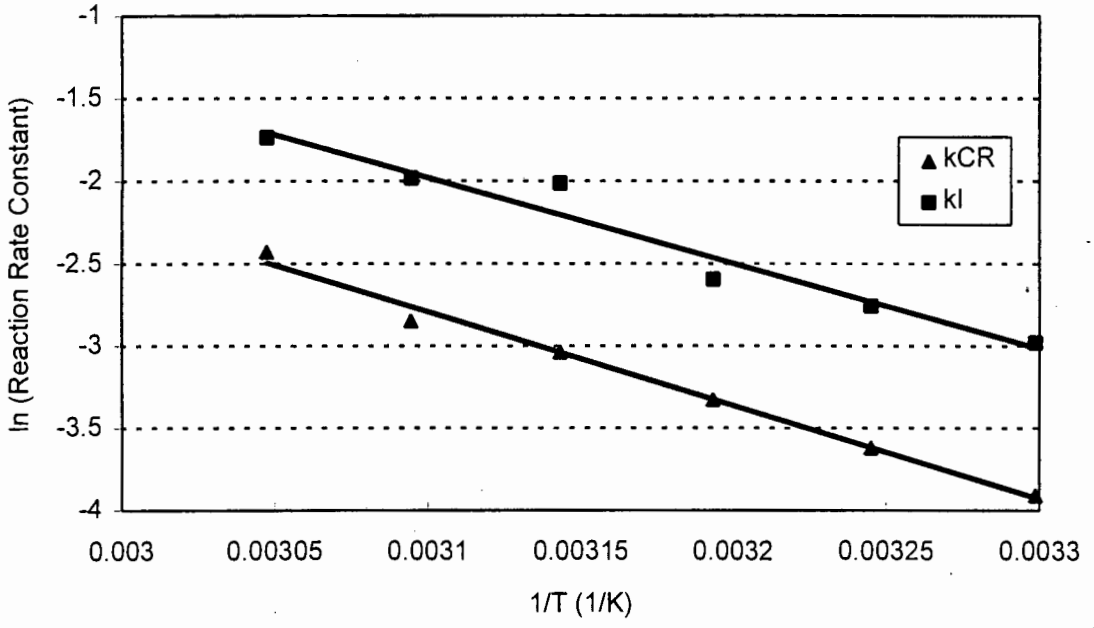

Figure 5-2 Arrhenius plot to determine the activation energy.

By fitting the data to the Surface Area Deactivation Model (Figure 5-1), the chemical reaction rate constant, k_{CR}, and the surface area deactivation rate constant, k_I, were determined over the range of temperatures studied. Variation of these rate constants with temperature was used to calculate the activation energy of the reaction from the Arrhenius equation as plotted in Figure 5-2.

This gave a value of 47.2 kJ.mol^{-1} for the chemical reaction rate constant, k_{CR} and 43.1 kJ.mol^{-1} for the surface area deactivation rate constant, k_I.

The value of the activation energy for the chemical reaction can be compared to a value of 46 kJ.mol^{-1} that Crundwell (1988b) obtained for the same sphalerite concentrate. Rath *et al.* (1988) and Jin *et al.* (1984) reported activation energies of 58 and 58.3 kJ.mol^{-1} respectively for the dissolution of sphalerite containing different amounts of iron (Figure 5-3). The discrepancies between these values from the literature of the activation energy of sphalerite and that calculated for the Gamsberg ore can be attributed to the iron within the sphalerite crystal lattice. This is due to the

alteration of the ionic strength of the energy bonds by the Fe in the ZnS crystal lattice (Crundwell, 1988b). This agrees with the results of Palencia-Perez and Dutrizac (1991) who found that the activation energy decreased with increasing iron content.

The activation energy, 47.2 kJ.mol^{-1}, calculated from this study was higher than that observed when a ferric chloride medium was used. This difference was supported by the work of Crundwell (1988b) in which both media, ferric chloride and ferric sulphate, were used. Figure 5-3 shows that the activation energy for the Gamsberg sphalerite leached in a sulphate medium by Crundwell (1988b) is comparable with that obtained in this study.

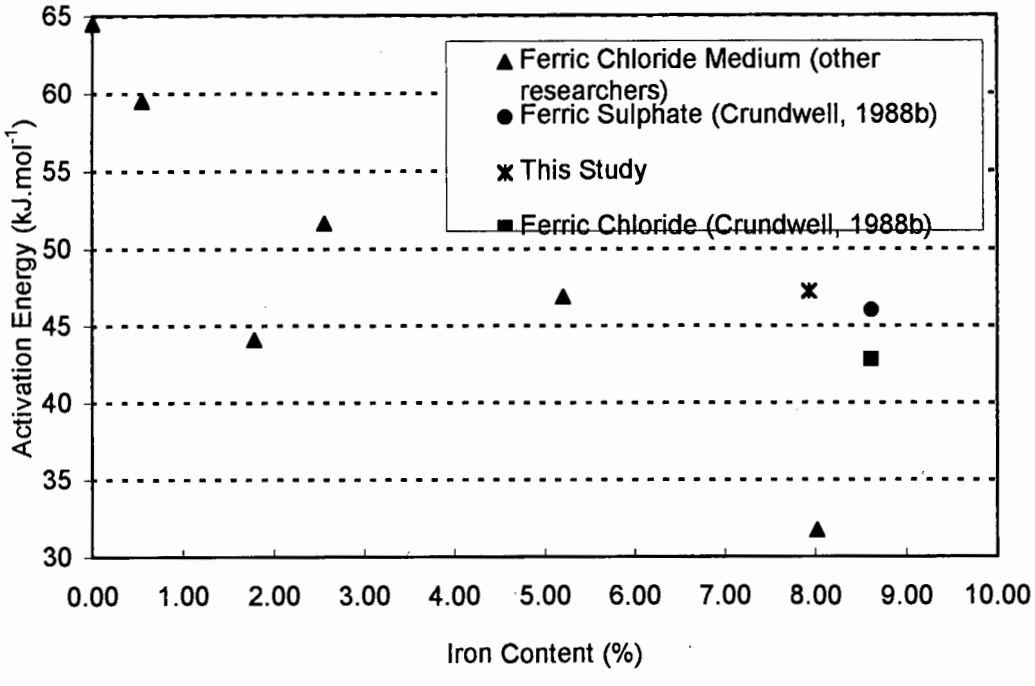

Figure 5-3 A plot of the activation energy calculated for ore samples with different iron content within the crystal lattice of the sphalerite. (Palencia-Perez and Dutrizac, 1991).

The activation energy evaluated is 43.1 kJ.mol $^{-1}$ for the surface area deactivation term. This is similar to that obtained for the initial stages of the reaction. This indicated that the chemical reaction was rate-limiting throughout the leaching process as a high activation energy indicates that the chemical reaction is rate-limiting (Jin *et al.*, 1984). This implied that the chemical reaction was rate-limiting throughout the process and the reaction does not become limited by the diffusion of

the reactants to the mineral surface or the products away from the reacting mineral surface. The values of the activation energies calculated for both the initial stages of the reaction and the later stages of the reaction were similar. This supports the assumption of the Surface Area Deactivation Model that the surface deactivation process was independent of the chemical reaction.

5.1.2 Particle Size and Surface Area Dependence of the Reaction

The distribution of particle size within a size fraction of each sample obtained by the Malvern Particle Size Analyser is shown in Figure 5-4. The B.E.T. specific surface area for each of these size fractions is given in Table 5-1. The size fraction -75+53 μm shows an unusually high surface area measurement. Chapman (1989) observed a similar trend for a pyrite sample from a different source and attributed it to etching or pitting on the mineral surface that increased the B.E.T. surface area. From the Malvern analysis of the particle size, an average particle size was calculated. The average particle size of the -75+53 μm fraction is low (57.50 μm). This too, will contribute to the higher B.E.T. surface area measurement. However, more work would be needed to clarify this unusual result. The specific surface area ($m^2.kg^{-1}$) for the respective size fractions was calculated. These calculations assumed that each particle was a sphere and the surface area values obtained do not allow for pitting or etching.

PARTICLE SIZE (μm)	B.E.T. SURFACE AREA ($m^2.kg^{-1}$)	SPHERICAL SURFACE AREA ($m^2.kg^{-1}$)
-106+90	2797	238
-75+53	5248	325
-53+45	3395	439
-45+38	4984	547

Table 5-1 The size fractions of ore used in the experimental study and their corresponding B.E.T. surface area and specific surface area measurements.

alteration of the ionic strength of the energy bonds by the Fe in the ZnS crystal lattice (Crundwell, 1988b). This agrees with the results of Palencia-Perez and Dutrizac (1991) who found that the activation energy decreased with increasing iron content.

The activation energy, 47.2 kJ.mol^{-1}, calculated from this study was higher than that observed when a ferric chloride medium was used. This difference was supported by the work of Crundwell (1988b) in which both media, ferric chloride and ferric sulphate, were used. Figure 5-3 shows that the activation energy for the Gamsberg sphalerite leached in a sulphate medium by Crundwell (1988b) is comparable with that obtained in this study.

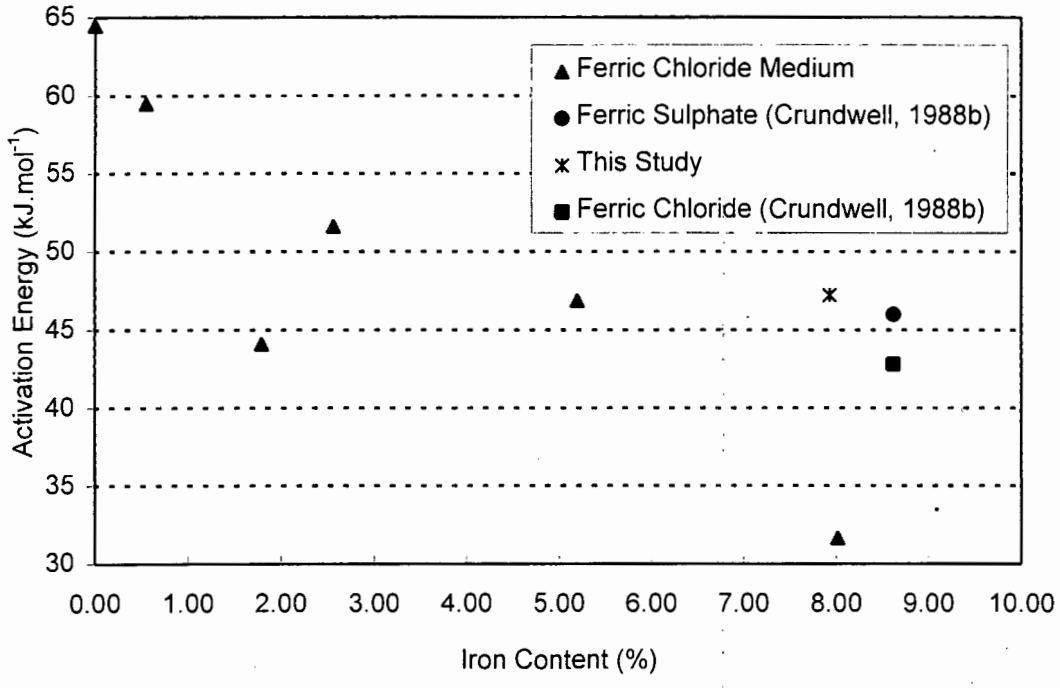

Figure 5-3 A plot of the activation energy calculated for ore samples with different iron content within the crystal lattice of the sphalerite. (Palencia-Perez and Dutrizac, 1991).

The activation energy evaluated for the surface deactivation term, k_I, is 43.1 kJ.mol^{-1}. This is similar to that obtained for the initial stages of the reaction. This indicated that the chemical reaction was rate-limiting throughout the leaching process as a high activation energy indicates that the chemical reaction is rate-limiting (Jin *et al.*, 1984). This implied that the chemical reaction was rate-limiting throughout the process and the reaction does not become limited by the diffusion of the reactants to the mineral

surface or the products away from the reacting mineral surface. The values of the activation energies calculated for both the initial stages of the reaction and the later stages of the reaction were similar. This supports the assumption of the Surface Area Deactivation Model that the surface deactivation process was independent of the chemical reaction.

5.1.2 Particle Size and Surface Area Dependence of the Reaction

The distribution of particle size within a size fraction of each sample obtained by the Malvern Particle Size Analyser is shown in Figure 5-4. The B.E.T. specific surface area for each of these size fractions is given in Table 5-1. The size fraction -75+53 μm shows an unusually high surface area measurement. Chapman (1989) observed a similar trend for a pyrite sample from a different source and attributed it to etching or pitting on the mineral surface that increased the B.E.T. surface area. From the Malvern analysis of the particle size, an average particle size was calculated. The average particle size of the -75+53 μm fraction is low (57.50 μm). This too, will contribute to the higher B.E.T. surface area measurement. The specific surface area ($m^2.kg^{-1}$) for the respective size fractions was calculated. These calculations assumed that each particle was a sphere and the surface area values obtained do not allow for pitting or etching.

PARTICLE SIZE (μm)	B.E.T. SURFACE AREA ($m^2.kg^{-1}$)	SPHERICAL SURFACE AREA ($m^2.kg^{-1}$)
-106+90	2797	238
-75+53	5248	325
-53+45	3395	439
-45+38	4984	547

Table 5-1 The size fractions of ore used in the experimental study and their corresponding B.E.T. surface area and specific surface area measurements.

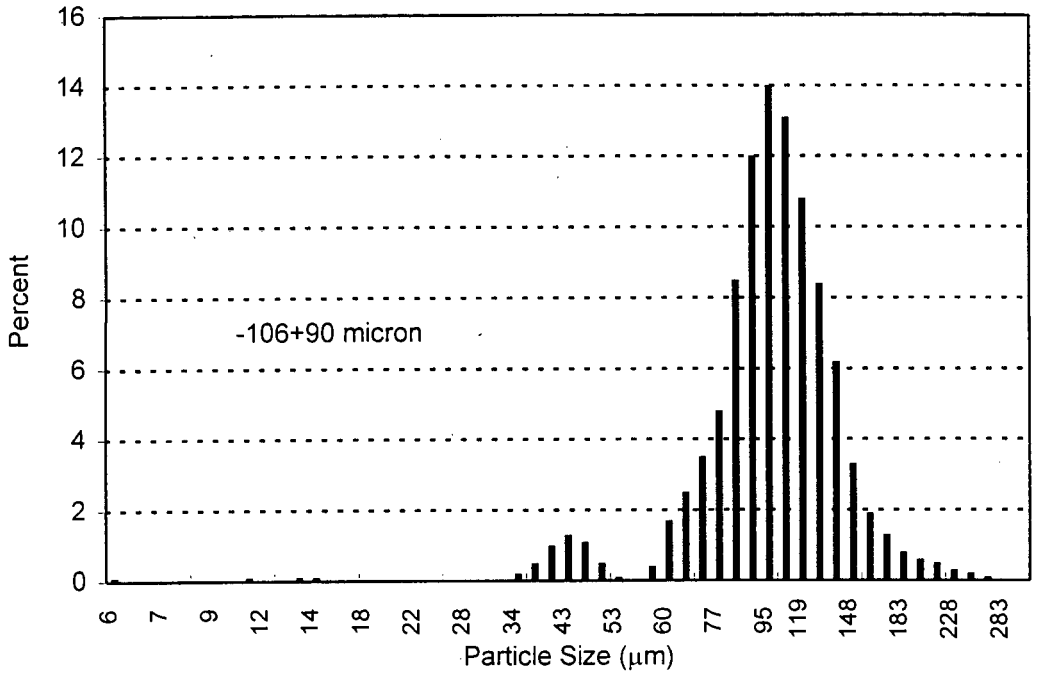
Percent
-106+90 micron
Particle Size (μm)
0
2
4
6
8
10
12
14
16
6
7
9
12
14
18
22
28
34
43
53
60
77
95
119
148
183
228
283

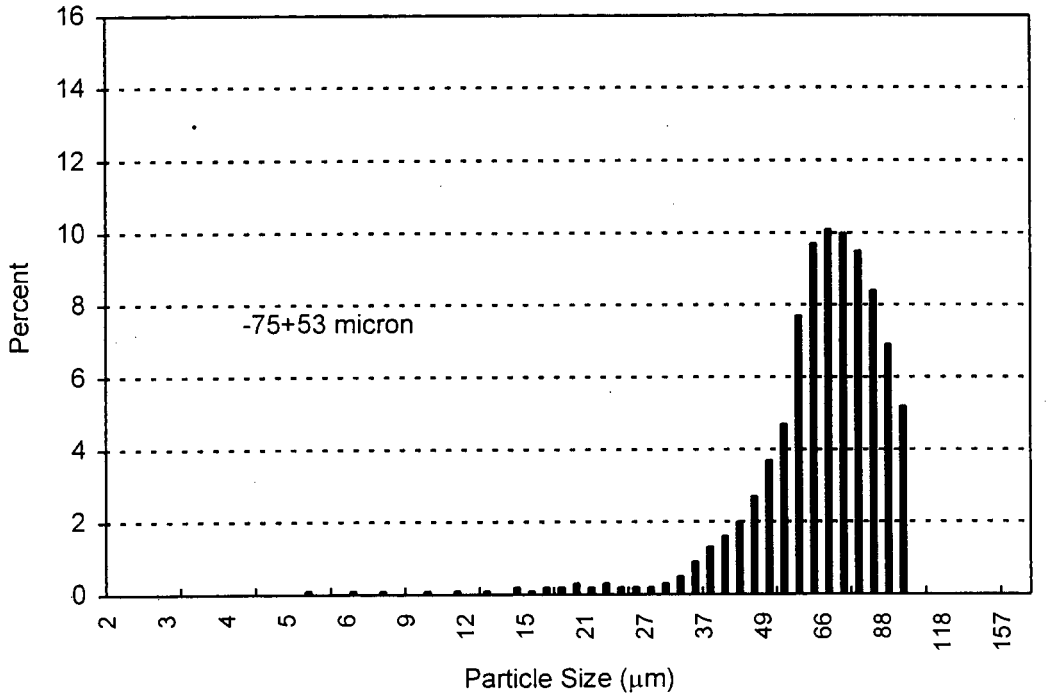
Percent
-75+53 micron
Particle Size (μm)
0
2
4
6
8
10
12
14
16
2
3
4
5
6
9
12
15
21
27
37
49
66
88
118
157

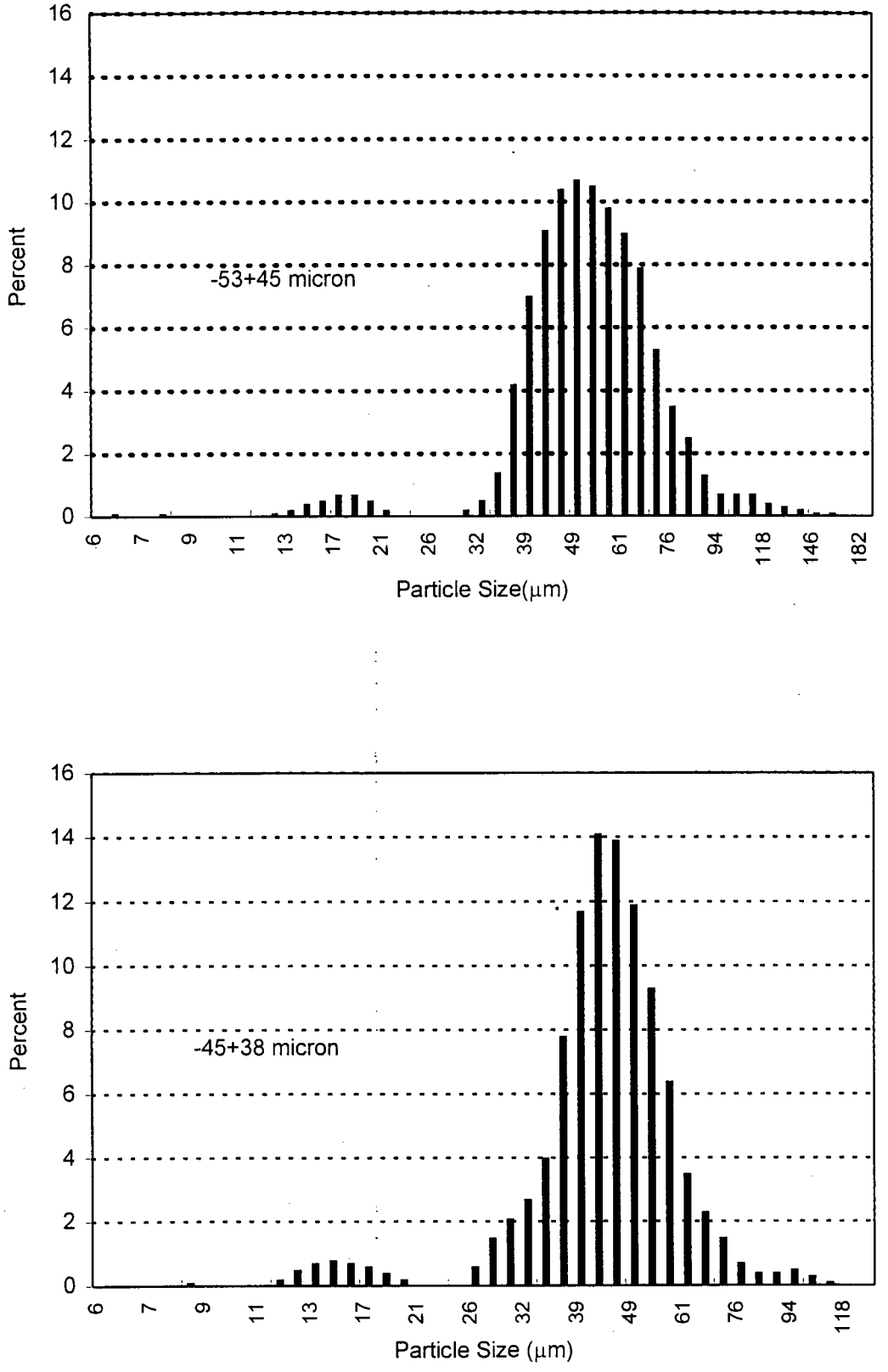

Figure 5-4 The Malvern Particle Size Analyser showing the size distribution for the different particle sizes.

The results obtained for this set of batch tests are presented in Figure 5-5. The experiments were run under the following conditions: $[Fe^{3+}]$ = 0.5 M, temperature = 40.5 °C and the redox potential controlled at 585 mV (vs Ag/AgCl). Figure 5-5 shows that as the particle size decreases, the rate of dissolution of the sphalerite increases. The rate of dissolution of the sphalerite is dependent on the surface area of the particles to be leached by the ferric iron in solution. An inverse relationship exists between the particle size and the surface area and thus as the particle diameter decreases, the faster the dissolution rate of the sphalerite.

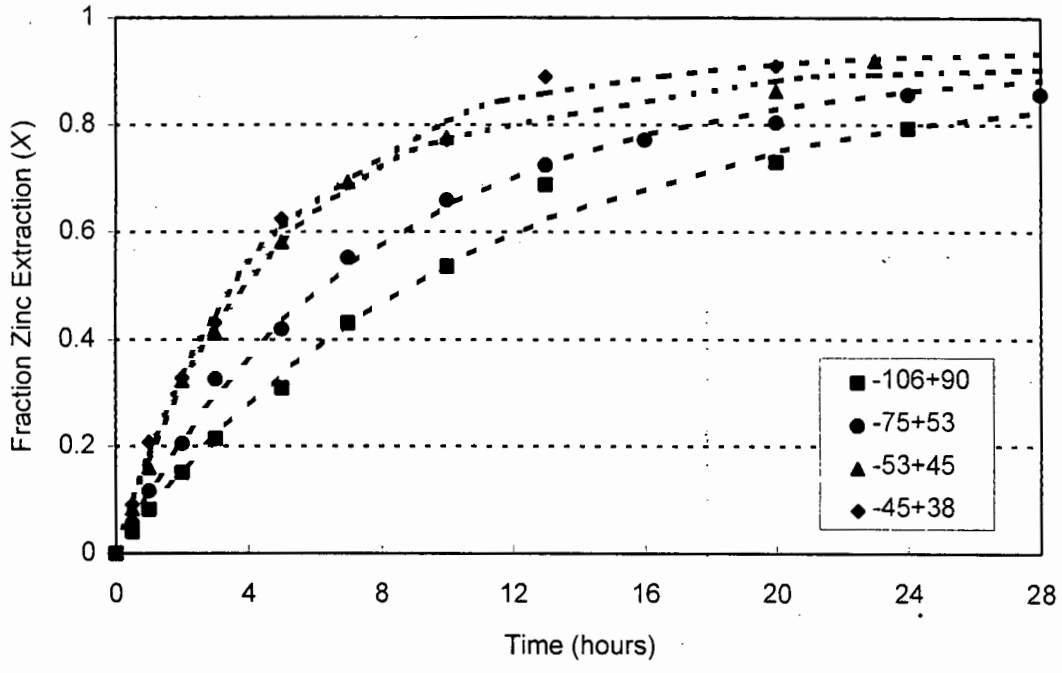

Figure 5-5 A plot of the fraction zinc extracted versus time for different particle sizes.

The Surface Area Deactivation Model was applied to the data (Figure 5-5) from which the chemical reaction rate constant and the surface area deactivation rate constant were determined. Particle sizes and the rate constants from Table 5-2 were used to determine the linear relationship between the reaction rate constants and the initial particle diameter (Figure 5-6).

PARTICLE SIZE (μm)	PARTICLE DIAMETER d_o (μm)	RATE CONSTANT k_{CR} (hours^{-1})	RATE CONSTANT k_I (hours^{-1})
-106+90	99.36	0.087775	0.051001
-75+53	57.50	0.126038	0.074597
-53+45	54.32	0.198279	0.115679
-45+38	45.00	0.210755	0.112921

Table 5-2 Effect of particle size on dissolution rate.

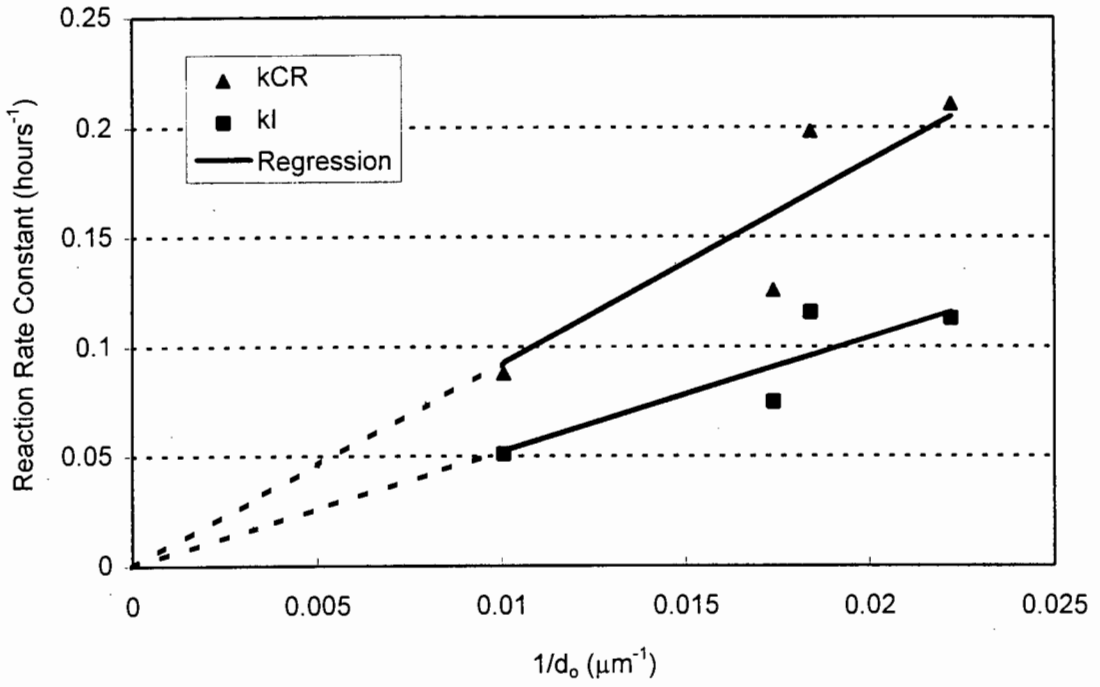

Figure 5-6 A plot of the reaction rate constant versus the inverse of the initial particle diameter.

The fraction of zinc extracted from the sphalerite was predicted by the Surface Area Deactivation Model. Figure 5-7 shows that for prolonged leach periods, the overall conversion of sphalerite is almost the same for each particle size. Figure 5-8 shows that the surface rate, r_{ao}, for each particle size. By definition, the surface area rate is independent of particle size and so the surface area rate is the same for each particle size as shown in Figure 5-8. This explains why the Surface Area De-activation Model predicts the same overall fractional extraction of zinc (Figure 5-7).

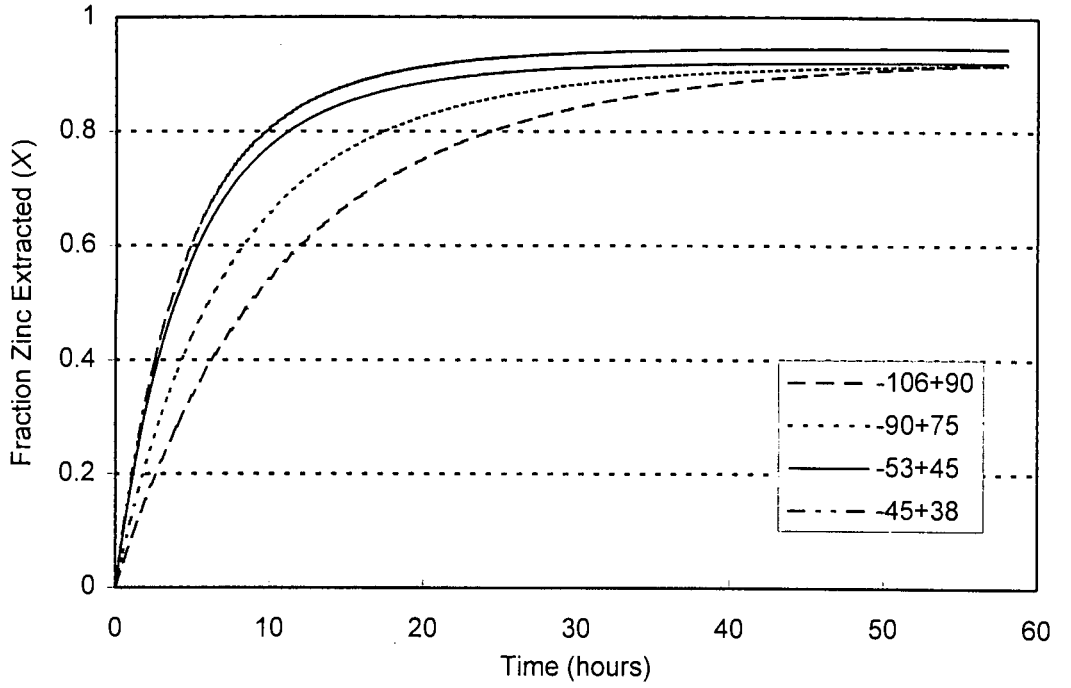

Figure 5-7 Model prediction of the leaching of sphalerite concentrates of different particle sizes.

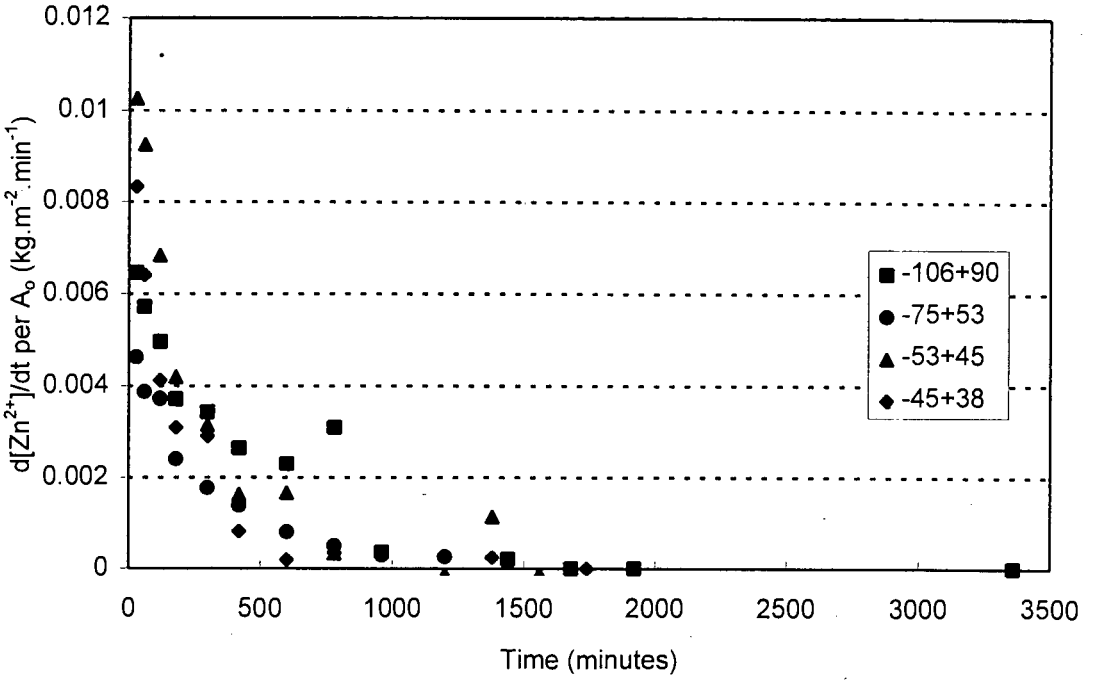

Figure 5-8 The surface area rate, r_{ao}, versus time for each particle size.

A plot of the surface deactivation term ($\exp\{-k_1 t\}$) versus time for each particle size shows that the smaller the particle, the greater the influence of the of the surface area deactivation term becomes (Figure 5-9). This shows that the surfaces of smaller particles are deactivated more rapidly. As the particle size decreases, the chemical reaction rate constant increases and so the rate of product formation is higher. The surfaces of smaller particles are deactivated more rapidly because of the higher rate of product formation.

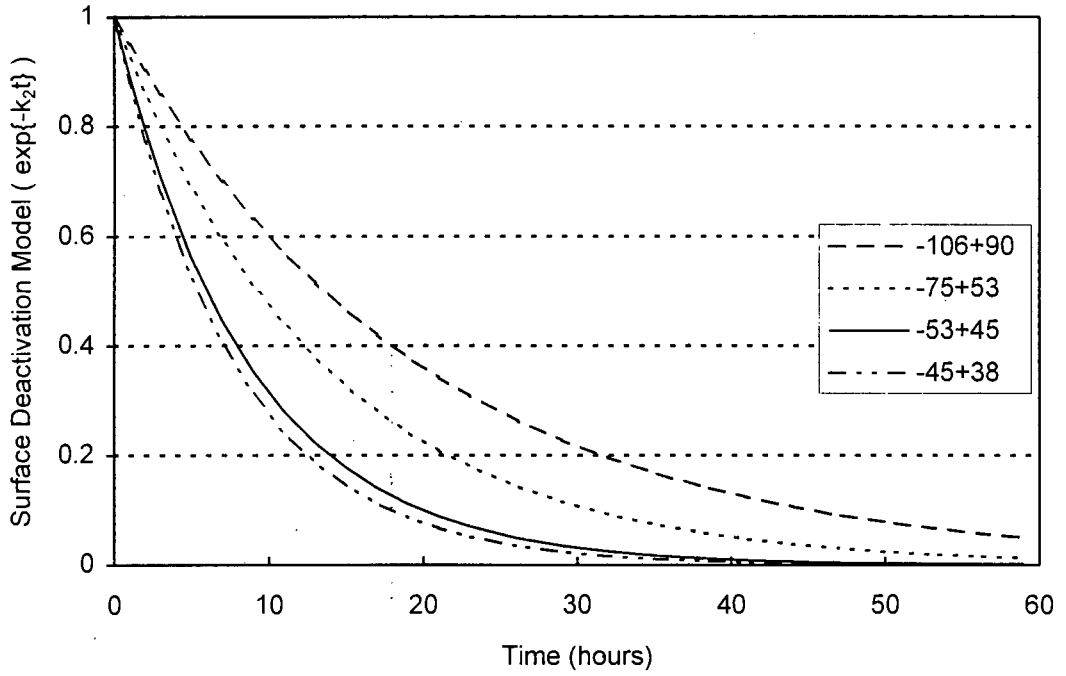

Figure 5-9 A plot of the surface deactivation term versus time showing the influence of this term as the reaction proceeds.

From their studies of the effect of particle size on the dissolution of sphalerite during prolonged leach periods, Bobeck and Su (1985) concluded that for smaller particles, the chemical reaction at the mineral surface was the rate-controlling step. For larger particles, diffusion limitations were more apparent.

The phenomenon described by Bobeck and Su (1985) can be explained in terms of the Surface Area Deactivation Model using the results of this study. The chemical reaction rate constant, k_{CR}, decreases as the particle gets larger, i.e., the rate of dissolution (or the rate of product formation) is slower. This is due to the fact that

surface area decreases as particle size increases and so the rate of dissolution of the sphalerite decreases.

If one considers the relationship of surface area available for leaching to the amount of product forming, then, for smaller particles, the apparent effect of the surface area deactivation term is less dominant. There is still enough surface area available to allow significant dissolution and the reaction rate for smaller particles is higher. Bobeck and Su (1985) conclude that this demonstrates that the chemical reaction is the rate limiting step for the dissolution of small particles.

For large particles, the ratio of surface area available to amount of product formed is lower than for small particles. The area available for the chemical reaction decreases more rapidly and so the apparent effect of the surface area deactivation term is larger. This causes the chemical reaction rate constant to be lower than that for smaller particles and explains why Bobeck and Su (1985) observe that the chemical reaction was limited by diffusion for large particles.

5.1.3 The Dependence of the Chemical Reaction on the Concentration of the Ferric Iron

The dependence of the chemical reaction on the concentration of ferric iron was studied under the following conditions:

1. the solution redox potential was not controlled and the initial ferric iron concentration was varied;
2. specific ferric iron concentrations and corresponding ferrous iron concentrations were chosen to maintain an almost constant total iron content. The resulting solution redox potential that was then measured at these conditions was the redox potential at which the experiment was controlled.

The ore used was a -75+53 μm size fraction of the Gamsberg sphalerite concentrate. The experiments were maintained at a temperature of 40.5 °C.

Figure 5-10 shows the extent of conversion of zinc sulphide under similar leach conditions with a varying initial concentration of ferric iron. The redox potential was not controlled by the addition of hydrogen peroxide. For high concentrations of ferric iron, the fraction of zinc extracted is higher when compared to the fraction of zinc

extracted where a low initial concentration of ferric iron is used in the leach medium. The rate of the dissolution of sphalerite is dependent on the initial concentration of ferric iron if the ferrous iron available for the chemical reaction is not regenerated. This occurs because the ferric iron is consumed by the dissolution reaction and the amount of ferric available becomes rate-limiting.

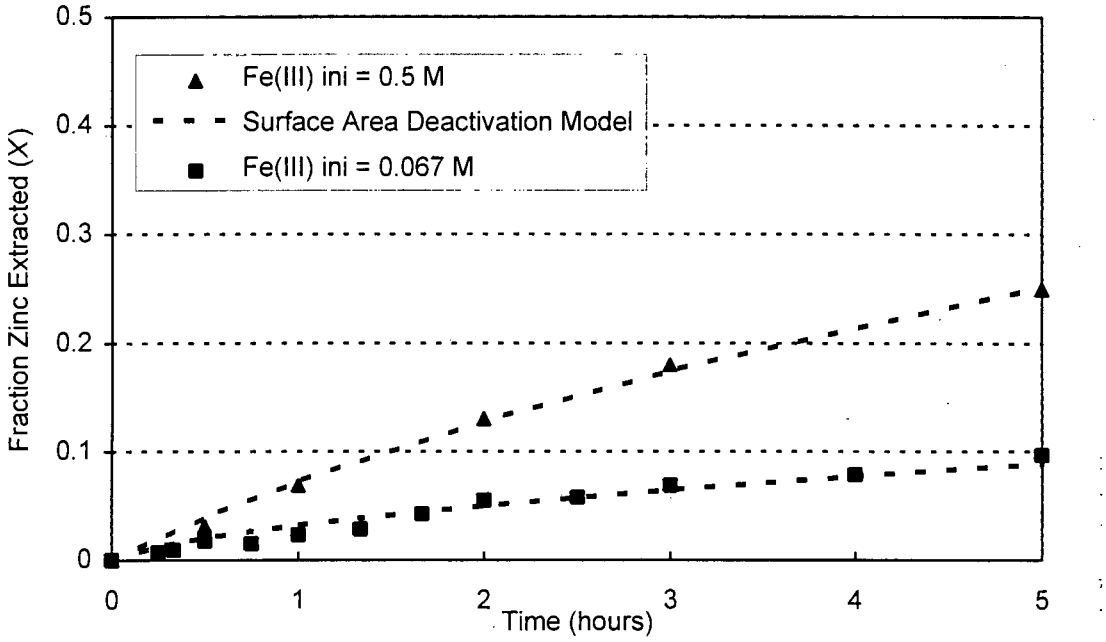

Figure 5-10 The dependence of the fractional extraction of zinc from sphalerite on the initial concentration of ferric iron if the redox potential is not controlled.

This plot shows that the amount of ferric iron available for the chemical reaction limits the extent of conversion of the sphalerite. The extent of conversion of the sphalerite is increased when the initial ferric iron concentration is increased, therefore the dissolution reaction is limited by the amount of ferric iron available for the chemical reaction.

Table 5-3 shows the iron concentrations and the corresponding redox potentials for the second set of experimental conditions.

RUN NUMBER	FERRIC IRON M	FERROUS IRON M	Fe^{3+}/Fe^{2+} RATIO	TOTAL IRON $g.\ell^{-1}$	FERROUS SULPHATE $g.\ell^{-1}$	FERRIC SULPHATE $g.\ell^{-1}$	REDOX POTENTIAL mV
4A	0.500	0.0001	3735	27.93	0.0558	196.8500	673
4B	0.500	0.0003	1493	27.94	0.1396	196.8500	656
4C	0.500	0.0007	746	27.96	0.2792	203.8400	609
4D	0.500	0.0013	373	28.00	0.5585	203.8400	601
4E	0.500	0.0200	25	29.04	8.3409	198.6900	554
4F	0.500	0.0500	10	30.72	20.8523	198.6900	492
4G	0.260	0.2602	1	29.05	108.4317	144.0300	443

Table 5-3 The ferric iron and ferrous iron concentrations used to determine the effect of solution redox potential on the rate of dissolution. The values for the redox potential are those measured with a Ag/AgCl electrode.

The results of leaching under the conditions presented in Table 5-3 are shown in Figure 5-11 for the experiments numbered 4C, 4D, 4E and 4F. These results show that as the ratio of ferric iron to ferrous iron in solution is increased, the faster the initial rate of zinc extraction becomes. In the experiment where the redox potential was not controlled, 4H, the rate of dissolution of the sphalerite was approximately as that observed in experiments numbered 4E and 4F. However, after four hours of leaching, the rate of extraction of zinc from the sphalerite decreased more rapidly and so the overall dissolution of the sphalerite was less than the overall dissolution of zinc in experiments where the redox potential was controlled. This can be attributed to a decrease in the redox potential or a decrease in the ferric iron concentration either (or both) of which become rate-limiting.

The reaction rate constants, k_{CR} and k_I, are calculated from the Surface Area Deactivation Model and are shown in Table 5-4.

RUN NUMBER	Fe^{3+}/Fe^{2+} RATIO	k_{CR} (hours^{-1})	k_I (hours^{-1})
4A	3735	0.12656	0.12641
4B	1493	0.10524	0.00843
4C	746	0.13994	0.13376
4D	373	0.10352	0.10157
4E	25	0.08971	0.08722
4F	10	0.08173	0.07205
4G	1	0.04519	0.03776

Table 5-4 The reaction rate constants calculated from the Surface Area De-activation Model (hours^{-1}).

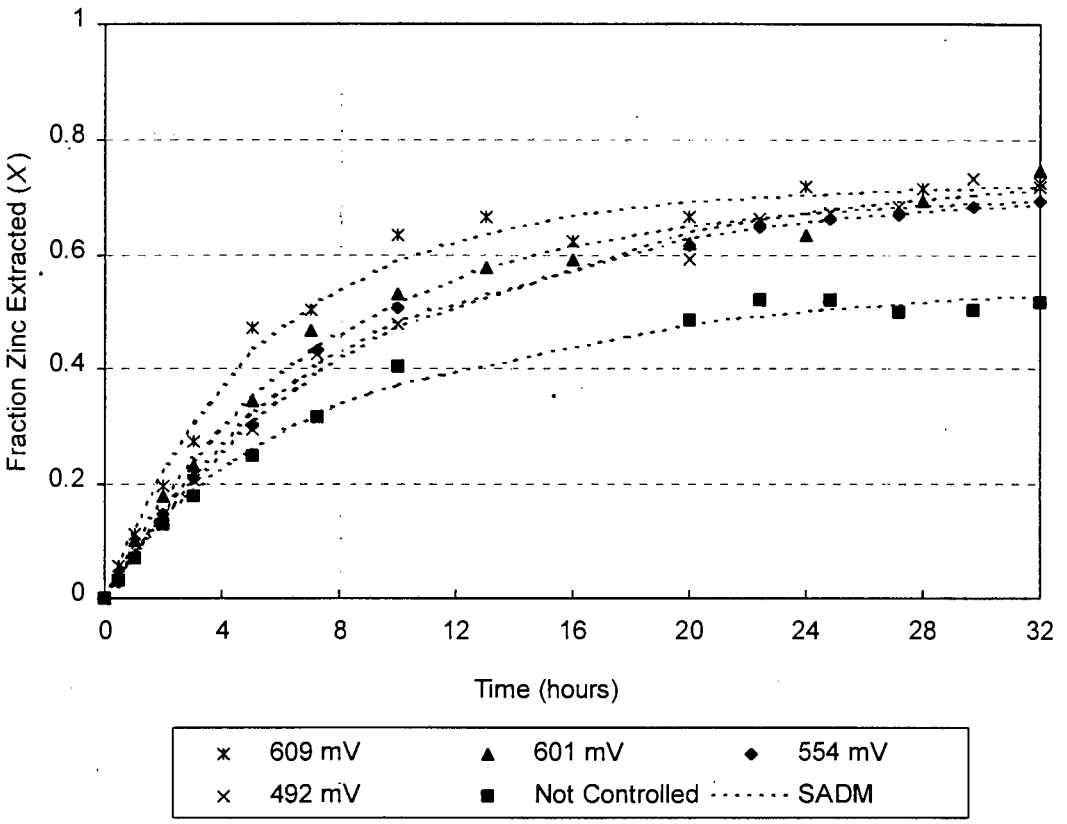

Figure 5-11 A plot of the fraction of zinc extracted versus time at varying redox potentials.

In the formulation of the Surface Area Deactivation Model, the chemical reaction rate constant and the surface area deactivation rate constant are dependent on the ferric iron concentration and the ferrous iron concentration. The Electrochemical Model assumes that the reaction rate is dependent on the ferric/ferrous iron ratio where the reaction order is one-half. A logarithmic plot of the chemical reaction rate constant versus the ferric/ferrous iron ratio using the results obtained in this study would show the dependence of the reaction on the ratio of ferric iron to ferrous iron and determine whether this assumption is valid.

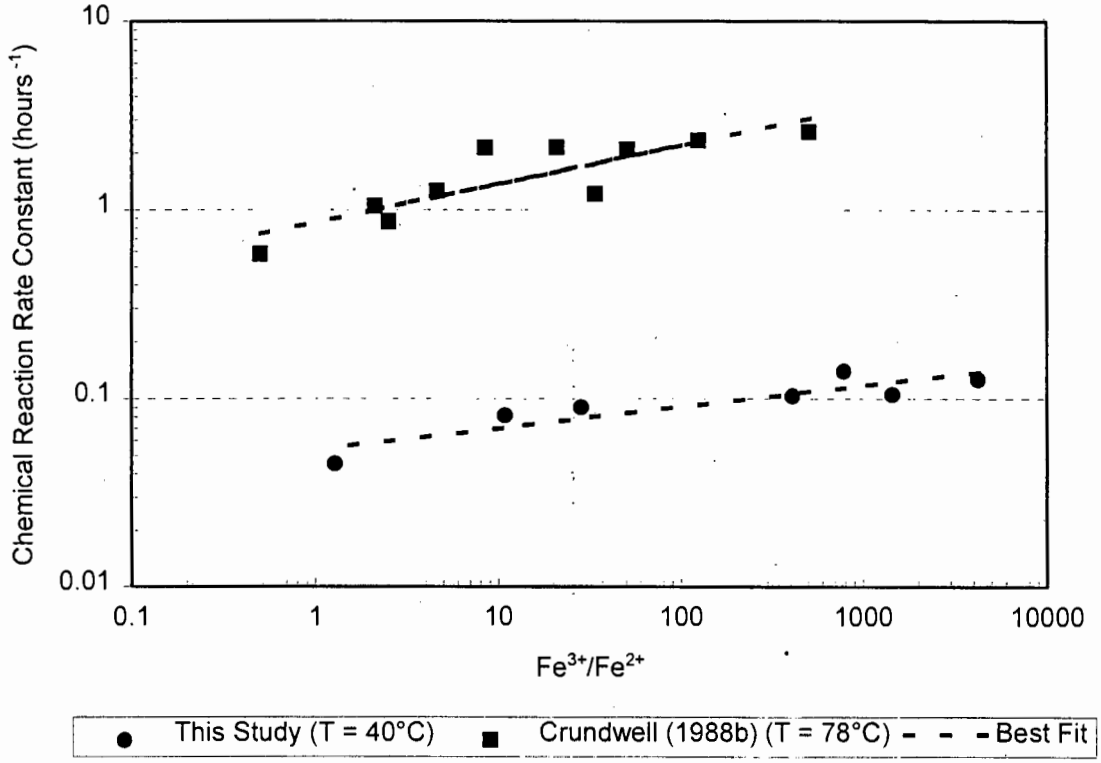

Figure 5-12 The chemical reaction rate constant as a function of the Fe^{3+}/Fe^{2+} ratio.

Figure 5-12 shows the relationship between the chemical reaction rate constant and the ferric/ferrous iron ratio. The slope of the linear regression through the data points was 0.113. The expected slope of this straight line is one-half corresponding to the half-order electrochemical reaction described for the Electrochemical Model. In comparison to this, the value of the slope for the same linear regression calculated for the data presented by Crundwell (1988b) was 0.206. The deviation of the two results from the expected value of 0.5 shows that this was an inadequate description of the relation of the chemical reaction rate constant to the ferric/ferrous

iron ratio. The difference in order of magnitude of the chemical reaction rate constants for this study and those for the work of Crundwell (1988b), were attributed to the difference in temperature of the experimental work that was used in the calculation of the chemical reaction rate constant and the surface area deactivation rate constant.

The chemical reaction rate constant (expressed logarithmically) was plotted against measured solution redox potential. The relationship can be described by a straight line below 500 mV (vs Ag/AgCl) and a straight line above 500 mV (vs Ag/AgCl). However, these two lines do not have the same gradient: at potentials below 500 mV (vs Ag/AgCl), the increase in reaction rate constant per incremental increase in redox potential is greater than the corresponding increase in reaction rate constant at potentials above 500 mV (vs Ag/AgCl). This implies that the dependence of the chemical reaction rate constant changes at an approximate redox potential of 500 mV (vs Ag/AgCl). The chemical reaction rate constant evaluated by the Surface Area Deactivation Model for the data presented by Crundwell (1988b) shows the same trend where the increase in the chemical reaction rate constant at redox potentials lower than 500 mV is greater than the increase in the chemical reaction rate constant at redox potentials greater than 500 mV.

This relationship is significant in that the surface area deactivation term shows the same dependence on the ferric iron equilibrium species as does the chemical reaction term. This supports the assumption in the definition of the Surface Area Deactivation Model that the two processes are independent of each other. This result also implies that the chemical reaction at the mineral surface is rate-limiting for the entire leach period. Apparent diffusion limitations are only observed because surface area decreases as product is formed, resulting in a decrease in the reaction rate until total surface area is deactivated and no more dissolution can occur. The further implications of this point are two-fold:

- the product formed results in complete deactivation of that portion of the surface on which it forms by filling the crevices and pits that are formed by leaching;
- reaction will cease prior to complete conversion of the sphalerite.

This result is in agreement with Crundwell (1988b) who showed that the dependence of the chemical reaction rate constant on the redox potential was an inadequate

description of the chemical reaction kinetics. His study showed that the dependence of the rate of the chemical reaction on the solution redox potential was linear in terms of the Nernst Equation, with a slope = nF/RT, if the ferrous iron in solution was held constant and the ferric iron concentration was varied. However, if the ferric iron concentration was held constant and the ferrous iron concentration was varied, the dependence of the reaction rate constant was linear, however the slope ≠ nF/RT and was termed "non-Nernstian".

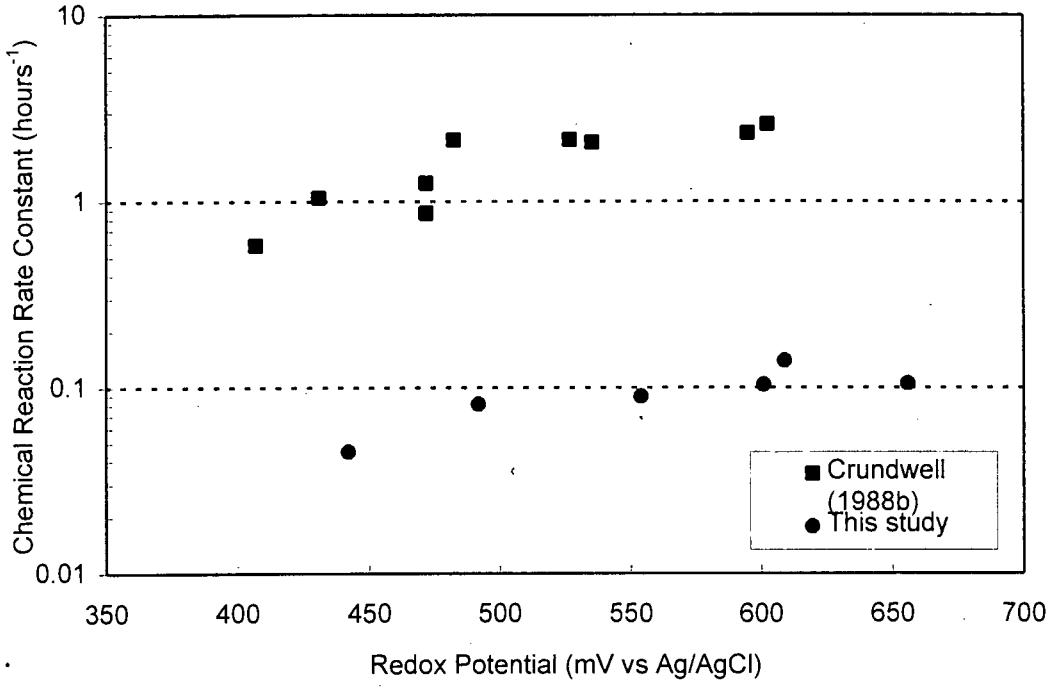

Figure 5-13 The dependence of the reaction rate constant on the redox potential.

By determining the ionic equilibria for the various species in solution, Crundwell (1988b) accounted for the "non-Nernstian" behaviour. He argued that the reaction was dependent on the electro-active outer-sphere equilibrium species (Fe^{3+}_{AQ} and $FeHSO_4^{2+}$) and showed the reaction rate constant (k_{CR}) to be linear with respect to the sum of these two species (Figure 3-11).

Crundwell (1988b) adapted the work of Dry and Bryson (1988) to determine the solution equilibria. The aim of the work by Dry and Bryson (1988) was to determine the solution redox potential by calculating the ionic equilibria of the uncomplexed ferric and ferrous iron in solution. The complex species that were accounted for, were the ferric iron species Fe^{3+}_{AQ}, $FeSO_4^+$ and $FeHSO_4^{2+}$; the ferrous iron species Fe^{2+}_{AQ},

$FeSO_4$ and $FeHSO_4^+$; and the bisulphate ion HSO_4^-. The activity coefficients of these species in solution were determined in an ionic strength range of 0 to 4 and a temperature range of 22°C to 90°C. The Debye-Hückel equation was used to estimate these activity coefficients except the HSO_4^- ion, where Pitzer's correlation was used (Pitzer *et al.*; 1977). The ratio of the activity coefficients multiplied by the concentrations of the uncomplexed ferric iron and the uncomplexed ferrous iron was used in the Nernst Equation for the prediction of the redox potential of the solution.

This work was combined with the numerical procedure developed by I and Nancollas (1972) for the calculation of the equilibrium concentrations of the species present. A listing of the TURBO C computer program, EQUIL, adapted from the work of Crundwell (1988b), is presented in Appendix F.

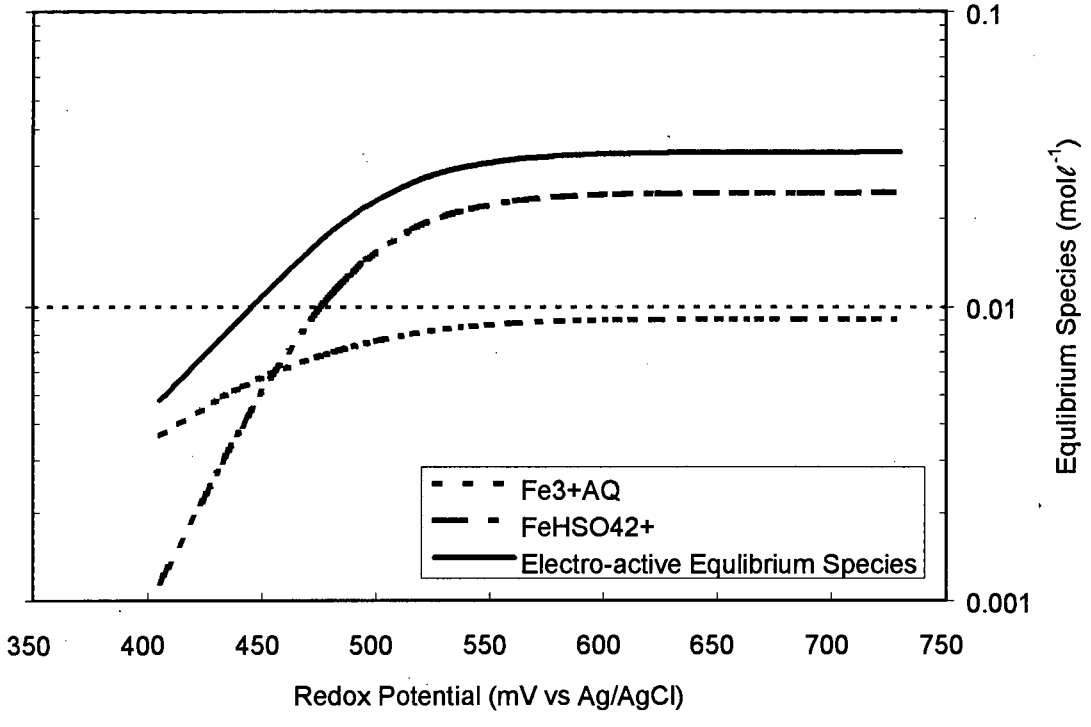

Figure 5-14 The equilibrium species, with particular reference to the electro-active species - Fe^{3+}_{AQ} and $FeHSO_4^{2+}$, as a function of the redox potential.

The dependence of the solution equilibrium of the electro-active species, Fe^{3+}_{AQ} and $FeHSO_4^{2+}$, on the redox potential was determined. The solution equilibria were determined at a constant ferric iron concentration of 0.5 M and the ferrous iron concentration ranging from 10 to 0.0001 M. The redox potential was calculated

using the Nernst equation dependent on the ratio of the concentration of the Fe^{3+}_{AQ} and Fe^{2+}_{AQ} species (Dry 1985). Using solution equilibria determined by EQUIL, the proposed electro-active species, Fe^{3+}_{AQ} and $FeHSO_4^{2+}$, and the sum of these species were plotted against redox potential (Figure 5-14).

This plot shows that the sum of the two electro-active species that Crundwell (1988b) proposed the electrochemical reaction was dependent on, changed slope in a similar manner to the data presented in Figure 5-11. The electro-active equilibrium species did not show a constant linear relationship with the redox potential. This explains the inconsistency of the model presented by Verbaan and Crundwell (1986) where the rate of dissolution was dependent on the redox potential defined by the ratio of the ferric iron to ferrous iron in solution.

Figure 5-15 shows that the reaction rate constant and the equilibrium species, when plotted versus the redox potential, changes slope at approximately 520 mV (vs Ag/AgCl), implying that the reaction rate is dependent on the equilibrium species. The results imply that the chemical reaction rate constant and the surface area deactivation rate constant are dependent on the equilibrium species.

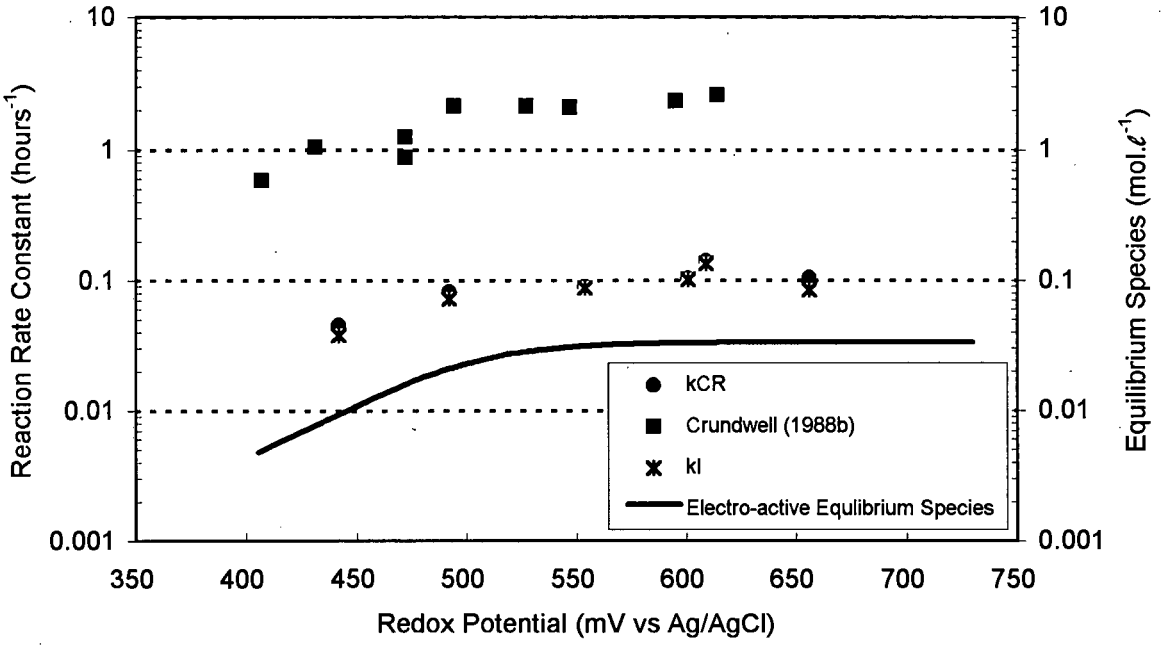

Figure 5-15 The reaction rate constant and the equilibrium species plotted versus the redox potential showing the same shape.

The equilibria species for the experiments numbered 4A to 4G were calculated using EQUIL. The results are presented in Table 5-5.

Equilibrium Species mol.ℓ^{-1}	Experiment Number						
	4A	4B	4C	4D	4E	4F	4G
Fe^{3+}	0.00904	0.00904	0.00904	0.00904	0.00894	0.00879	0.00492
Fe^{2+}	0.00003	0.00010	0.00023	0.00042	0.00645	0.01606	0.09055
H^{+}	0.05196	0.05195	0.05191	0.05187	0.05044	0.04828	0.04170
SO_4^{2-}	0.23536	0.23545	0.23636	0.23591	0.24438	0.25783	0.23100
$FeHSO_4^{2+}$	0.02430	0.02430	0.02428	0.02426	0.02370	0.02284	0.01026
$FeSO_4^{+}$	0.46665	0.46666	0.46668	0.46670	0.46736	0.46836	0.24482
HSO_4^{-}	0.23713	0.12369	0.12363	0.12355	0.12101	0.11702	0.09447
$FeSO_4$	0.00004	0.00013	0.00030	0.00056	0.00869	0.02209	0.11608
$FeHSO_4^{+}$	0.00003	0.00007	0.00017	0.00032	0.00486	0.01185	0.05358

Table 5-5 The equilibrium species as calculated by EQUIL.

To determine the dependence of the chemical reaction rate constant and the surface area deactivation rate constant on the equilibrium species, a logarithmic graph of the reaction rate constant versus the equilibrium species was plotted. A linear regression of the data for the chemical reaction rate constant yields a slope equal to 0.476. The slope of the linear regression for the surface area deactivation rate constant (k_I) is equal to 0.528. These values of the reaction order are significantly close to the expected value of 0.5 if the reaction is dependent on the electro-active species (Crundwell; 1988b).

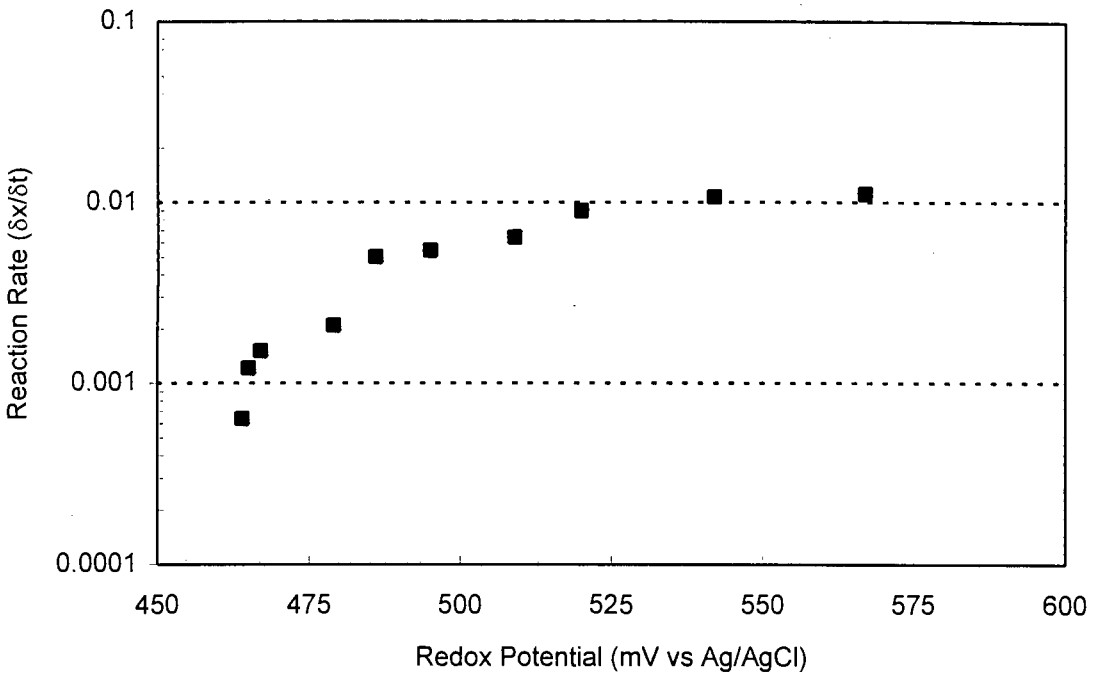

Figure 5-16 A plot of the chemical reaction versus redox potential where the redox potential was not controlled by the addition of H_2O_2.

The rate of zinc dissolution (dX/dt) was plotted against the redox potential (Figure 5-16) as the reaction proceeds without the regeneration of ferric iron. The results of Figure 5-16 show that the slope of the plot of the reaction rate changes at approximately 520 mV. This observation is significant in that the reaction rate shows the same dependence on the redox potential as does the chemical reaction rate constant for experiments where the redox potential was controlled. These results show that the rate of the reaction is limited by the concentration of the electro-active species and not by diffusion limitations. This supports the assumption used in the development of the Surface Area Deactivation Model that the chemical reaction at the mineral surface is rate limiting throughout the period of dissolution. The extent of dissolution of sphalerite is limited by the amount of ferric available for the leaching reaction.

5.2 The Effect of the Solids Concentration

The dependence of the fraction of zinc extraction on the solids concentration was studied. The sphalerite concentrate, of size fraction -75+53 μm, was leached at a temperature of 40.5 °C where the redox potential was not controlled by the addition of

hydrogen peroxide. There was no initial addition of ferrous sulphate to reduce the initial measured redox potential. The solids concentrations used were 0.2 % (w/v), 1.0 % (w/v) and 2.0 % (w/v). Figure 5-17 shows the results of the fraction of zinc extracted from the sphalerite for each experiment.

As the solids concentration decreased, the chemical reaction rate constant decreased. During a high solids concentration experiment, the dissolution reaction proceeds at a fast rate initially because there is a large amount of ferric iron available for the chemical reaction. As the reaction proceeds, the amount of ferric iron available for the chemical reaction becomes limiting as the ferric iron is reduced to ferrous iron.

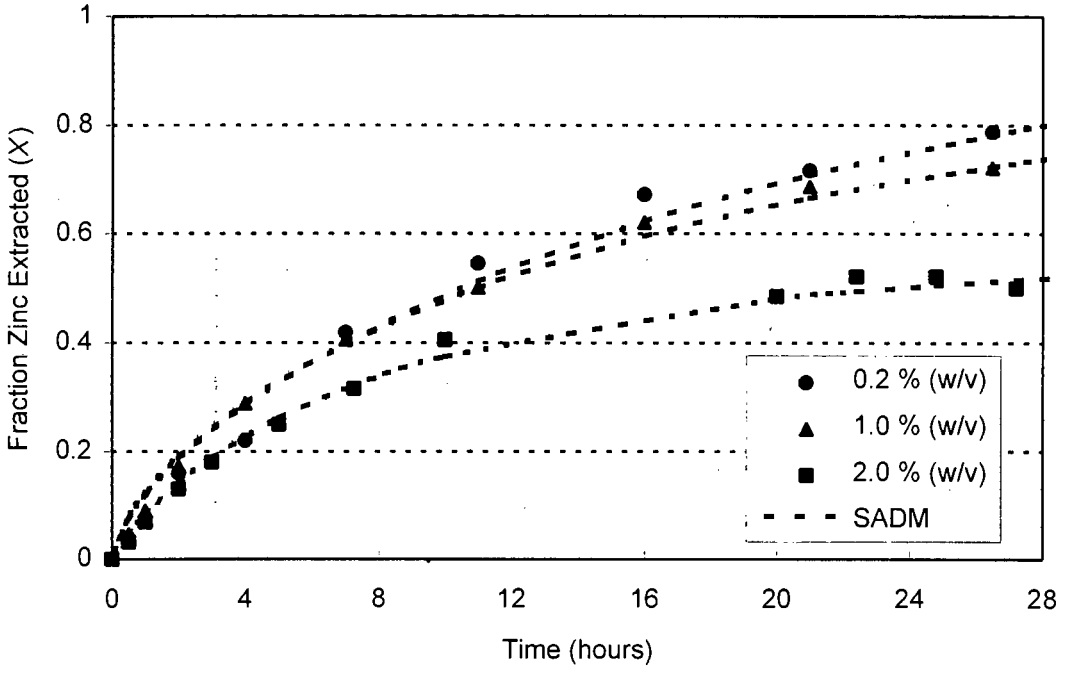

Figure 5-17 The effect of changing the solids concentration if the redox potential is not controlled.

The overall dissolution of zinc decreased as the solids concentration increased due to the limiting effect of the reduced amount of ferric iron available for reaction. Where the solution redox potential was controlled, the ferric iron was always regenerated from the ferrous iron. The amount of ferric iron in the solution thus did not limit the reaction and the overall conversion of zinc into solution was increased for the same solids concentration (Figure 5-18).

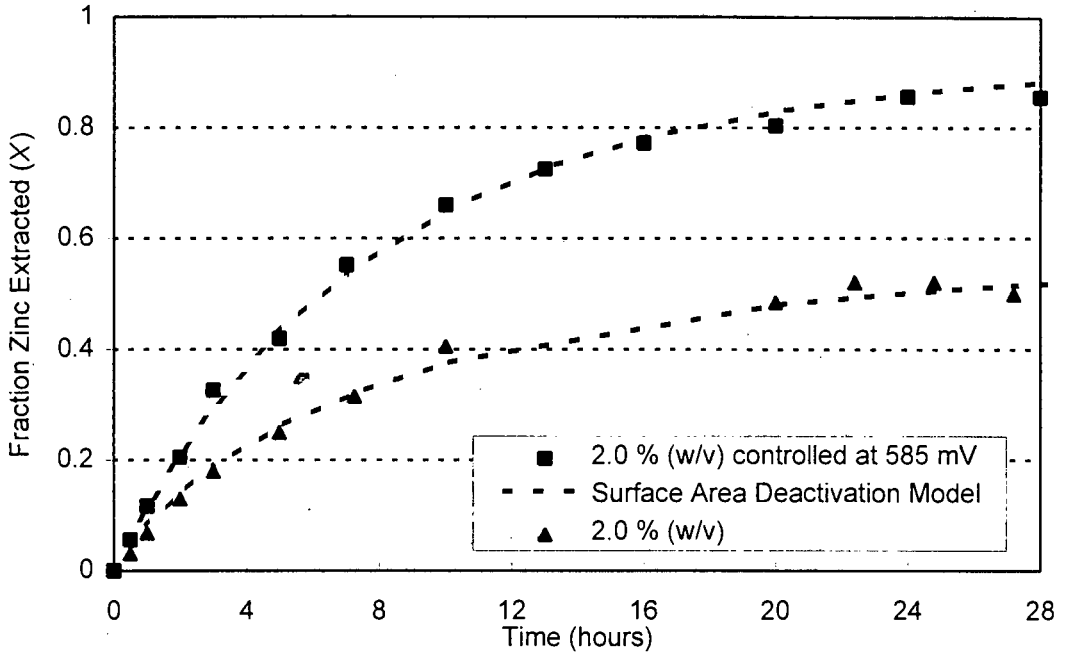

Figure 5-18 The overall conversion of zinc is increased if the solution redox potential is controlled.

5.3 The Effect of the Addition of Pyrite to a Chemical Leach of Sphalerite

The following experiments were performed to determine whether the addition of pyrite would enhance the leaching of sphalerite. Pyrite, of size fraction -53+45 μm, was added to a sphalerite concentrate of size fraction -106+90 μm. These size fractions were based on the work of Natarajan (1988) who showed that a smaller anodic surface area (i.e. the sphalerite surface area) in contact with a larger cathodic surface area enhanced the rate of reaction (discussed in the literature review in Chapter 2.5.3). The redox potential was controlled at 585 mV (vs Ag/AgCl) and the temperature was kept constant at 40.5 °C. Figure 5-19 shows the results of these experiments where the amount of sphalerite is kept constant and the amount of pyrite added is varied.

The results show that the addition of a pyrite concentrate to the leaching system does not have any direct effect on the dissolution rate of the sphalerite or the overall fraction of zinc extracted from the sphalerite.

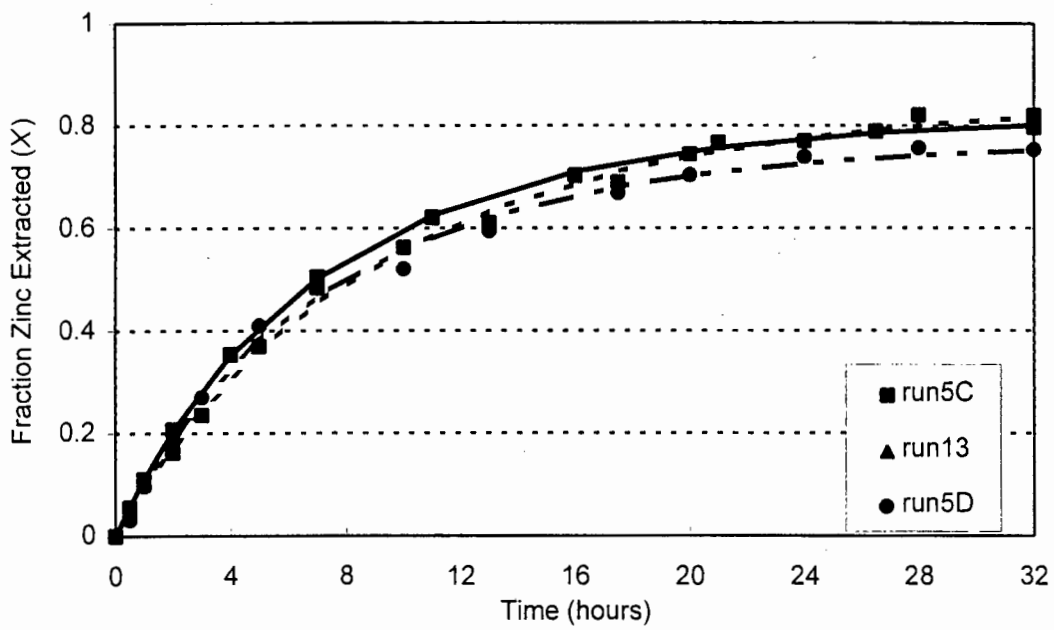

Figure 5-19 The effect of the addition of pyrite in trace amounts to the extraction of zinc.

Table 5-6 is a summary of the experimental conditions and results for the data plotted in Figure 5-19.

EXPERIMENT NUMBER	ZnS ADDED g	FeS_2 ADDED g	RATIO OF MINERAL	k_{CR} (hours^{-1})	k_I (hours^{-1})
5 C	15.00	1.50	0.1	0.09816	0.06658
5 D	15.00	0.15	0.01	0.11120	0.09474
13	15.00	0.00	0	0.12057	0.09123

Table 5-6 The conditions of experimental results shown in Figure 5-17 and the reaction rate constants evaluated from this plot.

The chemical reaction rate constant and the surface area deactivation rate constant were calculated using the Surface Area Deactivation Model. The surface area deactivation rate constant calculated for experiment numbered 5C is lower than the other two surface area deactivation rate constants (Table 5-6). This means that the apparent effect deactivation of the mineral surface was lower because the fraction of zinc measured in the solution was still increasing during prolonged leach periods thus

indicating that the dissolution reaction was not complete. This was attributed to the pyrite dissolution at a later stage than the sphalerite and the zinc within the pyrite increasing the fraction of zinc in solution. These results imply that the rate of pyrite dissolution in the presence of sphalerite was retarded.

The rest potential of sphalerite is -240 mV in a 1 M H_2SO_4 solution at 25°C (Attia and El Zeky, 1991). Under the same conditions, the rest potential of pyrite is 630 mV. This large difference between the rest potentials of pyrite and sphalerite indicates that possible galvanic interactions may occur if they are in contact with each other (Natarajan, 1988). However, the results of this experiment show that when added in trace amounts, pyrite does not seem to have any direct effect on the rate of dissolution of sphalerite.

These experiments were carried out under conditions where the ratio of pyrite to sphalerite was relatively small. Natarajan (1988) did similar work but the ratio of pyrite to sphalerite was at least ten times more than in this study. He showed that the ratio of the relative surface area of the anode (sphalerite) to the surface area of and the cathode (pyrite) was a controlling factor in the selective oxidation rates. He demonstrated that the larger the ratio of pyrite to sphalerite, the higher the expected rate of dissolution of the sphalerite. Comparing those results with the results from the experimental conditions of this study an expected increase in the rate of dissolution of sphalerite in the presence of trace amounts of pyrite cannot be expected as the amounts of pyrite used are too small.

However, the results show that in the last eight hours of experimentation, the amount of zinc in solution (Zn^{2+}) increased more than expected when compared to the results from previous experiments. This observation can be attributed to the dissolution of the pyrite, and in turn, the release of the zinc present within the pyrite ore. Thus the increased fractions of zinc measured during prolonged leach periods resulted partially from zinc released by pyrite.

These results support the theory that selective leaching may occur in a mixed sulphide ore where the one mineral acts as the anode and the other as the cathode. This is further supported by the fact that the surface deactivation rate constant for experiment 5C was smaller than those calculated from the other two experiments. However, the expected increase in the rate of dissolution is not apparent. The chemical reaction rate constant does not increase with increasing amounts of pyrite present.

EXPERIMENT NUMBER	ZnS ADDED g	FeS_2 ADDED g
15	15.00	0.00
5A	7.50	7.50

Table 5-7 The mixing ratios of the sulphide concentrates.

The total solids concentration was varied for a mixture of pyrite and sphalerite using the same weight ratio. These results were compared with the data obtained in Chapter 5.2. The redox potential was not controlled by the addition of hydrogen peroxide for these experiments. Figures 5-18 to 5-20 shows the results. Table 5-7 is a summary of the different mixing ratios of the sulphide concentrates, the results of which are shown in Figure 5-20.

Figure 5-20 shows the difference in the extent of conversion of zinc where pyrite was added in the same weight ratio as sphalerite, and where no pyrite was added. The solids concentration is the same for both experiments (10 $g.\ell^{-1}$ solids or 1.0 % w/v). For the experiment labelled 5A, the overall conversion of zinc was higher. This can be explained by the fact that there was half the amount of sphalerite available for reaction in experiment 5A as opposed to experiment 15. As the initial amount of solid available for the dissolution reaction was the same, the limiting factor in the overall extent of dissolution is the available ferric iron as the reaction proceeds.

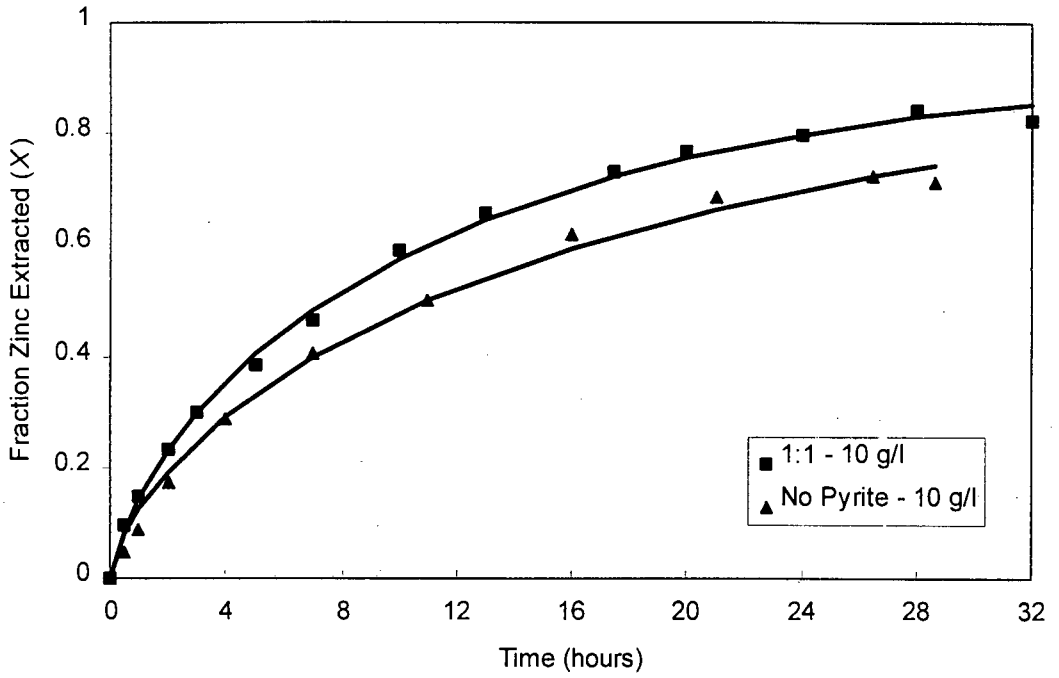

Figure 5-20 A plot of the extent of fractional conversion of sphalerite showing the difference where pyrite in the same weight ratio (10 g.ℓ^{-1} or 1.0 % w/v) as sphalerite was added, and where no pyrite was added.

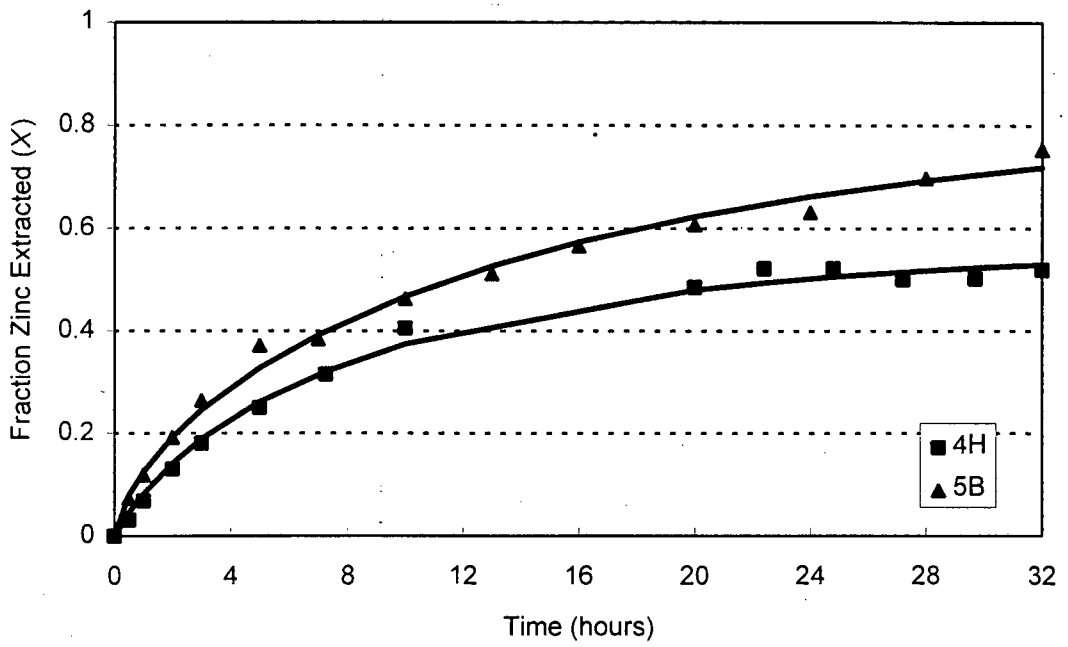

Figure 5-21 A plot of the extent of fractional conversion of sphalerite showing the difference where pyrite in the same weight ratio (20 g.ℓ^{-1} or 2.0 % w/v), as sphalerite was added, and where no pyrite was added.

Figure 5-21 supports the contention that the amount of ferric iron available for the dissolution reaction was limiting. For the same solids concentration (20 $g.\ell^{-1}$ solids or 2.0 % w/v), where pyrite was added in the same mass ratio as sphalerite, the overall extraction of zinc was higher.

If the amount of ferric iron available for the dissolution reaction was not limiting, then it would be expected that the addition of pyrite of the same mass weight of sphalerite would increase the rate of dissolution of sphalerite. Figure 5-22 shows the results of two experiments at the following mixing ratio:

EXPERIMENT NUMBER	ZnS ADDED g	FeS_2 ADDED g
15	15.00	0.00
5B	15.00	15.00

Table 5-8 The mixing ratios of the sulphide concentrates.

This plot (Figure 5-22) showed that there is no difference in the extent of dissolution of sphalerite. This result confirms that the addition of pyrite does not increase the rate of dissolution of sphalerite or the overall fraction of zinc extracted. This can apparently be attributed to a low level of contact between the sphalerite particles and pyrite particles, i.e., the probability of a sphalerite particle touching a pyrite particle decreases as the amount of pyrite added decreases. Another contributing factor would appear to be duration of contact: once contact occurs, the duration of that contact may not be long enough to allow sufficient charge transfer.

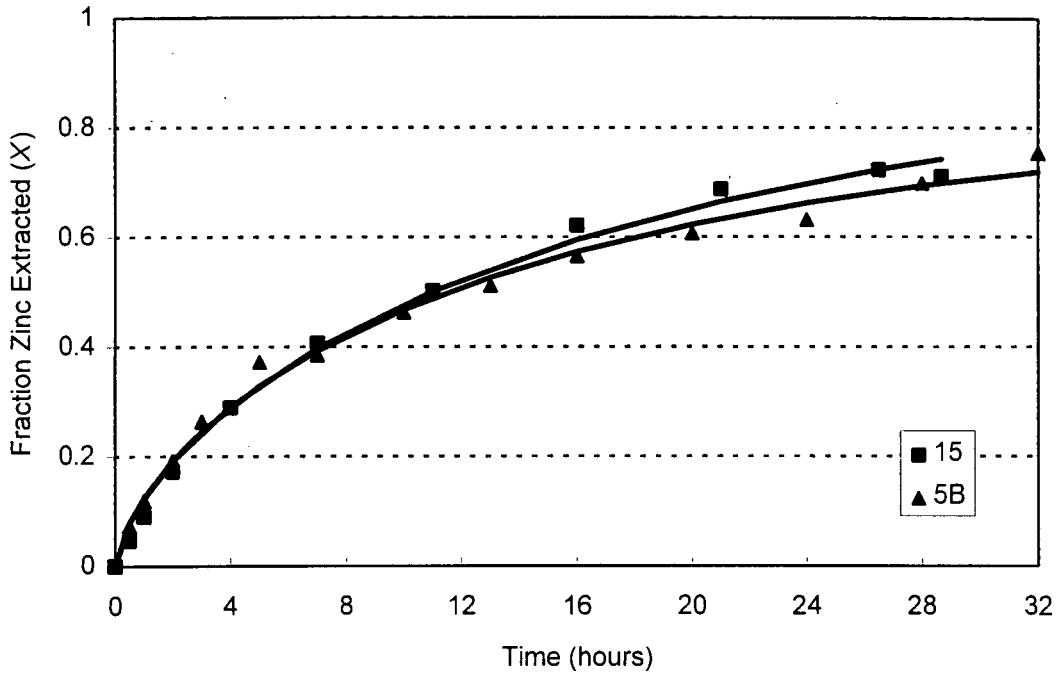

Figure 5-22 A plot of the extent of fractional conversion of sphalerite showing the difference where pyrite in the same weight ratio (10 g.ℓ^{-1} or 1.0 % w/v), as sphalerite was added, and where no pyrite was added.

5.4 Ferric Leaching of Sphalerite in Direct Contact with Pyrite and the Effect of the Galvanic Interactions

The ore used for these experiments was that hand-picked from the Pyrrhotite zone with zinc sulphide finely disseminated throughout each rock (ore sample E), the bore core samples from the Pyrrhotite zone (ore sample F) and the Gamsberg concentrate (ore sample G). The chemical analysis of these three samples is given in Table 4-1. The XRD analysis, which determines the relative amount of each mineral in each ore sample, is as follows:

ORE SAMPLE	MINERALOGICAL ANALYSIS (%)	
	SPHALERITE ZnS	PYRITE FeS_2
E	31.3	8.6
F	10.7	16.2
G	9.3	7.8

Table 5-9 The mineralogical analysis of the different ores used in the experimental work.

The results of the extent of the leaching of the zinc from these different ore samples are shown in Figure 5-23. These results show that as the ratio of sphalerite to pyrite increases, the initial rate of the reaction of sphalerite increases. The overall extent of conversion of the sphalerite from samples E, F and G were higher than that of the sphalerite concentrate. The chemical reaction rate constants and the surface area deactivation rate constants calculated by the Surface Area Deactivation Model are given in Table 5-9. It can be seen that the values of the chemical reaction rate constant were greater for the ore samples E, F and G than for the sphalerite concentrate (ore sample B).

EXPERIMENT NUMBER	ORE TYPE	k_{CR} ($hours^{-1}$)	k_I ($hours^{-1}$)
6 A	E	0.19749	0.10530
6 B	F	0.18075	0.10534
6 C	G	0.15915	0.09660
2 b	B	0.12604	0.07460

Table 5-10 The reaction rate constants calculated from the Surface Area Deactivation Model for the data presented in Figure 5-23.

The surface area deactivation rate constants are approximately equal for the ore samples E, F and G, whereas the surface area deactivation rate constant for the sphalerite concentrate (ore sample B) is much lower. It was assumed that ore samples, E, F and G had a large majority of particles that were each made up of

sphalerite, pyrite and to a lesser extent pyrrhotite. This meant that the minerals were in direct contact with one another and so the possibility of galvanic interactions as a result of contact was increased when compared to the experiments where mineral concentrates were added together. The results of the extent of the leaching of the zinc from these different ore samples are shown in Figure 5-23.

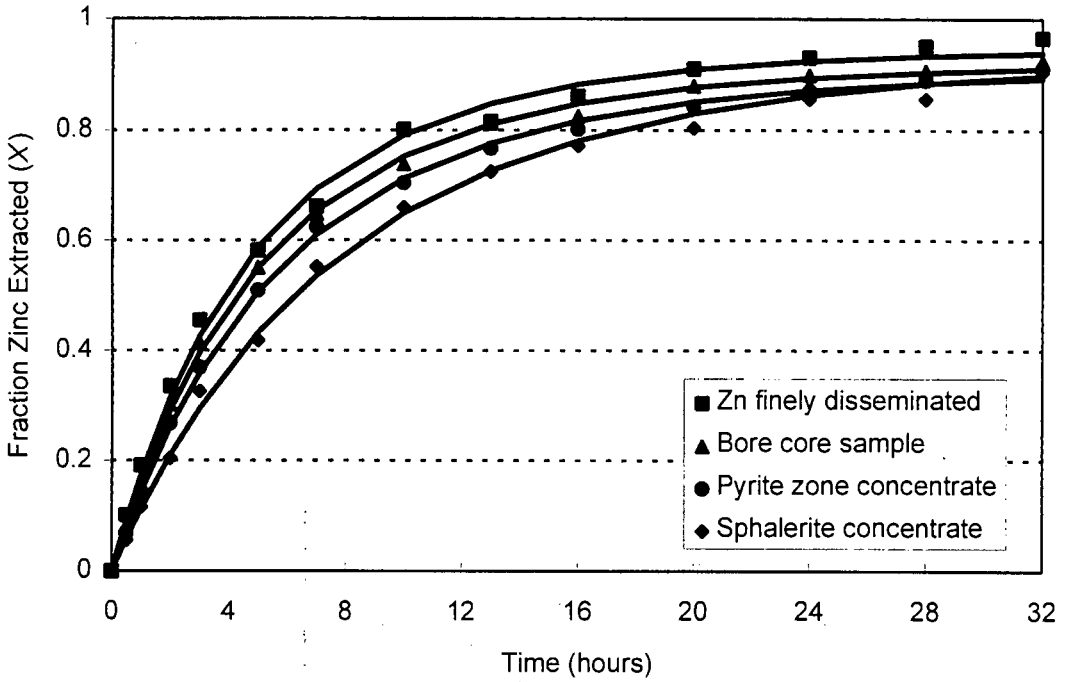

Figure 5-23 The dissolution of the ore where the sulphide minerals present are in direct contact with one another.

These results imply that the presence of pyrite in direct contact with the sphalerite does increase the initial chemical reaction rate.

The work of Natarajan (1988) showed that the greater the amount of pyrite in contact with sphalerite, the higher the rate of dissolution of the sphalerite became. If this is considered, a higher rate of dissolution of sphalerite is expected if the ratio of pyrite to sphalerite is large. However, the results show that as the ratio of pyrite to sphalerite is decreased, the rate of reaction also increases and the overall extent of dissolution of sphalerite is not influenced. This contradiction in the results can be attributed to the difference in experimental procedures followed. Natarajan (1988) leached a mixture of sphalerite and pyrite in a shake flask and did not control the solution redox potential, whereas the redox potential was controlled during the experiments performed in this study.

5.5 The Nature of the Products Formed and Their Influence on Reaction Kinetics

All the ore used for the experimentation work was investigated using a scanning electron microscope (SEM). Both fresh and leached samples were studied and the nature of the products formed were analysed using XRD analytical techniques.

Photomicrographs 1 and 2 show the Gamsberg pyrrhotite concentrate before and after it was conditioned with Na_2S. Photomicrographs 3 to 9 show the sphalerite concentrate at different stages of the leaching process. Photomicrographs 11 and 12 show the leached sample.

Photomicrograph 1 is a photomicrograph of the fresh sample of the pyrrhotite concentrate of size fraction -75+53 μm. The fresh sample is covered with a fine layer of oxidised material and a large number of particles adhering to the mineral surface. This can be compared with the ore sample shown in Photomicrograph 2 that was conditioned with Na_2S. The particle surface was clean and any oxidised mineral had been sulphidised.

Photomicrographs 3 to 5 are the photomicrographs of the sphalerite concentrate at different stages of the dissolution process at a solution temperature of 35 °C; and photomicrographs 6 to 8 are the photomicrographs of the sphalerite concentrate at different stages of the dissolution process at a solution temperature of 45 °C. Both sets of photomicrographs show that the surface gradually becomes covered with a product layer as the mineral becomes more leached by the ferric sulphate medium. The photomicrograph shows that the layer surrounds each particle. The layer was confirmed to be sulphur by XRD analysis of this product layer (see Appendix I).

The formation of the sulphur layer is shown in Photomicrograph 9 and Photomicrograph 10. Although the sulphur layer was assumed to be porous, (Jin et al.; 1984; Rath et al., 1988; Crundwell, 1988b) it is assumed to deactivate the mineral surface by filling the crevices and pits that are formed by leaching (Photomicrographs 11 and 12).

Photomicrograph 1 A fresh sample of the Gamsberg pyrrhotite concentrate of size fraction -75+53 µm.

Photomicrograph 2 The ore sample shown in Photomicrograph 1 after it was conditioned with Na_2S.

Photomicrograph 3 The sphalerite concentrate (size fraction -75+53 μm) after one hour of leaching at 35 °C.

Photomicrograph 4 The sphalerite concentrate (size fraction -75+53 μm) after twenty four hours of leaching at 35 °C.

Photomicrograph 5 The sphalerite concentrate (size fraction -75+53 μm) after thirty two hours of leaching at 35 °C.

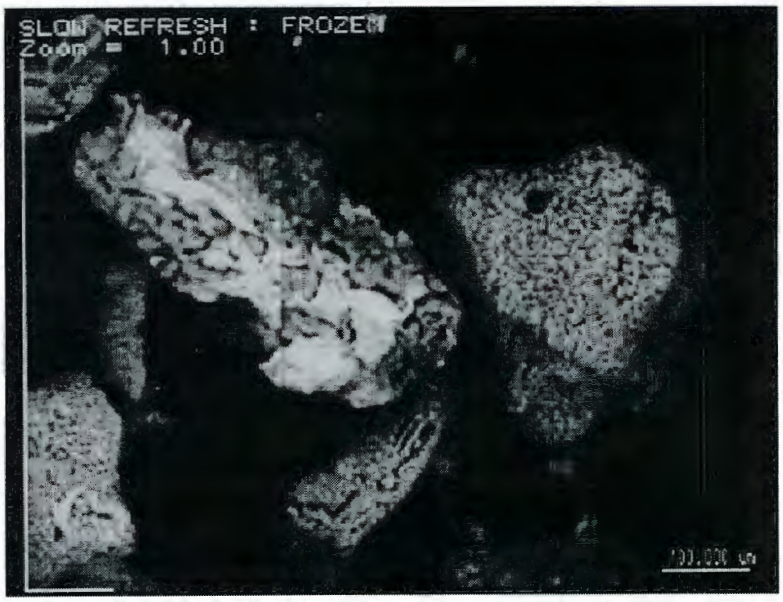

Photomicrograph 6 The sphalerite concentrate (size fraction -75+53 μm) after one hour of leaching at 45 °C.

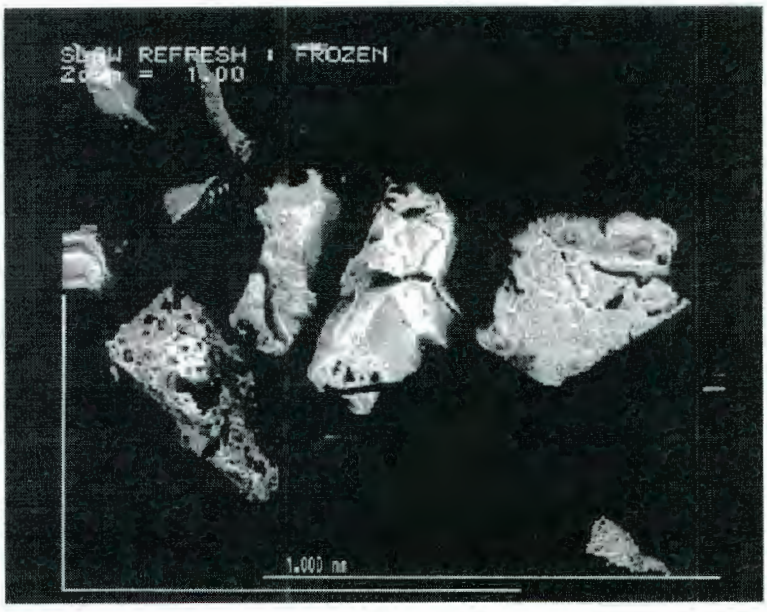

Photomicrograph 7 The sphalerite concentrate (size fraction -75+53 μm) after twenty four hours of leaching at 45 °C.

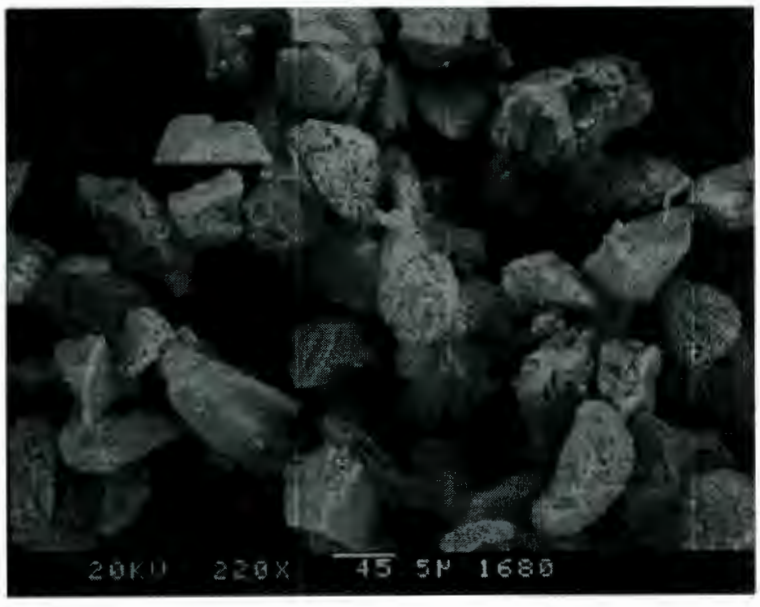

Photomicrograph 8 The sphalerite concentrate (size fraction -75+53 μm) after thirty two hours of leaching at 45 °C.

Photomicrograph 9 Sulphur formation of the sphalerite particles after thirty two hours of leaching.

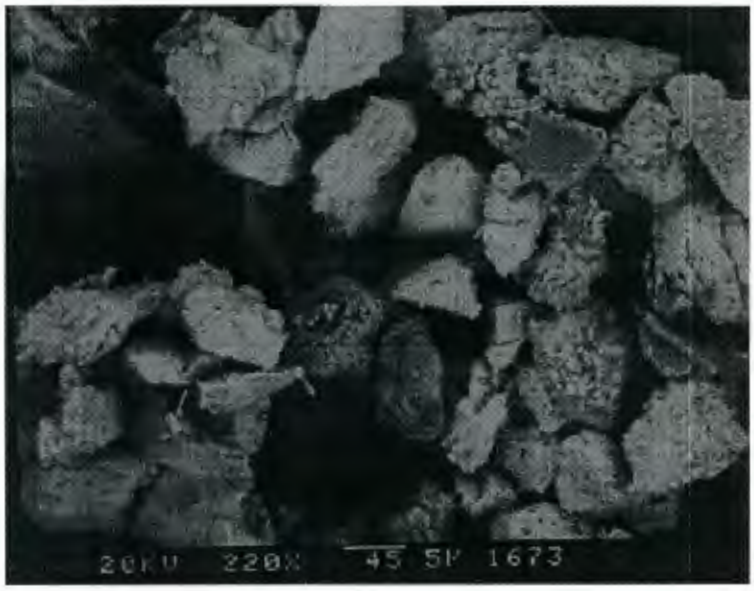

Photomicrograph 10 Massive sulphur formation of the sphalerite particles after thirty two hours of leaching.

Photomicrograph 11 The sphalerite concentrate after leaching for thirty two hours at 40 °C showing the altered mineral surface caused by the dissolution process.

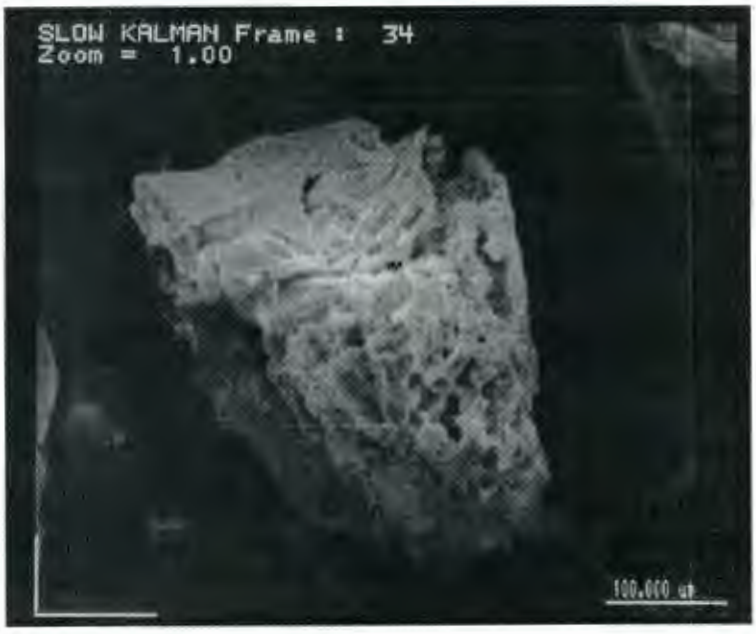

Photomicrograph 12 Single sphalerite particle showing pits and crevices that form due to chemical leaching.

6. CONCLUSIONS

The literature review emphasised the need to investigate the following:

- the chemical oxidation of sphalerite in a sulphate medium for prolonged leach periods;
- the presence of other sulphide minerals in trace amounts and the effect they have in a chemical leaching system;
- the nature of the products formed where ferric sulphate is used as the main constituent of the leach medium and their influence on reaction kinetics.

In order to investigate these issues, the following objectives were determined for this study:

1. to define a kinetic model for the chemical leaching of zinc from a sphalerite concentrate;
2. to investigate the sub-process of chemical oxidation of sphalerite by ferric iron and to test the applicability of the model defined;
3. to determine the overall effect of the galvanic interactions inherent in a multi-sulphide system and to determine whether the data can be modelled in terms of the model developed for the sphalerite concentrate.

6.1 The Kinetic Model for the Chemical Leaching of Zinc from a Sphalerite Concentrate

The Surface Area Deactivation Model that assumes that the surface area decreases as leaching progresses was an adequate fit of the data. The use of this model was verified by modelling the data presented by Crundwell (1988b) on the ferric sulphate leaching of the Gamsberg sphalerite concentrate.

The results obtained by the application of the Surface Area Deactivation Model confirmed the results of the experimental investigation of Crundwell (1988b). He investigated the kinetics of the dissolution of sphalerite in terms of the iron concentration within the crystal lattice and the transfer of charge at the phase boundary.

6.2 The Sub-Process of Chemical Oxidation of Sphalerite by Ferric Iron

The Surface Area Deactivation Model was used to determine the reaction rate constants from the experimental results. These constants were evaluated in terms of the activation energy of the reaction, the influence of the size of the leaching particle and the dependence of the concentrations of the ferric iron and ferrous iron in solution.

The values of the activation energy calculated from the reaction rate constants suggested that the chemical reaction is the rate-limiting step throughout the leaching process. These results confirmed the assumption made by the Surface Area Deactivation Model that the surface area deactivation process is independent of the chemical reaction.

The rate at which the dissolution reaction proceeded increased as the initial particle size decreased. The Surface Area Deactivation Model predicted that for prolonged leach periods, particles with different initial particle size will dissolute to the same extent and that the sphalerite will never undergo complete dissolution. A surface area oxidation rate was applied to the leaching data. This showed that the surface rate of dissolution was constant for all particles of different initial size.

The effect of the surface area deactivation term was less for large particles than for small particles. However, the apparent effect of this term was greater for larger particles because of the smaller surface area available for the chemical reaction. This explained the phenomenon in the literature (Bobeck and Su, 1985) that for chemical leaching of a sphalerite concentrate, the rate-limiting step apparently changed from the chemical reaction at the mineral surface to a diffusion limited reaction.

The rate of dissolution of the sphalerite is dependent on the initial concentration of the ferric iron in solution if the redox potential is not controlled by oxidising the ferrous iron to ferric iron. However, if the ferric iron is regenerated continuously,

then the chemical reaction is not limited by the amount of ferric iron available for the chemical reaction.

The rate of the chemical reaction increased linearly with increasing solution redox potential. At redox potentials greater than approximately 520 mV (vs Ag/AgCl) the dependence of the reaction rate constants on the redox potential changed but remained linear. This was explained in terms of the theory developed by Crundwell (1988b) that the chemical reaction was dependent on the solution equilibrium and the ionic species responsible for transfer of charge. This phenomenon was also observed for the change in the rate of reaction when the ferrous iron was not oxidised to ferric iron. The extent of dissolution of sphalerite was limited by the amount of ferric iron available for the leaching reaction.

This conclusion is supported by the results of leaching the sphalerite concentrate at different solids concentration (0.2 % to 2.0 % w/v) and not controlling the redox potential. As the solids concentration increased, the overall dissolution of sphalerite decreased because of the limiting effect of the ferric iron available for the reaction.

6.3 The Overall Effect of the Galvanic Interactions Inherent in a Multi-Sulphide System

Pyrite concentrate was added in trace amounts to the sphalerite concentrate. The addition of pyrite in small amounts did not have any direct effect on the rate of dissolution. However, the amount of zinc in solution did increase in the later stages of the dissolution reaction. This was attributed to the pyrite dissolution and in turn, to the zinc present in the pyrite. This supported the phenomenon of selective leaching of two minerals, having different rest potentials, in contact with each other. Pyrite, added to sphalerite in equal mass ratios, does not increase the rate of dissolution of sphalerite.

The extent of dissolution of sphalerite was not influenced by the addition of pyrite and so the Surface Area Deactivation Model was applied to the data presented.

For ore samples that had a large majority of particles each made up of sphalerite, pyrite and pyrrhotite, the extent of conversion increased as the amount of sphalerite increased. When compared to the sphalerite concentrate, the overall extent of conversion increased because of the observed increase in the rate of dissolution.

The Surface Area Deactivation Model was applied to the leaching data. However, the chemical reaction rate constant and the surface area deactivation rate constant are now a function of the sum of the oxidation kinetics of sphalerite, pyrite, pyrrhotite and the rate of transfer of charge from one mineral to the next.

6.4 The Products Formed and their Influence on the Dissolution Process

The SEM photographs show the need for the mineral surface area deactivation term to be included in the model derivation so that the data for leaching for prolonged periods can be modelled. However, this may have to be revised in the case of bacterial leaching as the bacteria may attack the products formed during the leaching reaction. This would ensure that the mineral surface is not covered or deactivated by the products as the leaching process proceeds.

6.5 Recommendations for Further Work

The kinetic model proposed must be applied to sphalerite concentrates from different origins to determine whether or not a common chemical reaction rate constant and surface area deactivation rate constant can be applied. This model can then be extended to the modelling of the kinetics of dissolution of other mineral sulphides.

The Surface Area Deactivation Model describes the kinetics of the ferric leaching of sphalerite. It must be tested in the presence of bacteria. This would help establish the role of the bacteria using ferric sulphate to leach sulphide minerals. From this, the bacterial leaching kinetics can be determined and then modelled.

Galvanic interactions or the transfer of charge due to particles being in direct contact with each other must be quantified to determine the extent of dissolution caused by this. This would establish the kinetics of a mixed mineral system. This can then be extended to the addition of bacteria from which an overall reaction kinetics can be determined.

REFERENCES

1. Attia, Y.A. and El-Zeky, M. (1990) Effects of Galvanic Interactions of Sulfides on Extraction of Precious Metals from Refractory Complex Sulfides by Bioleaching; **International Journal of Mineral Processing**, Vol 30, 99-111.

2. Bailey, A.D. (1993) An Assessment of Oxygen Availability, Iron Build-up and the Relative Signifiance of Free and Attached Bacteria as Factors Affecting Bio-oxidation of Refractory Gold-Bearing Sulphides at High Solids Concentrations; PhD Thesis: University of Cape Town, South Africa.

3. Bailey, A.D. and Hansford, G.S. (1993) Factors Affecting Bio-Oxidation of Sulphide Minerals at High Concentrations of Solids: A Review; **Biotechnology and Bioengineering**, Vol 42, 1164-1174.

4. Berry, V.K.; Murr, L.E. and Hiskey, J.B. (1978) Galvanic Interaction Between Chalcopyrite and Pyrite During Bacterial Leaching of Low-Grade Waste; **Metallurgical Transactions B: Process Metallurgy**, Vol 3, 309-326.

5. Bobeck, G.E. and Su, H. (1985) The Kinetics of Dissolution of Sphalerite in Ferric Chloride Solution; **Metallurgical Transactions B: Process Metallurgy**, Vol 16, 413 - 424.

6. Boon, M. and Heijnen, J.J. (1993) Mechanisms and Rate Limiting Steps in Bioleaching of Sphalerite, Chalcopyrite and Pyrite with *Thiobacillus Ferrooxidans;* In: **Biohydrometallurgical Technologies** (Eds: A.E. Torma, J.E. Wey, V.L. Lakshmanan), The Minerals, Metals and Materials Society, 217-235.

7. Brierley, C.L. (1978) Bacterial Leaching; **Critical Reviews in Microbiology**; Vol 6, Issue 3, 207-262.

8. Bryner, L.C. and Anderson, R. (1957) Microorganisms in Leaching Sulphide Minerals; **Industrial and Engineering Chemistry**, Vol 49, No. 10, 1721-1724.

9. Buehler, H.A. and Gottschalk, V.H. (1910) **Economic Geolology**, Vol 5, 28-35.

10. Chapman, J.T (1989) The Batch and Continuous Bacterial Leaching Kinetics of a Refractory Gold-Bearing Pyrite Concentrate; MSc Thesis: University of Cape Town, South Africa.

11. Crundwell, F.K. (1987) Kinetics and Mechanism of the Oxidative Dissolution of a Zinc Sulphide Concentrate in Ferric Sulphate Solution; **Hydrometallurgy**, Vol 19, 227 - 242.

12. Crundwell, F.K. (1988a) Effect of Iron Impurity in Zinc Sulphide Concentrates on the Rate of Dissolution; **American Institute of Chemical Engineering Journal**, Vol 34, No. 7 1128 - 1134.

13. Crundwell, F.K. (1988b) The Role of Charge-Transfer Mechanisms in the Oxidative and Non-Oxidative Dissolution of Sphalerite; PhD Thesis: University of the Witwatersrand, South Africa.

14. Dry, M.J. (1985) PhD Thesis: University of the Witwatersrand, South Africa.

15. Dry, M.J. and Bryson, A.W. (1988) Prediction of Redox Potential in Concentrated Iron Sulphate Solutions; **Hydrometallurgy**, Vol 21, 59 - 72.

16. Dutrizac, J.E.and MacDonald, R.J.C. (1973) Kinetics of Cubanite, and Effect NaCl Additions on Rate of Dissolution of Cubanite and Chalcopyrite in Acidified Ferric Sulphate Solutions; **Canadian Metallurgical Quarterly**, Vol 12, 409-420.

17. Dutrizac, J.E., and MacDonald, R.J.C. (1978) The Dissolution of Sphalerite in Ferric Chloride Solutions; **Metallurgical Transactions B: Process Metallurgy**, Vol 9, 543 - 551.

18. Gormely, L.S.; Duncan, D.W.; Branion, R.M.R. and Kinder, K.L. (1975) Continuous Culture of *Thiobacillus ferrooxidans* on a Zinc Sulphide Concentrate; **Biotechnology and Bioengineering**, Vol 17, 31-49.

19. Gottschalk, V.H. and Buehler, H.A. (1912) **Economic Geology**, Vol 7, 15-34.

20. Graham, R. (1993) Gamsberg Zinc Column Leaches; Suggested Zinc Dissolution Mechanism. Goldfields Research Laboratories, Southdale, Johannesburg, Memorandum.

21. Hansford, G.S. and Chapman, J.T. (1992) Batch and Continuous Bio-oxidation Kinetics of a Refractory Gold-Bearing Pyrite Concentrate; **Minerals Engineering**, Vol 5, No 6, 597-612.

22. Hansford, G.S. and Bailey, A.D. (1992) The Logistic Equation for Modelling Bacterial Oxidation Kinetics; **Minerals Engineering**, Vol 5, No's.10-12, 363-369.

23. I, T-P and Nancollas, G.H. (1972) EQUIL - A General Computational Method for the Calculation of Solution Equilibria; **Analytical Chemistry,** Vol 44, 1940 - 1950.

24. Jin, Z-M; Warren, G.W. and Henein, H. (1984) Reaction Kinetics of the Ferric Chloride Leaching of Sphalerite - an Experimental Study; **Metallurgical Transactions B: Process Metallurgy**, Vol 15, 5 - 12.

25. Jin, Z-M; Warren, G.W. and Henein, H. (1985) Reaction Kinetics and Electrochemical Model for the Ferric Chloride Leaching of Sphalerite; In: **Proceedings of the International Symposium of Extractive Metallurgy of Zinc** (Eds: K.Towaza), Mineralogical and Metallurgical Institute of Japan, 111 - 125.

26. Jyothi, N.; Sudha, K.N. and Natarajan, K.A. (1989) Electrochemical Aspects of Selective Bioleaching of Sphalerite Chalcopyrite from Mixed Sulphides; **International Journal of Mineral Processing**, Vol 27, No 3-4, 189-203.

27. Komnitsas, C. and Pooley, F.G. (1990) Optimisation of the Bacterial Oxidation of an Arsenical Gold Sulphide Concentrate from Olympias, Greece; **Minerals Engineering**, Vol 3, No. 3-4, 295-306.

28. Levenspiel, O. (1972) **Chemical Reaction Engineering**, John Willey and Sons, USA.

29. Lochmann, J. and Pedlik, M. (1995) Kinetic Anomolies of Dissolution of Sphalerite in Ferric Sulfate Solution; **Hydrometallurgy**, Vol 37, 89-96.

30. Majima, H. (1969) How an Oxidant Affects Selective Flotation of Complex Sulphide Ores; **Canadian Metallurgical Quarterly**, Vol 8, 269-273.

31. Malouf, E.E. and Prater, J.D. (1968) The Effects of Environment on Bacterial Leaching Rates; **Proceedings - Australasian Institute of Mining and Metallurgy**, Vol 225, 15-.

32. Marchant, P.B. (1986) Commercial Piloting and the Economic Feasibility of Plant Scale Continuous Tank Leaching at Equity Silver Mines Limited; In: **Fundamental and Applied Biohydrometallurgy**, (Eds: R.W.Lawrence; R.M.R.Branion; H.G.Ebner), Elsevier, Amsterdam, 53-76.

33. Mehta, A.P. and Murr, L.E. (1982) Kinetic Study of Sulfide Leaching by Galvanic Interaction between Chalcopyrite, Pyrite and Sphalerite in the Presence of *T. ferrooxidans* (30°C) and a Thermophilic Microorganism (55°C); **Biotechnology and Bioengineering**, Vol 24, 919-940.

34. Mehta, A.P. and Murr, L.E. (1983) Fundamental Studies of the Contribution of Galvanic Interaction to Acid-Bacterial Leaching of Mixed Metal Sulfides; **Hydrometallurgy**, Vol 9, 235-256.

35. Morin, D.; Gaunand, A. and Renon, H. (1985) Representation of the Kinetics of Leaching of Galena by Ferric Chloride in Concentrated Sodium Chloride Solutions by a Modified Mixed Kineics Model; **Metallurgical Transactions B: Process Metallurgy**, Vol 16, 31 - 39.

36. Murr, L.E. (1980) Theory and Practice of Copper Sulphide Leaching in Dumps and In-Situ; **Minerals Science and Engineering**, Vol 12, No. 3, 121-189.

37. Nagata,S. (1975) **Mixing: Principles and Applications**, Kodansha Ltd., Halstead Press, Japan.

38. Natarajan, K.A. (1988) Electrochemical Aspects of Bioleaching Multisulphide Minerals; **Minerals and Metallurgical Processing**, Vol 5, No. 2, 61-65.

39. Natarajan, K.A. and Iwasaki, I. (1983) Role of Galvanic Interactions in the Bioleaching of Duluth Gabbro Copper-Nickel Sulfides; **Separation Science and Technology**, Vol 18, No 12-13, 1095-1111.

40. Natarajan, K.A. (1992a) Electrobioleaching of Base Metal Sulphides; **Metallurgical Transactions B: Process Metallurgy**, Vol 23, Part 1, 5-11.

41. Natarajan, K.A. (1992b) Bioleaching of Sulphides under Applied Potentials; **Hydrometallurgy**, Vol 29, No 1-3, 161-172.

42. Nicol, M.J. (1993) The Role of Electrochemistry in Hydrometallurgy; Plenary Lecture: IV International Symposium on Hydrometallurgy, Salt Lake City.

43. Palencia-Perez, I. and Dutrizac, J.E. (1991) The Effect of the Iron Content of Sphalerite on its Rate of Dissolution in Ferric Sulphate and Ferric Chloride Media; **Hydrometallurgy**, Vol 26, 211 - 232.

44. Peters, E. and Majima, H. (1968) The Physical Chemistry Of Leaching Sulphide Minerals; Paper Presented at the 97th Annual Meeting, **AIPIE**, New York.

45. Pitzer, K.S.; Roy, R.N. and Sylvester, L.F. (1977) Thermodynamics of Electrolytes. 7. Sulfuric Acid; **Journal of the American Chemical Society**, Vol 99, 4930 - 4936.

46. Rath, P.C.; Paramguru, R.K. and Jena, P.K. (1988) Kinetics of Dissolution of Sulphide Minerals in Ferric Chloride Solution, 1: Dissolution of Galena, Sphalerite and Chalcopyrite; **Transactions of the Institute of Mining and Metallurgy**, Vol 97, 150 - 158.

47. Romankiw, L.T. and De Bryn, P.L. (1965) The Kinetics of Dissolution of Zinc Sulphide in Aqueous Sulphuric Acid; In: **Unit Operations in Hydrometallurgy** (Eds: M.Wadsworth), Gordon and Breach.

48. Rozendaal, A. (1982) The Gamsberg Zinc Deposit; Unpublished Work.

49. Rozendaal, A. (1986) The Gamsberg Zinc Deposit, Namaqualand District; **Mineral Deposits of Southern Africa**, 1477-1488.

50. Sakaguchi, H.; Silver, M. and Torma, A.E. (1976) Microbiol Leaching of a Chalcopyrite Concentrate by *Thiobacillus ferrooxidans*; **Biotechnology and Bioengineering**, Vol 18, 1091-1101.

51. Somasundaran, P. and Moudgil, B.M. (1988) **Reagents in Mineral Technology**, Marcel Dekker Incorporated, USA.

52. Su, H. (1976) The Kinetics on Dissolution of Sphalerite in Ferric Chloride Solutions; PhD Thesis: University of Idaho, USA.

53. Suni, J., Henein, H., Warren, G.W. and Reddy, D. (1989) Modelling the Leaching Kinetics of a Sphalerite Concentrate Size Distribution in Ferric Chloride Solution; **Hydrometallurgy**, Vol 22, 22 - 38.

54. Torma, A.E. and Bosecker, K. (1982) Bacterial Leaching; In: **Progress in Industrial Microbiology** (Eds: M.J.Bull), 77-118.

55. Torma, A.E. and Subramanian, K.N. (1974) Selective Bacterial Leaching of a Lead Sulphide Concentrate; **International Journal of Mineral Processing**, Vol 1, Part 2, 125-134.

56. Torma, A.E.; Walden, C.C. and Branion, R.M.R. (1970) Microbial Leaching of a Zinc Sulphide Concentrate; **Biotechnology and Bioengineering**, Vol 12, 501-517.

57. Torma, A.E.; Walden, C.C.; Duncan, D.W. and Branion, R.M.R. (1972) The Effect of Carbon Dioxide and Particle Surface Area on the Microbiological Leaching of a Zinc Sulphide concentrate; **Biotechnology and Bioengineering**, Vol 14, 777-786.

58. Verbaan, B. and Crundwell, F.K. (1986) An Electrochemical Model for the Leaching of a Sphalerite Concentrate; **Hydrometallurgy**, Vol 16, 345 - 359.

APPENDIX A

The Geology and Mineralogy of Gamsberg

The Gamsberg to which the zinc deposit is confined, is a steep-sided inselberg - 7 km long and 5 km across, rising by approximately 250 m from the general level of the surrounding plane. The flat top of the mountain has been eroded to form an internal basin. The base metal deposit is exposed as a prominent gossan along the inner periphery of this erosional basin (Rozendaal, 1986).

The mineralogically complex unit is known as the Gams Iron Formation. It is exposed along the inner periphery of the Gamsberg erosional basin and its stratigraphic width measures from 0 to 80 m. Variations in the thickness have been attributed to facies change, deformation and possibly to intraformational erosion.

The Gams Formation is further subdivided into the A, B and C members. The A and C members are not economically mineralised. The B member consists of the mineralised layer consisting of the complex sulphide ore. This layer has a gossan capping exposed for a strike length of 5300 m. The stratigraphic thickness of this layer varies from 0 to 50 m. A complete transition from gossan to sulphide takes place within 3 to 4 m (Rozendaal, 1986).

The stratabound Gamsberg ore body can be divided into three zones each characterised by certain mineralogical and/or geochemical criteria (Martin, 1989). They are known as the *Magnetite Ore Zone* - the base of a Banded Iron Formation - consisting of a high grade of zinc but also having a high manganese content; the *Pyrite Ore Zone* - the stratigraphic base of the ore zone - primarily consisting of pyrite and sphalerite with minor amounts of other iron sulphides; and the *Pyrrhotite Ore Zone* which consists of pyrrhotite, pyrite, sphalerite and minor amounts of galena. The main difference between the *Pyrite Ore Zone* and the *Pyrrhotite Ore Zone* is the presence of minor amounts of **graphite** in the former that has influenced precipitation of FeS_2 instead of $Fe_{1-x}S$.

Some important characteristics about each zone follow:

1. The *Magnetite Ore Zone*

- this is characterised by the presence of magnetite together with sphalerite;

- this always occurs at the base of the iron formation;
- pyrite and/or pyrrhotite are often present and when abundant may lead to the ore zone being misinterpreted;
- the immediate hanging wall is usually of the same rock-type except for the absence of sphalerite;
- from geochemical profiles, this zone has a higher grade than the other two zones;
- microprobe analysis of the sphalerite grain have an average of 57 % Zn and 0.83 % Mn.

2. The *Pyrrhotite Ore Zone*

- contact between the *Magnetite Ore Zone* and the *Pyrrhotite Ore Zone* is the contact between the iron formation and the metapelic assemblage at which point the magnetite disappears and the ore zone is characterised by the presence of abundant pyrrhotite and pyrite;
- this zone has undergone partial to severe degrees of alteration with which the occurrence of thallium is associated;
- the zinc grade is lower than the *Magnetite Ore Zone* but higher than the *Pyrite Ore Zone;*

3. The *Pyrite Ore Zone*

- transition from the *Pyrrhotite Ore Zone* to the *Pyrite Ore Zone* is marked by the sudden presence of graphite;
- the ore body is banded caused by the parallel trains of subidioblastic pyrite grains which have formed parallel to the bedding;
- the zinc and manganese content in this zone are lower than the other two zones.

APPENDIX B

The Shrinking-Core Model

Basic Assumptions

The following assumptions have been made in deriving the shrinking-core model:

- the mineral particles are considered to be spheres;
- the particles consist of a single mineral;
- the rate of mineral dissolution per unit solids surface area is constant throughout the leaching process;
- the number of particles per unit volume of solution does not change during leaching.

As the reaction rate is assumed to be directly proportional to the mineral surface area the following equation can be used to describe the dissolution process: (Boon and Heijnen, 1993)

$$\frac{d[MS]}{dt} = -k_A A_S \qquad [B\text{-}1]$$

where [MS] - metal sulphide concentration ($mol_{MS}.m^{-3}_{slurry}$)

t - time (s)

k_A - rate constant 1st order in surface reaction rate ($mol.m^{-2}.s^{-1}$)

A_s - specific particle area (m^2_{solid}/m^3_{slurry})

k_A may be described as $k_{A,\ sphere}$ or $k_{A,BET}$ depending on the method used for calculation of the particle surface area. Boon and Heijnen (1993) used the BET method for chemical leaching as they proposed that is was a more accurate method of measuring k_A as the chemical reaction area is better described by the BET surface area.

The decrease in volume (diameter) of the unreacted particle accompanying the disappearance of dM moles of the solid reactant can be described by: (Levenspiel, 1972):

$$-d\,M = \frac{-\pi\,\rho_{MS}\,d_o\,d\,d_o}{2} \qquad [\text{B-2}]$$

Writing M_{MS} in terms of the shrinking diameter where the decrease in the particle diameter is constant

$$\frac{d\,d_o}{d\,t} = \frac{2\,k_A M_{MS}}{\rho_{MS}} \qquad [\text{B-3}]$$

where d_o - particle diameter (m)
M_{MS} - molar weight of MS ($kg.mol^{-1}$)
ρ_{MS} - MS density ($kg.m^{-3}$)

Integration of this equation yields:

$$1 - (1 - X)^{1/3} = \frac{2\,k_A\,M_{MS}}{\rho_{MS}\,d_o}\,t \qquad [\text{B-4}]$$

In this equation k_A ($mol_{MS}.m^{-2}_{MS}.s^{-1}$) is dependent on process conditions.

APPENDIX C

The Nernst Equation

$$E = E^{o} + \frac{RT}{nF} \ln\left(\frac{[Fe^{3+}]}{[Fe^{2+}]}\right) \qquad [C\text{-}1]$$

where E is the redox potential
E^{o} is the standard redox potential
R is the gas constant
T is the temperature
F is the Faraday constant
$[Fe^{3+}]$ and $[Fe^{2+}]$ the concentrations of ferric iron and ferrous iron respectively

The Butler-Volmer Equation

$$j = j_{o}\left\{\exp\left(\frac{\alpha_{A} nF\eta}{RT}\right) - \exp\left(\frac{\alpha_{C} nF\eta}{RT}\right)\right\} \qquad [C\text{-}2]$$

where j is the experimental current density at redox potential E
j_{o} is the exchange current density
$a_{A/C}$ is the anodic/cathodic transfer coefficient
n is the number of electrons involved in the reaction
η is the overpotential

APPENDIX D

Other Reasearchers' Work

(See pages 112 and 113)

REFERENCE	AIM	MATERIAL	EQUIPMENT	pH	TEMPERATURE	REDOX POTENTIAL	ANALYSIS	OTHER
Bobeck and Su Huai (1985)	To study the important factors involved in the leaching of ZnS by ferric chloride and to determine whether the rate-determining step is the diffusion of Fe^{3+} through S°, the chemical reaction at the liquid-solid interface or a combination	ZnS concentrate 1) Zn 61.6% Fe 5.17% 2) Zn 64.2% Fe 6.25% 3) Zn 44.3% Fe 8.06%	1l Pyrex reaction flask fitted with temperature measurement, gas inlet, stirrer (15 rpm) condenser and sampling port	< 2.0 Controlled	317 - 363 K Controlled	-	Metallic elements by AA $[Fe^{2+}]$ by dichromate titration X-ray diffraction to verify S°	Ore washed in acetic acid
Jin *et al.* (1984)	To investigate the reaction mechanism for the dissolution of sphalerite concentration in ferric chloride	ZnS concentrate (from flotation) 90% ZnS Major impurity FeS_2	1l reaction vessel fitted with thermometer, condenser and sampling device	Initial pH 0.3 - 1.0	300 - 366 K Controlled	-	Zn by AA Residues - SEM, X-ray diffraction	Ore washed in Na_2S
Verbaan and Crundwell (1986)	To apply an electrochemical leaching model to dissolution of a sphalerite concentrate	Flotation concentrate (Gamsberg) Zn 60.9% Fe 9.1% S 30.8% Mn 2.5%	1) 10 l glass vessel fitted with robes for E_h, sampling 2) stainless steel stirred pressure reactor	0.7	298 - 368 K Controlled	Pt electrode; Ag/AgCl reference	$[Zn^{2+}]$ AA $[Fe_{TOTAL}]$ AA $[Fe^{3+}]$ Titration	BET surface area: 1471 m_2/kg
Crundwell (1987)	To understand the effect of the Fe^{3+}/Fe^{2+} redox couple by addition of Fe^{2+}	Flotation concentrate (Gamsberg) Zn 60.9% Fe 9.1% S 30.8% Mn 2.5%	2l cylindrical glass vessel fitted with baffles, impeller, condenser	1.0 - 1.5	298 - 368 K Controlled	with 30% H_2O_2 (SCE)	$[Fe_{TOTAL}]$ AA $[Fe^{3+}]$ Titration	Ore washed in Na_2S
Rath *et al.* (1988)	To establish kinetic data for the dissolution of sphalerite	Zn 49.62% Fe 10.86% Cu 0.2% S 37.0% Major part ZnS with traces of $CuFeS_2$, FeS_2	1l flanged corning reactor vessel fitted with stirrer, condenser, thermometer, sampling port	1.45	303 - 333 K Controlled	-	[Zn] AA X-ray diffraction $[Fe^{2+}]$ by dichromate titration	-
Suni *et al.* (1989)	To present a mathematical model (verified by experimental data) for the agitation leaching of mineral concentrates that have any type of size distribution	2 different concentrates % Zn Fe Cu A 60.9 3.6 0.7 B 57.3 5.3 0.1	1 and 2l baffled reactors fitted with thermometers, condenser, sampling device	0.3 - 1.0	T unknown Controlled	-	Chemical analysis by AA	Ore washed in Na_2S
Palencia-Perez and Dutrizac (1991)	To clarify the increase in leaching rate with increasing iron content in terms of its magnitude and form of the resulting curve	15 different samples Zn 67.6% - 51.5% Fe 0.04% - 14.7% S 33%	3l reactor fitted with stirrer, thermometer, sampling device	- (Boon 0.6)	323 - 363 K Controlled	-	[Zn] AA	-

REFERENCE	MODEL	REACTION CONDITIONS				CALCULATED PARAMETERS		VARIED ?
		MEDIUM	PARTICLE SIZE	SOLID-TO-LIQUID RATIO ($g.l^{-1}$)	$[Fe^{3+}]$ M	K (s^{-1})	E_A $kJ.mol^{-1}$	
Bobeck and Su Huai (1985)		Ferric chloride	-100 + 150 MESH	1 2 10	0.25	1.1×10^{-3} $cm.min^{-1}$ T = 44°C	60	Temperature Particle size Speed of impeller
Jin *et al.* (1984)	$1-(1-X)^{\frac{1}{3}} = \left[8.86x10^{3} r_o^{-1} [Fe^{3+}]^{0.5} \exp\left(\frac{-E_A}{RT}\right)\right] t$	Ferric chloride	-63 + 53 μm	1	0.2		68.4	Temperature Particle size Speed of impeller $[Fe^{3+}]$
Verbaan and Crundwell (1986)	$1-(1-X)^{\frac{1}{3}} = \left[\frac{6.605}{3M_o} A_o \exp(17.3E_h) \exp\left(\frac{-E_A}{RT}\right)\right] t$	Ferric sulphate	Varied	1	0.0179 0.0931 0.1719 0.4656 0.9382	1.1×10^{-4} 1.8×10^{-4} 2.5×10^{-4} 4.0×10^{-4} 5.2×10^{-4} T = 65°C	79	Temperature $[Fe^{3+}]$ $[Fe^{2+}]$ = Eh
Crundwell (1987)	$1-(1-X)^{\frac{1}{3}} = \left[\frac{\tau}{3M_o} A_o \exp\left(\frac{-E_A}{RT}\right)\left\{[Fe^{3+}_{Ad}] + [FeHSO_4^{2+}]\right\}^{1-\alpha}\right] t$	Ferric sulphate	-53 + 45 μm	2	0.123 0.336 0.993	1.146×10^{-4} 1.411×10^{-4} 1.975×10^{-4} T = 78°C	46	Temperature $[Fe^{3+}]$ $[Fe^{2+}]$ Addition of $ZnSO_4$
Rath *et al.* (1988)	$1-(1-X)^{\frac{1}{3}} = \left[\phi\ d_o^{-1} [Fe^{3+}]^{0.62} \exp\left(\frac{-E_A}{RT}\right)\right] t$	Ferric chloride	Varied	6	0.8 0.6 0.4 0.2	2.07×10^{-5} 1.86×10^{-5} 1.57×10^{-5} 0.87×10^{-5} T = 60°C	68	Temperature Particle size $[Fe^{3+}]$
Suni *et al.* (1989)	$X_T = \frac{\sum \left(\omega_i G_i [1-(1-(\frac{k_2}{r_{oi}} + \beta) t)^3]\right)}{\sum \omega_i G_i}$	Ferric chloride	-20.8 + 14.3 μm -36.7 + 27.9 μm -63 + 53 μm -150 + 125 μm	1 - 2	0.2	7.16×10^{-5} 4.11×10^{-5} 2.66×10^{-5} 1.48×10^{-5} T = 65°C	68.4	Particle size within leaching system
Palencia-Perez and Dutrizac (1991)	$1-(1-X)^{\frac{1}{3}} = K t$ *where* $K = 0.219 + 0.258\ [\%Fe]$	Ferric chloride Ferric sulphate	-104 + 76 μm	0.37	$[Fe^{3+}]$ M: 0.3 Fe content: 12.6 7.5 6.0 1.29 0.19 0.04	8.86×10^{-5} 6.33×10^{-5} 4.04×10^{-5} 1.27×10^{-5} 0.76×10^{-5} 0.45×10^{-5}	Range 39-81	Samples with differing iron content Temperature

APPENDIX E

First-Order Model

The reaction is dependent on the concentration of ferric iron in solution.

$$-\rho_B \frac{d\,d}{d\,t} = bk' \left[Fe^{3+}\right] \qquad [\text{E-1}]$$

In terms of fractional conversion where

$$\begin{aligned} 1 - X &= \left(\frac{\text{Volume of Unreacted Core}}{\text{Total Volume of Particles}}\right) \\ &= \frac{\frac{1}{6}\prod d^3}{\frac{1}{6}\prod d_o^3} \\ &= \left(\frac{d}{d_o}\right)^3 \\ \frac{d}{d_o} &= (1 - X)^{1/3} \end{aligned}$$

Equation 0-2 becomes:

$$\begin{aligned} -\rho_B\left(\frac{d\,d_o\,(1 - X)^{1/3}}{d\,t}\right) &= bk' \left[Fe^{3+}\right] \\ (1 - X)^{-2/3} \frac{d_o\,\rho_B}{3bk'} \frac{d\,X}{d\,t} &= \left[Fe^{3+}\right] \\ \frac{d\,X}{d\,t} &= (1 - X)^{2/3} \frac{3\,b\,k'}{d_o\,\rho_B}\left[Fe^{3+}\right] \end{aligned}$$

Electrochemical Model

The reaction is dependent on the ratio of ferric iron to ferrous iron determined from the electrochemical model presented by Verbaan and Crundwell (1986).

$$-\rho_B \frac{d\,d}{d\,t} = bk' \left(\frac{[Fe^{3+}]}{[Fe^{2+}]}\right)^{1/2} \qquad [\text{E-2}]$$

In terms of fractional conversion where

$$1 - X = \left(\frac{\text{Volume of Unreacted Core}}{\text{Total Volume of Particles}}\right)$$

$$= \frac{\frac{1}{6}\prod d^3}{\frac{1}{6}\prod d_o^3}$$

$$= \left(\frac{d}{d_o}\right)^3$$

$$\frac{d}{d_o} = (1 - X)^{1/3}$$

Equation E-2 becomes:

$$-\rho_B\left(\frac{d\,d_o\,(1 - X)^{1/3}}{d\,t}\right) = bk'\left(\frac{[Fe^{3+}]}{[Fe^{2+}]}\right)^{1/2}$$

$$(1 - X)^{-2/3}\frac{d_o\,\rho_B}{3\,bk'}\frac{d\,X}{d\,t} = \left(\frac{[Fe^{3+}]}{[Fe^{2+}]}\right)^{1/2}$$

$$\frac{d\,X}{d\,t} = (1 - X)^{2/3}\frac{3\,b\,k'}{d_o\,\rho_B}\left(\frac{[Fe^{3+}]}{[Fe^{2+}]}\right)^{1/2}$$

Half-Order Kinetics Model

The reaction is controlled by both the chemical reaction at the mineral surface and the product layer diffusion. The reaction is dependent on the half-order ratio of ferric iron to ferrous iron.

$$\begin{aligned}
\frac{-d\,N_{[Fe^{3+}]}}{d\,t} &= \Pi d^2 Q_{[Fe^{3+}]_c} \\
Q_{[Fe^{3+}]} &= D_e \frac{d\,[Fe^{3+}]}{d\,d} \\
\frac{-d\,N_{[Fe^{3+}]}}{d\,t} &= \Pi d^2 \frac{d\,[Fe^{3+}]}{d\,d} \\
\frac{-d\,N_{[Fe^{3+}]}}{d\,t} \int_{d_o}^{d} \frac{d\,d}{d^2} &= \Pi D_e \int_{Q_{[Fe^{3+}]_g}}^{Q_{[Fe^{3+}]_c}} d\,[Fe^{3+}] \\
\frac{d\,N_{[Fe^{3+}]}}{d\,t}\left(\frac{1}{d} - \frac{1}{d_o}\right) &= \Pi D_e \left([Fe^{3+}]_c - [Fe^{3+}]_g\right)
\end{aligned} \qquad [\text{E-3}]$$

Now the mass balance for reaction control gives:

$$\frac{-d\,N_{[Fe^{3+}]}}{d\,t} = k_s [Fe^{3+}]_c^{\alpha}\ \Pi d^2 \qquad [\text{E-4}]$$

If the reaction kinetics are half-order:

$$\frac{-d\,N_{[Fe^{3+}]}}{d\,t} = k_s [Fe^{3+}]_c^{1/2}\ \Pi d^2 \qquad [\text{E-5}]$$

If you substitute Equation E-5 into the final form of Equation E-3 then:

$$\begin{aligned}
-k_s [Fe^{3+}]^{1/2}\ d^2 \left(\frac{1}{d} - \frac{1}{d_o}\right) &= D_e \left([Fe^{3+}]_c - [Fe^{3+}]_g\right) \\
[Fe^{3+}]_g &= [Fe^{3+}]_c + k_s [Fe^{3+}]^{1/2} \frac{d\,(d_o - d)}{d_o\,D_e}
\end{aligned} \qquad [\text{E-6}]$$

This is a quadratic in $[Fe^{3+}]^{1/2}$

$$0 = \left(\left[Fe^{3+}\right]_c^{1/2}\right)^2 + \left[Fe^{3+}\right]_c^{1/2} \frac{d\,(d_o - d)\,k_s}{d_o\,D_e} - \left[Fe^{3+}\right]_g^{1/2}$$

$$\left[Fe^{3+}\right]_c^{1/2} = \frac{-d\,(d_o - d)\,k_s}{d_o\,D_e} \pm \sqrt{\left(\frac{d\,(d_o - d)\,k_s}{d_o\,D_e}\right)^2 + 4\left[Fe^{3+}\right]_g} \qquad [E\text{-}7]$$

And since $[Fe^{3+}]^{1/2}$ is positive:

$$\left[Fe^{3+}\right]_c^{1/2} = \frac{-d\,(d_o - d)\,k_s}{d_o\,D_e} + \sqrt{\left(\frac{d\,(d_o - d)\,k_s}{d_o\,D_e}\right)^2 + 4\left[Fe^{3+}\right]_g} \qquad [E\text{-}8]$$

Knowing that :

$$1 - X = \left(\frac{d}{d_o}\right)^3$$

and letting:

$$k_2 = \left(\frac{k_s d_o}{4D_e}\right) \qquad [E\text{-}9]$$

$$\left[Fe^{3+}\right]_c^{1/2} = -k_2(1-X)^{1/3}\left[1-(1-X)^{1/3}\right] + \sqrt{\left\{k_2(1-X)^{1/3}\left[1-(1-X)^{1/3}\right]\right\}^2 + \left[Fe^{3+}\right]} \qquad [E\text{-}10]$$

From the mass balance:

$$\begin{aligned}
\frac{-d\,N_{[Fe^{3+}]}}{d\,t} &= \Pi d^2\,k_s\left[Fe^{3+}\right]^{1/2} \\
d\,N_{[Fe^{3+}]} &= \frac{\rho_B \Pi d^2\,k_s}{b}\,d\,d \\
-\frac{\rho_B}{b}\,\frac{d\,d}{d\,t} &= k_s\left[Fe^{3+}\right]_c^{1/2} \qquad [E\text{-}11] \\
-\frac{\rho_B}{b}\,\frac{d\,d_o(1-X)^{1/3}}{d\,t} &= k_s\left[Fe^{3+}\right]_c^{1/2} \\
\frac{d\,X}{d\,t} &= \frac{3\,k_s\,b}{\rho_B\,d_o}(1-X)^{2/3}\left[Fe^{3+}\right]_c^{1/2}
\end{aligned}$$

Diffusion Coefficient Decay Model

This model is similar to that derived as the Half-Order Kinetics Model, but the diffusion coefficient decays with time as in the Surface Deactivation Model. The rate controlling steps are the chemical reaction at the mineral surface and the product layer diffusion limitations. The reaction order is equal to one-half. This is very similar to the model described by Morin *et al.* (1985), the difference being that their derivation did not include the half order reaction.

$$k_{22} = k_2 \exp(k_D t) \qquad [\text{E-12}]$$

where k_{22} contains the diffusion coefficient.

This changes the dependence on ferric iron to be:

$$[Fe^{3+}]_c^{1/2} = -k_{22}(1-X)^{1/3}\left[1-(1-X)^{1/3}\right] + \sqrt{\left\{k_{22}(1-X)^{1/3}\left[1-(1-X)^{1/3}\right]\right\}^2 + \left[Fe^{3+}\right]} \qquad [\text{E-13}]$$

And the final form of the model is:

$$\frac{dX}{dt} = \frac{k_1}{[Fe^{2+}]^{1/2}} (1-X)^{2/3} [Fe^{3+}]_c^{1/2} \qquad [\text{E-14}]$$

APPENDIX F

```
/* PROGRAM EQUIL */

/* This program calculates the equilibrium distribution of the ferric and ferrous
species in solution given the total concentrations of ferric ferrous, H+ and Zn2+. The
sulphate is also input but is completely specified in terms of the electroneutrality of
the solution. */

/* NOMENCLATURE

c(1)=Fe3+++
c(2)=Fe2++
c(3)=H+
c(4)=SO4--
c(5)=Zn2+
c(6)=FeHSO4++
c(7)=Fe(SO4)2 -
c(8)=FeSO4+
c(9)=HSO4-
c(10)=FeHSO4+
c(11)=FeOH++
c(12)=Fe(OH)2+
c(13)=Fe2(OH)2++++
c(14)=FeOH+
c(15)=Fe(OH)2
*/

#include "c:\tc\programs\nrutil.h"

#include <stdio.h>
#include <stdlib.h>
#include "c:\tc\programs\ludcmp.cpp"
#include "c:\tc\programs\lubksb.cpp"
```

```
#define NP 20
#define MAXSTR 80

static float sqrarg, cubearg;
#define SQR(ab) ((sqrarg=(ab)) == 0.0 ? 0.0 : sqrarg*sqrarg)
#define CUBE(ab) ((cubearg=(ab)) == 0.0 ? 0.0 : cubearg*cubearg*cubearg)


/* prototypes */

void lubksb (float **a, int n, int *indx, float b[]);
void ludcmp (float **a, int n, int *indx, float *d);
void equilb (float *tc, float *c, float temp);

int main (void)

{
int i;
float temp, *tc, *c;
char filename[MAXSTR], dummy[MAXSTR];
FILE *fp;

tc=vector(1,5);
c=vector(1,15);

/* entering the data file name */

//printf("enter the name of the data file:\n");
//scanf("%s",filename);
//printf("Filename: %s",filename,"\n");

/* read data from file */

//if ((fp = fopen(filename,"r")) == NULL)
if ((fp = fopen("terry.dat","r")) == NULL)
nrerror("Data file not found\n");
```

```
fgets(dummy,MAXSTR,fp);
fscanf(fp,"%f ",&temp);printf("temperature %f\n",temp);
for (i=1;i<=5;i++) fscanf(fp,"%f ",&tc[i]);
fclose(fp);

/* calculate the equilibrium concentrations */

equilb(tc,c,temp);

/* write out results to screen */

printf("Equilbrium concentrations\n");
        //for (i=1;i<=10;i++) printf ("%d %f ",i,c[i]);
printf("\nFe+++ \t\t%e\n",c[1]);
printf("Fe++ \t\t%f\n",c[2]);
printf("H+ \t\t%f\n",c[3]);
printf("SO4-- \t\t%f\n",c[4]);
printf("Zn++ \t\t%f\n",c[5]);
printf("FeHSO4++ \t%e\n",c[6]);
printf("FeSO4+ \t\t%f\n",c[7]);
printf("HSO4- \t\t%f\n",c[8]);
printf("FeSO4 \t\t%f\n",c[9]);
printf("FeHSO4+ \t%f\n",c[10]);

free_vector(tc,1,5);
free_vector(c,1,15);

return 0;

}
/*============================================================*/

void equilb (float *tc,float *c,float temp)
```

```
/* Program to evaluate the equilibrium conditions of a solution given the total species
concentration and the equilibrium constants. The activity coefficients are evaluated
using the Debye-Huckel equation. */
{
int i,j,n,itr,*indx;
float alfamn; int nerror;
float eq[14],ceq[14],diag[5],y[10];
float atemp,a,b,xions,p;
float **q,*x,*g,*ga,a0[10],z[10];

q=matrix(1,5,1,5);
x=vector(1,5);
g=vector(1,5);
ga=vector(1,5);

/* calculate equilibrium constants */

eq[1]=0.0;
eq[2]=exp(33.334-7629.9/temp);
eq[3]=0.0;
eq[4]=exp(-900.421+39110.926/temp+136.626*log(temp));
eq[6]=pow(10.0,(3.339-337.37/temp));
eq[7]=exp(30.692-7290.4/temp);
eq[8]=pow(10.0,2.38)*exp(-754.8/temp+2.533);
eq[9]=exp(10.9609-4727.1523/temp);
eq[10]=exp(35.5599-15515.302/temp);
eq[11]=exp(13.4335-5965.1007/temp);
eq[12]=0.0;
eq[13]=pow(10.0,(-14.01));
eq[14]=1.6505*pow(10.0,-14.01);
eq[9]=0.0;
eq[10]=0.0;
eq[11]=0.0;
eq[12]=0.0;
//for(i=1;i<=10;i++) printf("%d Equilb const %e\n",i,eq[i]);
/* calculate constants for the Debye-Huckel equation */
```

```
atemp=temp-298.15;

a0[1]=9.;a0[2]=6.;a0[3]=9.;a0[4]=4.;a0[5]=4.;a0[6]=8.;a0[7]=8.;a0[8]=8.;a0[9]=4.;a0[1
0]=4.;
z[1]=3.;z[2]=2.;z[3]=1.;z[4]=2.;z[5]=2.;z[6]=2.;z[7]=1.;z[8]=1.;z[9]=1.;z[10]=1.;


a=0.4919+7.143e-4*atemp+2.113e-6*SQR(atemp)+1.172e-8*CUBE(atemp);
b=0.3249+2.099e-4*atemp-2.582e-8*SQR(atemp)+2.589e-9*CUBE(atemp);


/* assume total dissociation, and calculate ionic strength, and set guess for the initial
concentrations as the total dissociation concentration */

tc[4]=3./2.*tc[1]+tc[2]+0.5*tc[3]+tc[5];

xions=0.0;

for (i=1;i<=5;i++)
        {
        c[i]=tc[i];
        xions=xions+SQR(z[i])*c[i];
        }
xions=xions/2.;
c[9]=c[3]/2.;

/* conditions for loop */

itr=0;//nerror=1;

/* begin loop */

do {
        itr += 1;
```

```
/* calculate activity coefficients from Debye-Huckel equation */

for (i=1;i<=10;i++)
        {
        y[i]=pow(10.0,(-a*z[i]*z[i]*sqrt(xions)/(1.0+a0[i]*b*sqrt(xions))));
        }

/* calculate the equilibrium constants in terms of concentration */

ceq[1]=eq[1]*y[1]*y[3]*SQR(y[4]);
ceq[2]=eq[2]*y[1]*y[3]*y[4]/y[6];
ceq[3]=eq[3]*y[1]*SQR(y[4])/y[7];
ceq[4]=eq[4]*y[1]*y[4]/y[8];
ceq[6]=eq[6]*y[2]*y[4];
ceq[7]=eq[7]*y[2]*y[3]*y[4]/y[10];
ceq[8]=eq[8]*y[5]*y[4];
ceq[9]=eq[9];
ceq[10]=eq[10];
ceq[11]=eq[11];
ceq[14]=eq[14];


/* calculate the concentration quotient for the bisulphate equilibrium using Pitzer's
correlation */

float k2,mh,m1,m2,bh10,bh11,bh20,ch20,a1,u,f,bh1,bh2,ch2,actvty;

k2=exp(14.03231-2825.2/temp);
bh10=0.05584+46.04/temp;
bh11=-0.65758+336.514/temp;
bh20=-0.32806+98.607/temp;
ch20=0.25333-63.124/temp;
a1=0.377+4.68e-4*(temp-273.15)+3.74e-6*SQR(temp-273.15);
u=sqrt(xions)/(1.0+1.2*sqrt(xions));
f=-a1*(u+(2./1.2)*log(1.0+1.2*sqrt(xions)));
bh1=bh10+bh11/xions/2.*(1.-(1.+2.*sqrt(xions))*exp(-2.*sqrt(xions)));
```

```
bh2=-1.+(1.+2.*sqrt(xions)+2.*xions)*exp(-2.*sqrt(xions));
bh2=bh11/(SQR(xions)/2.)*bh2;
ch2=ch20/(pow(2.,1.5));
mh=c[3];
m1=c[9];
m2=c[4];
actvty=4.*f+2.*(m1-mh)*bh1+2.*(m2+mh)*bh20;
actvty=exp(actvty+2.*mh*(2.*m2+mh)*ch2+4.*m1*mh*bh2);

ceq[5]=k2*actvty;

/* calculate vector for the solution of the non-linear equations using the Newton-
Raphson technique */

g[1]=c[1]+ceq[1]*c[1]*c[3]*SQR(c[4])+ceq[2]*c[1]*c[3]*c[4];
g[1]=g[1]+ceq[3]*c[1]*SQR(c[4])+ceq[4]*c[1]*c[4]-tc[1];

g[2]=c[2]+ceq[6]*c[2]*c[4]+ceq[7]*c[2]*c[3]*c[4]-tc[2];

g[3]=c[3]+ceq[1]*c[1]*c[3]*SQR(c[4])+ceq[2]*c[1]*c[3]*c[4];
g[3]=g[3]+ceq[5]*c[3]*c[4]+ceq[7]*c[2]*c[3]*c[4]-tc[3];

g[4]=c[4]+2.0*ceq[1]*c[1]*c[3]*SQR(c[4])+ceq[2]*c[1]*c[3]*c[4];
g[4]=g[4]+2.0*ceq[3]*c[1]*SQR(c[4])+ceq[4]*c[1]*c[4];
g[4]=g[4]+ceq[5]*c[3]*c[4]+ceq[6]*c[2]*c[4];
g[4]=g[4]+ceq[7]*c[2]*c[3]*c[4]+ceq[8]*c[5]*c[4]-tc[4];

g[5]=c[5]+ceq[8]*c[5]*c[4]-tc[5];


for (i=1;i<=5;i++)
        {
        ga[i]=g[i];
        g[i]=-g[i];
        }
```

```
/* calculate the matrix Q */

q[1][1]=1.+ceq[1]*c[3]*SQR(c[4])+ceq[2]*c[3]*c[4]+ceq[3]*SQR(c[4])+ceq[4]*c[4];
q[1][2]=0.0;
q[1][3]=ceq[1]*c[1]*SQR(c[4])+ceq[2]*c[1]*c[4];
q[1][4]=2.*ceq[1]*c[1]*c[3]*c[4]+ceq[2]*c[1]*c[3]+2.*ceq[3]*c[1]*c[4]+ceq[4]*c[1];
q[1][5]=0.0;

q[2][1]=0.0;
q[2][2]=1.0+ceq[6]*c[4]+ceq[7]*c[3]*c[4];
q[2][3]=ceq[7]*c[2]*c[4];
q[2][4]=ceq[6]*c[2]+ceq[7]*c[2]*c[3];
q[2][5]=0.0;

q[3][1]=ceq[1]*c[3]*SQR(c[4])+ceq[2]*c[3]*c[4];
q[3][2]=ceq[7]*c[3]*c[4];
q[3][3]=1.0+ceq[1]*c[1]*SQR(c[4])+ceq[2]*c[1]*c[4]+ceq[5]*c[4]+ceq[7]*c[2]*c[4];
q[3][4]=2.0*ceq[1]*c[1]*c[3]*c[4]+ceq[2]*c[1]*c[3]+ceq[5]*c[3]+ceq[7]*c[2]*c[3];
q[3][5]=0.0;

q[4][1]=2.*ceq[1]*c[3]*SQR(c[4])+ceq[2]*c[3]*c[4]+2.0*ceq[3]*SQR(c[4])+ceq[4]*c[4];
q[4][2]=ceq[6]*c[4]+ceq[7]*c[3]*c[4];
q[4][3]=2.*ceq[1]*c[1]*SQR(c[4])+ceq[2]*c[1]*c[4]+ceq[5]*c[4]+ceq[7]*c[2]*c[4];
q[4][4]=1.0+4.*ceq[1]*c[1]*c[3]*c[4]+ceq[2]*c[1]*c[3]+4.*ceq[3]*c[1]*c[4]+ceq[4]*c[1]+
ceq[5]*c[3]+ceq[6]*c[2]+ceq[7]*c[2]*c[3]+ceq[8]*c[5];
q[4][5]=ceq[8]*c[4];

q[5][1]=0.0;
q[5][2]=0.0;
q[5][3]=0.0;
q[5][4]=ceq[8]*c[5];
q[5][5]=1.0+ceq[8]*c[4];

/* arrange in terms of fractional shifts */

for (i=1;i<=5;i++)
```

```
        {
        for (j=1;j<=5;j++)
                {
                q[i][j]=q[i][j]*c[j];//printf("%d %d %f \n",i,j,q[i][j]);
                }
        diag[i]=q[i][i];
        if (c[i]<=0.0) diag[i]=1.0;
        }

/* matrix scaling */

for (i=1;i<=5;i++)
{
g[i]=g[i]/sqrt(diag[i]);
for (j=1;j<=5;j++)
        {
        q[i][j]=q[i][j]/sqrt(diag[i]*diag[j]);
        }
}
```

/* calculate the vector X in the equation QX = G the method of LU decomposition is first called, and then the back-substitution procedure is used to calculate G ludcmp performs the LU decomposition of the matrix q, and then lubksb solves the set of linear equations QX=G where Q is input as the LU decomposition of Q, G is the input of the right-hand side vector, and output as the solution. There are limited error checking routines in the programs from Numerical Recipes */

```
n=5;
ludcmp(q,n,indx,&p);
lubksb(q,n,indx,g);
/* calculate the fractional shifts */

for (i=1;i<=5;i++)
        {
        x[i]=g[i]/sqrt(diag[i]);
        if (x[i]>1.0) x[i]=0.95;
```

```
        if (x[i]<-1.0) x[i]=-0.95;
        }

/* calculate concentrations c[1] to c[5] for next iteration */

alfamn=1.0; nerror=0;
for (i=1;i<=5;i++)
        {
        c[i]=c[i]*(1.+alfamn*x[i]);
        if (c[i]<0.0) c[i]=1.0e-10;
        if (fabs(alfamn*x[i])>0.00001) nerror=nerror+1;
        }

/* calculate concentrations c[6] thru c[10] for next iteration    */

c[6]=ceq[2]*c[1]*c[3]*c[4]; //FeHSO4++
c[7]=ceq[3]*c[1]*SQR(c[4]); //Fe(SO4)-
c[8]=ceq[4]*c[1]*c[4];      //FeSO4+
c[9]=ceq[5]*c[3]*c[4];      //HSO4-
c[10]=ceq[7]*c[2]*c[3]*c[4];//FeHSO4+

//for(i=1;i<=10;i++) printf("%d c[i] %e ceq[i] %e\n",i,c[i],ceq[i]);
//printf("mass Ferric total in %e Mass Ferric total out %e\n",tc[1],(c[1]+c[6]+c[8]));

/* calculate the ionic strength */

xions=0.0;
for (i=1;i<=10;i++)
        {
        xions=xions+SQR(z[i])*c[i];
        }
xions=xions/2.;

} while (nerror>0); // end of do while loop

/* calculate concentrations for values of interest */
```

```
c[6]=ceq[2]*c[1]*c[3]*c[4]; //FeHSO4++
c[7]=ceq[4]*c[1]*c[4];      //FeSO4+
c[8]=ceq[5]*c[3]*c[4];      //HSO4-
c[9]=ceq[6]*c[2]*c[4];      //FeSO4
c[10]=ceq[7]*c[2]*c[3]*c[4];//FeHSO4+

free_vector(x,1,5);
free_vector(g,1,5);
free_vector(ga,1,5);
free_matrix(q,1,5,1,5); printf("number of iterations %d\n",itr);

}
// end of routine equilb

/*============================================================*/
```

APPENDIX G

Acid Digest Method

Acid digestion enables a mineral sample to be completely dissolved so that the resulting solution can be analysed for the presence of various metals, using atomic adsorption (AA) spectrophotometry. The method outlined below has been adapted from the procedure used by Anglo American Research Laboratories (South Africa).

Reagents Required

REAGENT	FORMULA	CONCENTRATION
Hydrochloric acid	HCl	30%
Nitric acid	HNO_3	60%
Perchloric acid	$HClO_4$	70%
Hydrofluoric acid	HF	40%

Hydrofluoric acid is extremely dangerous, causing severe burns if it comes in contact with the skin. Appropriate protective clothing (face shield, rubber gloves and plastic apron) must be worn when performing digests. The digestion should be performed in a fume cupboard.

Method

1. Make up 1 litre of solution by mixing 4 parts HCl to 1 part HF. Store in a plastic container as HF attacks glass.
2. Weigh approximately 0.2 g of sample accurately on a 4 decimal place balance. Let this be mass "a". The mass of sample may have to be reduced to 0.1 g if the mineral is a high grade material.
3. Put the weighed sample into an Erlenmeyer flask.

4. Pipette (using a plastic pipette) 10 ml of the HCl/HF mixture into the flask and heat until boiling.
5. When boiling, add 10 ml HNO_3 and boil till approximately 2 ml remains in the flask and the solution has become colourless.
6. Add 5 ml $HClO_4$ and boil till the white fumes that form lift to the neck of the flask and 2 ml remains.
7. Remove the flask from the hotplate and allow to cool.
8. Using a funnel, pour the contents of the flask into a 250 ml volumetric flask. Rinse the flask using distilled water and pour all washings into the volumetric flask.
9. Make up the remaining volume in the volumetric flask to 250 ml with distilled water.
10. Shake the volumetric flask to ensure that the solution is well mixed.
11. Filter the solution using Whatman No.1 filter paper and collect the filtrate in a 20 ml sample bottles. A half-filled sample bottle is generally sufficient for the determination of one element. It is advisable to retain excess solution, however, until the AA analysis has been performed.
12. Determine the concentration, R (ppm) of a particular element in the filtered solution using AA analysis.
13. The composition, C (%) of the element in the original sample is determined as follows:

R(ppm)	=	R/1000 ($g.\ell^{-1}$)
Mass of sample digested per litre	=	a x 1000/250
	=	4a ($g.\ell^{-1}$)
Concentration, C	=	(R/1000 x 1/4a) x 100 %
	=	R/40a %

APPENDIX H

Experimental Data

EXPERIMENT 1 The effect of temperature on the dissolution of zinc from sphalerite in a ferric sulphate solution.

CONDITIONS	1A	1B	1C	1D	1E	1F
Temperature (°C)	55	50	45	40	35	30
Particle Size (μm)	-75+53	-75+53	-75+53	-75+53	-75+53	-75+53
Fe(III) (M)	0.5	0.5	0.5	0.5	0.5	0.5
Fe(II) (M)	0.002	0.003	0.002	0.002	0.002	0.002
Redox Potential (mV vsAg/AgCl)	585	585	585	585	585	585

TIME	FRACTION ZINC EXTRACTED					
(hours)	1A	1B	1C	1D	1E	1F
0.00	0.000	0.000	0.000	0.000	0.000	0.000
0.25	0.058					
0.33		0.055	0.052			
0.50	0.127			0.056	0.043	0.024
0.67		0.137	0.113			
0.75	0.187					
1.00	0.235	0.206	0.173	0.117	0.085	0.048
1.50	0.317					
1.75		0.322	0.269			
2.00	0.379			0.205	0.164	0.121
2.50	0.471	0.409	0.354			
3.00	0.496			0.326	0.224	0.181
4.00	0.572	0.536	0.465			
5.00				0.419	0.321	0.263
6.00	0.689	0.567	0.559			
7.00				0.552	0.403	0.333
8.00	0.835	0.745	0.643			
10.00	0.782	0.783		0.660	0.492	0.418
11.00			0.714			
12.00	0.824	0.793				
13.00				0.725	0.565	0.486
14.00		0.824	0.774			
16.00		0.839		0.772	0.613	0.542
17.00			0.794			
18.00		0.857				
20.00				0.804	0.677	0.605
21.00			0.799			
24.00		0.901	0.840	0.856	0.722	0.652
28.00				0.856	0.754	0.677
32.00				0.905	0.768	0.716

EXPERIMENT 2 The effect of particle size on the dissolution of zinc from sphalerite in a ferric sulphate solution.

CONDITIONS	2A	2B	2C	2D
Temperature (°C)	40	40	40	40
Particle Size (μm)	-106+90	-75+53	-53+45	-45+38
Fe(III) (M)	0.5	0.5	0.5	0.5
Fe(II) (M)	0.008	0.011	0.009	0.015
Redox Potential (mV vsAg/AgCl)	585	585	585	585

TIME	FRACTION ZINC EXTRACTED			
	2A	2B	2C	2D
0.0	0.000	0.000	0.000	0.000
0.5	0.040	0.056	0.084	0.091
1.0	0.082	0.117	0.161	0.208
2.0	0.151	0.205	0.324	0.328
3.0	0.214	0.326	0.413	0.431
5.0	0.309	0.419	0.582	0.625
7.0	0.431	0.552	0.694	0.772
10.0	0.535	0.660	0.776	0.889
13.0	0.688	0.725		
16.0		0.772		
20.0	0.730	0.804	0.863	0.910
23.0			0.920	
24.0	0.793	0.856		
28.0		0.856		
29.0			0.899	0.933
32.0	0.827	0.905		

EXPERIMENT 4 The effect of the ferric iron concentration and ferrous iron concentration on the dissolution of zinc from sphalerite in a ferric sulphate solution.

CONDITIONS	4A	4B	4C	4D	4E	4F	4G	4H
Temperature (°C)	40	40	40	40	40	40	40	40
Particle Size (μm)	-75+53	-75+53	-75+53	-75+53	-75+53	-75+53	-75+53	-75+53
Fe(III) (M)	0.5	0.5	0.5	0.5	0.5	0.48	0.26	0.5
Fe(II) (M)	0.00013	0.00033	0.00067	0.00134	0.02	0.048	0.26	0.000
Redox Potential (mV vsAg/AgCl)	673	656	609	601	554	492	443	Not Controlled

TIME (hours)	FRACTION ZINC EXTRACTED			
	4A	4B	4C	4D
0	0.000	0.000	0.000	0.000
0.5	0.059	0.054	0.056	0.047
1	0.117	0.107	0.111	0.102
2	0.215	0.188	0.198	0.180
3	0.282	0.243	0.273	0.231
5	0.391	0.307	0.334	0.347
7	0.471	0.381	0.385	0.469
10	0.573	0.444	0.456	0.533
13	0.616	0.509	0.485	0.577
16	0.642	0.538	0.475	0.591
20	0.665	0.561	0.515	0.621
24	0.675	0.571	0.569	0.633
28	0.692	0.604	0.565	0.694
32	0.699	0.601	0.568	0.745

TIME (hours)	FRACTION ZINC EXTRACTED			
	4E	4F	4G	4H
0.0	0.000	0.000	0.000	0.000
0.5	0.028	0.030	0.015	0.031
1.0	0.069	0.070	0.032	0.069
2.0	0.149	0.148	0.067	0.131
3.0	0.213	0.209	0.104	0.180
5.0	0.304	0.295	0.201	0.250
7.3	0.432	0.426	0.280	0.315
10.0	0.506	0.478	0.353	0.405
20.0	0.616	0.592	0.491	0.485
22.4	0.647	0.663	0.518	0.525
24.8	0.661	0.674	0.536	0.537
27.2	0.670	0.682	0.620	0.569
29.7	0.683	0.731	0.628	0.597
32.0	0.694	0.726	0.624	0.608

EXPERIMENT 5 The effect of the addition of pyrite on the dissolution of zinc from sphalerite in a ferric sulphate solution.

CONDITIONS	5A	5B	5C	5D
Temperature (°C)	40	40	40	40
Sphalerite (g.ℓ^{-1})	5.00	10.00	10.00	10.00
Particle Size (μm)	-106+90	-106+90	-106+90	-106+90
Pyrite (g.ℓ^{-1})	5.00	10.00	1.00	0.10
Particle Size (μm)	-53+45	-53+45	-53+45	-53+45
Fe(III) (M)	0.5	0.5	0.5	0.5
Fe(II) (M)	0.009	0.000	0.009	0.014
Redox Potential (mV vsAg/AgCl)	Not Controlled	Not Controlled	585	585

TIME (hours)	FRACTION ZINC EXTRACTED			
	5A	5B	5C	5D
0.0	0.000	0.000	0.000	0.000
0.5	0.097	0.074	0.047	0.031
1.0	0.147	0.120	0.101	0.097
2.0	0.231	0.192	0.163	0.181
3.0	0.297	0.264	0.235	0.270
5.0	0.385	0.373	0.369	0.409
7.0	0.464	0.385	0.484	0.505
10.0	0.590	0.463	0.562	0.521
13.0	0.657	0.512	0.610	0.595
17.5	0.729	0.566	0.689	0.668
20.0	0.769	0.607	0.743	0.703
24.0	0.798	0.632	0.770	0.739
28.0	0.843	0.698	0.820	0.756
32.0	0.822	0.754	0.820	0.754

EXPERIMENT 6 The leaching of the different types of ores from the Gamsberg.

CONDITIONS	6A	6B	6C
Temperature (°C)	40	40	40
Particle Size (μm)	-75+53	-75+53	-75+53
Fe(III) (M)	0.5	0.5	0.5
Fe(II) (M)	0.009	0.009	0.006
Redox Potential (mV vsAg/AgCl)	585	585	585

TIME (hours)	FRACTION ZINC EXTRACTED		
	6A	6B	6C
0.0	0.000	0.000	0.000
0.5	0.101	0.082	0.069
1.0	0.191	0.159	0.136
2.0	0.335	0.303	0.268
3.0	0.455	0.414	0.369
5.0	0.582	0.551	0.509
7.0	0.661	0.648	0.624
10.0	0.801	0.739	0.705
13.0	0.815	0.814	0.767
16.0	0.861	0.826	0.801
20.0	0.910	0.880	0.842
24.0	0.930	0.899	0.871
28.0	0.950	0.907	0.889
32.0	0.966	0.924	0.911

6A Pyrrhotite Zone (Zn finely disseminated)
6B Bore Core Samples
6C Gamsberg Concentrate (zone unknown)

APPENDIX I

XRD Analysis

XRD analysis of the leached sphalerite after thirty two hours of leaching at 35 °C.

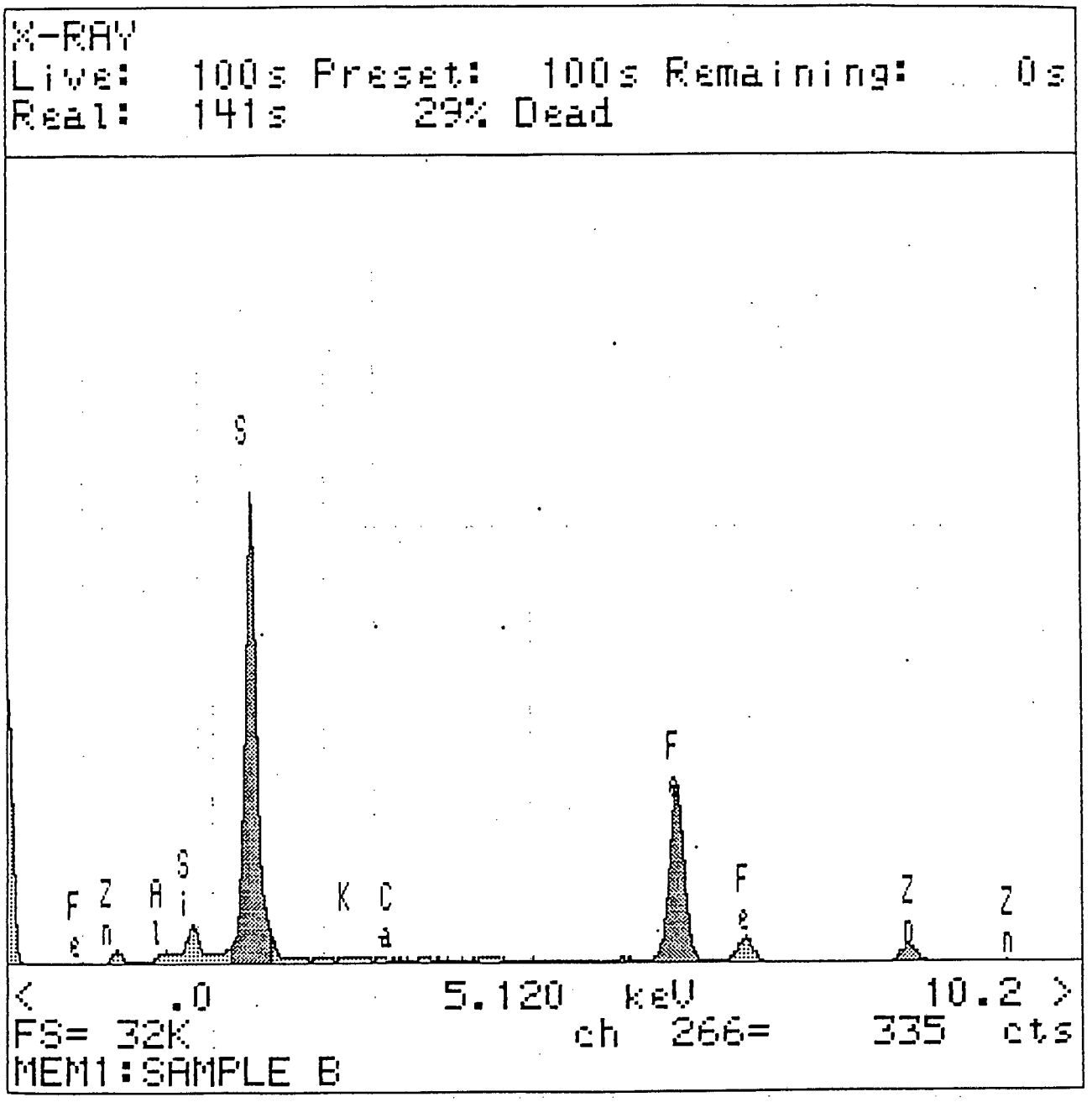

XRD analysis of the leached sphalerite after thirty two hours of leaching at 50 °C.

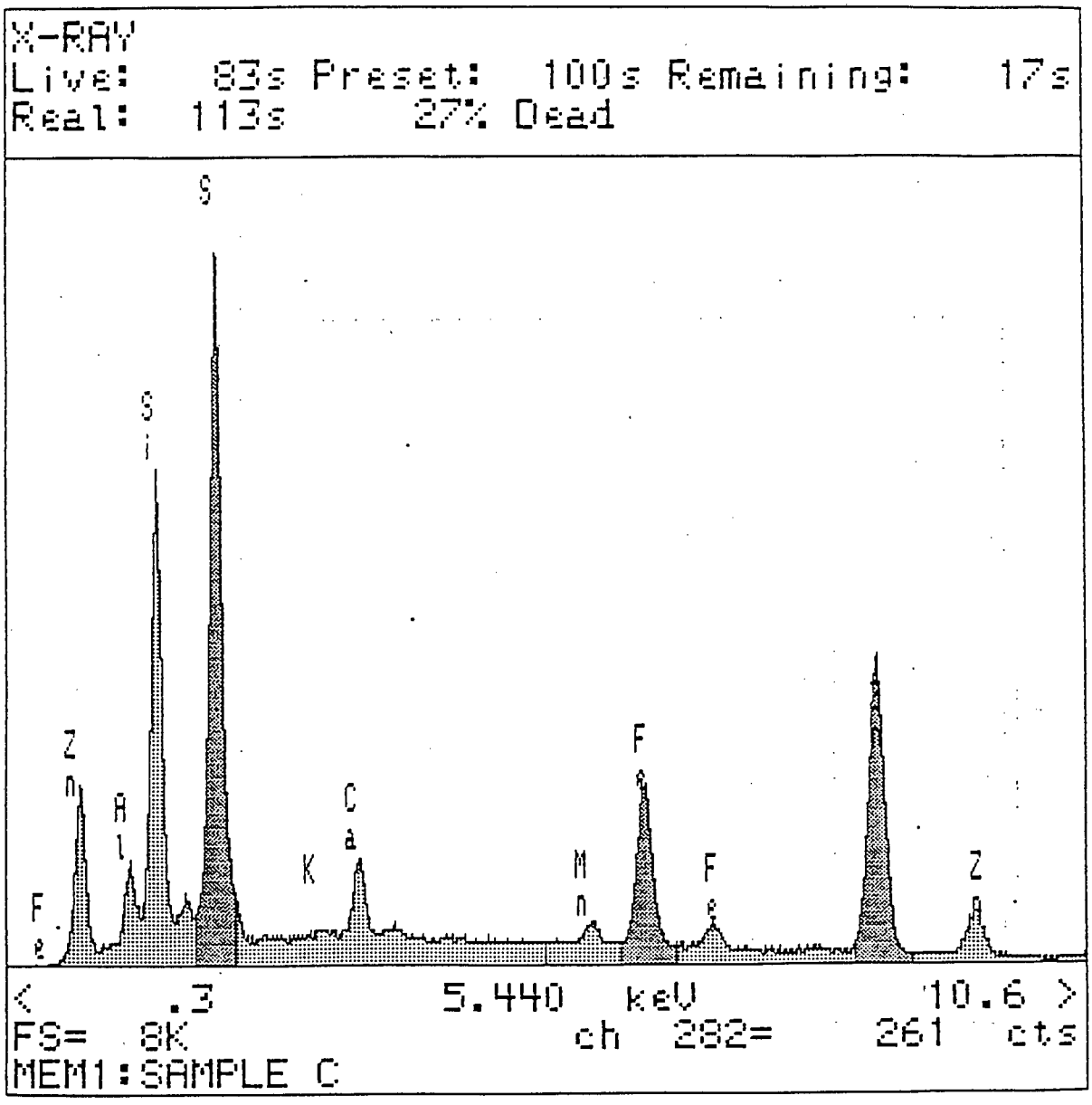

XRD analysis of the leached sphalerite after thirty two hours of leaching at 40 °C showing the large amount of sulphur present.

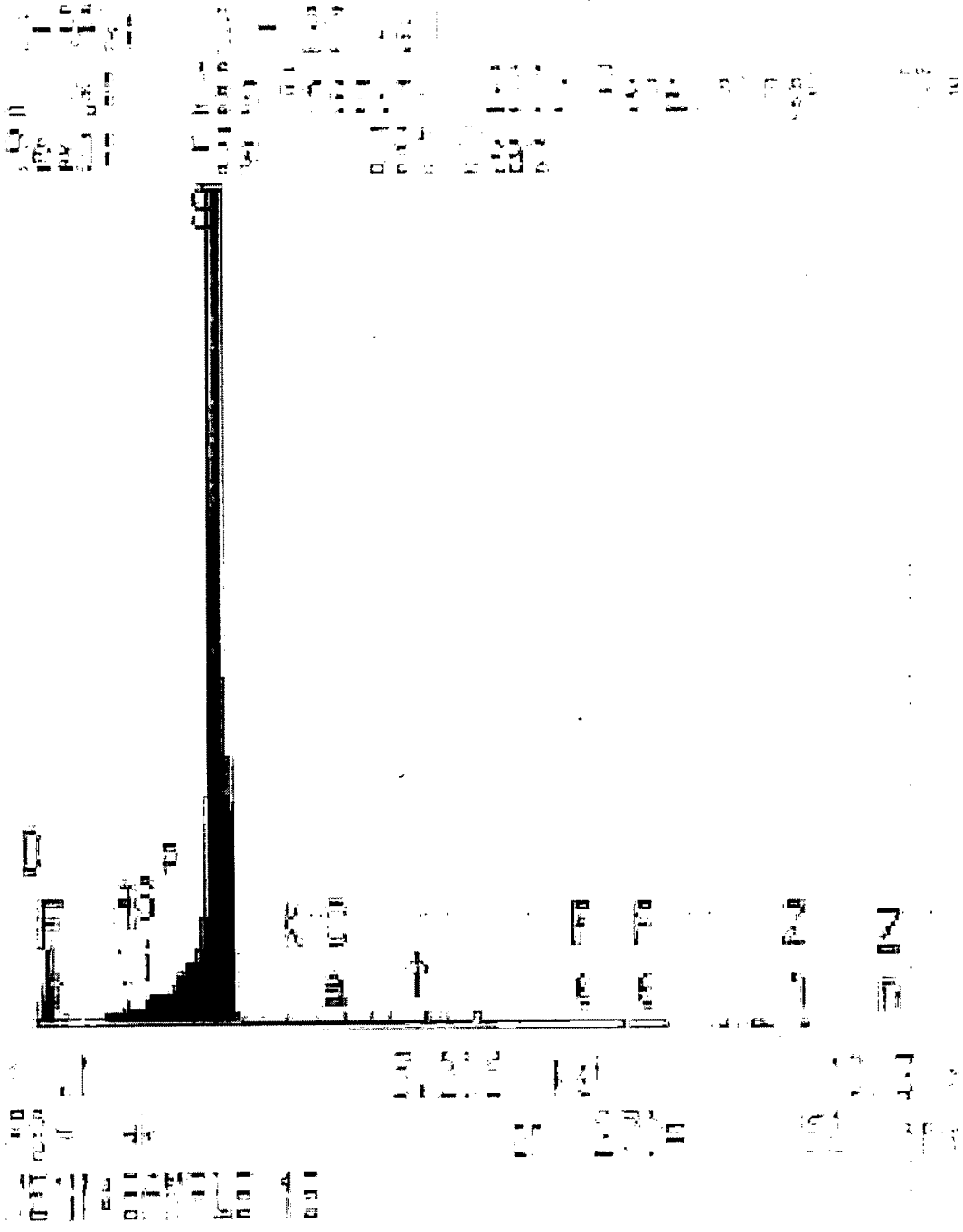

XRD analysis of the leached sphalerite after thirty two hours of leaching at 40 °C showing the large amount of sulphur present.